CENTRIFUGE MODELLING AND NUMERICAL ANALYSIS OF BEARING CAPACITY OF RING FOUNDATIONS ON SAND

CENTRE FOR NEWFOUNDLAND STUDIES

TOTAL OF 10 PAGES ONLY
MAY BE XEROXED

(Without Author's Permission)

FANYU ZHU

001311

CENTRE FOR NFLD. STUDIES
JUN 18 1978
MEMORIAL UNIVERSITY
OF NEWFOUNDLAND

INFORMATION TO USERS

This manuscript has been reproduced from the microfilm master. UMI films the text directly from the original or copy submitted. Thus, some thesis and dissertation copies are in typewriter face, while others may be from any type of computer printer.

The quality of this reproduction is dependent upon the quality of the copy submitted. Broken or indistinct print, colored or poor quality illustrations and photographs, print bleedthrough, substandard margins, and improper alignment can adversely affect reproduction.

In the unlikely event that the author did not send UMI a complete manuscript and there are missing pages, these will be noted. Also, if unauthorized copyright material had to be removed, a note will indicate the deletion.

Oversize materials (e.g., maps, drawings, charts) are reproduced by sectioning the original, beginning at the upper left-hand corner and continuing from left to right in equal sections with small overlaps. Each original is also photographed in one exposure and is included in reduced form at the back of the book.

Photographs included in the original manuscript have been reproduced xerographically in this copy. Higher quality 6" x 9" black and white photographic prints are available for any photographs or illustrations appearing in this copy for an additional charge. Contact UMI directly to order.

UMI

A Bell & Howell Information Company
300 North Zeeb Road, Ann Arbor MI 48106-1346 USA
313/761-4700 800/521-0600

CENTRIFUGE MODELLING AND NUMERICAL ANALYSIS OF BEARING CAPACITY OF RING FOUNDATIONS ON SAND

by

Fanyu Zhu, B. Eng., M. Eng.

A thesis submitted to the School of Graduate Studies
in partial fulfillment of the requirements for
the degree of Doctor of Philosophy

Faculty of Engineering and Applied Science
Memorial University of Newfoundland

August 1998

St. John's Newfoundland Canada

To my wife Ying

Abstract

Ring foundations are often adopted for large and tall structures to resist lateral loads and to increase the stability against overturning. They have been used worldwide under various structures, including telecommunication towers, liquid storage tanks, bridges and offshore structures. However, the behaviour of these foundations has not been well understood. An accepted method for estimating the bearing capacity is not available. In the design of ring foundations, very crude simplifications have to be made. Therefore, developing a rational and practical procedure for estimating the bearing capacity of ring foundations is of great importance.

This thesis presents research on the bearing capacity of ring footings on a dense sand under vertical loads. The effects of footing size, ring radii ratio and load eccentricity have been investigated by means of centrifuge modelling, the method of characteristics and the finite element technique. To support the research, triaxial and oedometer compression tests have been conducted to determine the soil friction angles, in situ stress ratios, and plastic and elastic behaviour of the sand. The peak and critical state friction angles of the sand from triaxial tests are reduced by 4° to 5° with a log-cycle increase of confining pressure.

Over 40 centrifuge tests of ring footings have been conducted at acceleration levels from 10 to 160 gravities. High quality sand test samples with density index of 90% were prepared using a developed raining technique. The aluminum model footings with a constant area of 15 cm^2 and with ring radii ratios from 0 to 0.9 were tested under load eccentricity ratios from 0 to 0.375. Test results indicate that the bearing capacity is significantly affected by footing size, ring radii ratio and load eccentricity. It is found that The bearing capacity of circular footings increases linearly with footing diameter in a double-log scale diagram. The bearing capacity of a vertically loaded ring footing can be expressed in terms of a bearing capacity ratio (B_r), a reduction factor (R_e) and the bearing capacity of an axially loaded circular footing with the same area. Test results show that the value of B_r is related only to the ring radii ratio (n), independent of footing size; when n is from 0 to 0.35, B_r increases slightly with n. Further increase of n beyond 0.35 results in significant decrease of B_r. The value of R_e decreases with load eccentricity and is independent of ring radii ratio. The procedure presented for evaluating the bearing capacity of ring foundations is very practical.

Circular footings under axisymmetric conditions have been analyzed by the method of characteristics to further study the effect of footing size on bearing capacity. In the analysis, the soil friction angle can be variable or assumed to be constant. The bearing capacities calculated also increase linearly with footing diameter in a double-log scale diagram and are close to the centrifuge test results. The compatibility of bearing capacities obtained from both variable and constant friction angle analysis provides a basis for the FE analysis using an equivalent constant friction angle for each footing.

The FE technique has been applied to circular and ring footings on the dense sand under axial vertical loads. In the analysis, a footing is represented by a rigid body consisting of rigid surface elements. Interface elements are used to model the interaction between the footing and soil. The elasto-plastic behaviour of soil is simulated by the Drucker-Prager/Cap constitutive model. Compared with centrifuge test data, the analytical results regarding the effect of footing size and ring radii ratio on bearing capacity are satisfactory. When calibrated with experimental data, the FE technique is very useful for analysis of very large foundations or for cases when experimental data are not available or difficult to obtain.

Acknowledgments

I would like to express my sincere appreciation to those who have supported me in pursuing the degree of Doctor of Philosophy. Particularly, I would like to thank my supervisor, Dr. Jack Clark, for his academic guidance and financial support provided through the research program. His broad knowledge of geotechnical engineering has contributed greatly not only to my Ph.D. research program but also to my professional development.

As my co-supervisor, Dr. Ryan Phillips has provided me detailed guidance in every phase of the research program. His expertise in geotechnical engineering, especially in experimental modelling, has kept me on a relatively straight line towards my research goal. I also wish to thank Dr. Gary Sabin, a member of my supervisor committee, for his enthusiastic guidance of my research. His support of my Ph.D. program was invaluable.

I am very grateful for the help provided by the staff members of the C-CORE Centrifuge Centre, particularly Don Cameron, Shawn Hurley, Stephen Smyth and Karl Tuff, in the development of the test equipment and in conducting the centrifuge tests. Gratitude is also due Dr. Jim Sharp and Mrs. Moya Crocker who have helped me in a variety of ways in my graduate studies at Memorial University, as well as the staff members of the machine shop of the Faculty of Engineering for manufacturing a large number of parts of my experimental equipment.

For years I have also benefited greatly from discussions of theoretical and experimental geotechnical problems with my colleagues and friends, Mr. Michael Paulin, Dr. Paul Lach and Mrs. Ling Lin. Thanks are also due Dr. Keith Kosar, a former staff member of C-CORE, and Dr. Radu Popescu, who has been recently appointed as a senior research engineer of C-CORE, for their helpful advice regarding my research.

I wish to acknowledge the generous financial support I have received for my graduate studies, including the graduate support from C-CORE, the scholarship entitled Atlantic Accord Career Development Awards through the government of the Province of Newfoundland and Labrador, and a fellowship provided by C-CORE. I am also grateful for the employment opportunities provided by the Faculty of Engineering and Applied Science as a teaching assistant.

In particular, I have to thank my wife, Ying, for her patience and devotion. As my fellow student and more recently officemate, she has accompanied me during so many long days at school.

This thesis is presented in memory of my parents. They have had to overcome numerous difficulties, for almost half a century, in order to provide their children with the opportunity to obtain higher education. In their minds, nothing has been more important to me than becoming a doctor.

Contents

List of Figures

List of Tables

List of Symbols

a	Centrifuge acceleration
A	Area of footings
a_m	Centrifuge model acceleration
a_p	Prototype acceleration
B	Footing width; footing diameter
B_r	Bearing capacity ratio
CPT	Cone penetration test
c	Cohesion of soil
C_u	Uniformity coefficient
d	Inside diameter of ring footings;
D	Diameter of circular footings; Outside diameter of ring footings
d, K, β	Drucker-Prager model parameters
d_{pl}, K_{pl}, β_{pl}	Drucker-Prager model parameters from plain strain tests
d_{tr}, K_{tr}, β_{tr}	Drucker-Prager model parameters from triaxial tests
d'_{tr}, K'_{tr}, β'_{tr}	Modified Drucker-Prager model parameters
d_{10}	Effective grain size
d_{50}	Mean grain size
e	Soil void ratio; Load eccentricity
E	Young's modulus

FE	Finite element
g	Gravitational acceleration
G	Shear modulus of soil
G_s	Specific gravity
h_m	Centrifuge model height
I_D	Density index of sand
K	Bulk modulus
K_o	Coefficient of earth pressure at rest
L_m	Model dimension
L_p	Prototype dimension
LDT	Linear displacement transducer
M	Slope of critical state line in p-q plane; Moment of load
n	Ring radii ratio
N	Dimension scale
N_c, N_q, N_γ	Bearing capacity factors
OCR	Overconsolidation ratio
p	Mean effective stress
q	Deviator stress; Surcharge or overburden pressure
Q	Vertical load
q_c	Cone tip resistance
q_u	Bearing capacity

q_{uc}	Bearing capacity of axially loaded circular footings
q_{uo}	Bearing capacity of axially loaded ring footings
r	Centrifuge rotational radius; Horizontal coodinate of axisymmetry
r_e	Load eccentricity ratio
R_e	Reduction factor of bearing capacity
$\bar{r}$	Normalized horizontal coodinate of axisymmetry
s	Mean stress; Settlement
v	Specific volume
z	Vertical coodinate of axisymmetry
$\bar{z}$	Normalized vertical coodinate of axisymmetry
α	Wedge angle under footings
γ	Unit weight of soil
γ_m	Unit weight of model material
γ_p	Unit weight of prototype material
ε	Strain
ε^e	Elastic strain
ε^p	Plastic strain
ε_v	Volumetric strain
κ	Slope of loading-reloading line in v-lnp' plane
λ	Slope of normal compression line in v-lnp' plane

μ_f	Coefficient of skin friction
ν	Poisson's ratio
ρ	Material density
σ	Stress
$\bar{\sigma}$	Normalized stress
σ_1, σ_2, σ_3	Principal stresses
σ_h	Lateral (horizontal) stress
σ_m	Mean normal stress
σ_p	Stress in prototype
σ_r	Stress in r-direction
σ_v	Vertical stress
σ_z	Stress in z-direction
σ_θ	Circumferential stress
τ	Shear stress
τ_f	Shear stress at failure
τ_{rz}	Shear stress in r-z plane
v	Specific volume
ϕ	Friction angle
ϕ_{cs}	Critical state friction angle
ϕ_{eq}	Equivalent friction angle
ϕ_{max}	Maximum friction angle
ϕ_{tr}	Friction angle from triaxial test

ψ	Direction of principal stress (σ_I)
ω	Angular velocity

Chapter 1

Introduction

1.1 Background and Previous Research

Ring foundations are often used for large and tall structures to resist lateral loads and to increase the stability against overturning. They have been applied worldwide for various structures, including liquid storage tanks (Bhushan and Boniadi, 1988), tower structures (Clark, 1972; and Daspupta and Sengupta, 1989) and radar stations (Veletsos and Tang, 1987). Many important structures in the world have been built on ring foundations. In the construction of the Northumberland Strait Crossing between Prince Edward Island and mainland Canada, ring-shaped piers with outside diameter of 22 m and inside diameter of 14 m have been adopted (Kosar *et al.*, 1994). The Manifold gravity platform MCP-01 in the North Sea resting on dense sand has a ring foundation of 101 m in diameter (Lacasse and Olsen, 1988). In Kuwait City, a 370 m high telecommunication tower is founded on a 55 m diameter ring foundation resting on dense calcareous sand (Brenner *et al.*, 1990; Al-Sanad *et al.*, 1993). The Leaning Tower of Pisa also has a ring foundation of 19.58 m in outside diameter and 4.50 m in inside diameter (Mitchell *et al.*, 1977). In Canada, a large number of agricultural silos for storing crops have been built on ring foundations providing increased stability against failure (Bozozuk, 1974; Bozozuk, 1979a,b; Lo and Becker, 1979; Morin and

Table 1.1: Settlement influence factor $\omega(n)$ of Egorov (1965)

n	0	0.2	0.4	0.6	0.8	0.9	0.95
$\omega(n)$	1.0	1.0	1.02	1.04	1.14	1.20	1.30

Bozozuk, 1983; and Morin and Gervais, 1985).

Egorov (1965) presents a method for calculating the settlement and reaction pressure of a rigid ring footing resting on elastic foundation under an axially symmetrical load. The settlement, s, is expressed as

$$s = \frac{2P(1-\nu^2)}{ED}\omega(n) \tag{1.1}$$

in which P is the load applied, E is the elastic modulus, ν is the Poisson's ratio, D is the outside diameter of the ring, $\omega(n)$ is an influence factor related to the ring radii ratio, n, defined as the ratio of the inside diameter to the outside diameter of the ring. The variation of $\omega(n)$ is listed in Table 1.1. It is shown that the settlements of circular and ring foundations are in the same order when n is within 0 to 0.60. After Egorov (1965), the behaviour of ring foundations on elastic media has been analyzed in many ways. Using the finite element method, Milovic (1973, 1982), Bowles (1977) and Kathroli *et al.* (1982) have studied the behaviour of ring footings on elastic foundations. Other elastic analyses of ring foundations have also been carried out by Bowles (1975), and Tassoulas and Kausel (1984). In the analysis of a ring footing on a layer of finite thickness, Madhav (1980) derived the allowable bearing capacity by utilizing the ultimate bearing capacity of a circular footing and the elastic settlement of circular and ring footings. In another analysis, Madhav and Karmarkar (1982) introduced a very simple method with restricted conditions for estimating the elasto-plastic settlement of ring foundation on cohesive soil. It is shown that for the same contacting pressure, the settlement of ring footings is smaller than that of circular footings.

In situ loading tests of small scale ring plates on dense, cemented calcareous sands have been carried out by Al-Sanad *et al.* (1993) and Ismael (1996). Using a set of plates with the same outside diameter of 0.6 m and different ring radii ratios, defined by Equation (1.2), of 0, 0.25, 0.5 and 0.75, Ismael (1996) has found that under applied pressure the settlement of the plates decreases with increasing ring radii ratio, while the ultimate bearing capacity of ring plates is close to that of the solid circular plate.

In spite of the continued effort in the investigation of ring foundation behaviour, a rational method for evaluating the bearing capacity of ring foundations is not available. In the design of ring foundations, simplifications have to be made. For instance, in the stability analysis of the aforementioned North Sea platform (Lacasse and Olsen, 1988) using Brinch-Hansen's method of limiting equilibrium, the ring-shaped base was represented by 4 independent rectangular base elements; the external loads were distributed so that the 4 bases mobilize the same safety factor and the total 4 base system was in equilibrium with the external loads. A similar procedure has been followed in the stability analysis of the ring-shaped piers of the Northumberland Strait Crossing (Kosar *et al.*, 1994). Therefore, conducting research on the bearing capacity of ring foundations and developing a practical procedure for engineering design are of great importance.

1.2 Scope of This Study

For a ring footing resting on soil, as shown in Figure 1.1, the ring radii ratio, n, is defined as

$$n = \frac{d}{D} \tag{1.2}$$

where d is the inside diameter of the ring footing and D is the outside diameter. The

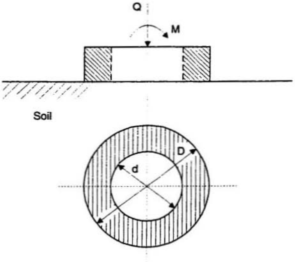

Figure 1.1: Geometry and load pattern of ring footing

area, A, can be expressed as

$$A = \frac{\pi}{4}(D^2 - d^2) = \frac{\pi}{4}D^2(1 - n^2) \tag{1.3}$$

When the vertical load Q and moment M applied to the ring footing are increased, the footing will eventually fail. The vertical load Q and moment M in Figure 1.1 can be replaced by an eccentric vertical load, P, which has the same magnitude as Q but locates from the center of the footing by a distance, e, calculated by

$$e = \frac{M}{Q} \tag{1.4}$$

where e is called load eccentricity. When e=0, the footing is under axial loading conditions otherwise it is under eccentric loading conditions.

The purpose of this study is to provide a practical procedure for evaluating the bearing capacity of ring footings on the surface of a dense sand subjected to vertical axial and eccentric loads. The behaviour of ring footings under various combinations of footing diameter D, ring radii ratio n, vertical load Q and moment M will be investigated by experiment and numerical analyses.

1.3 Methodology

The bearing capacity of foundations can be measured by laboratory experiment or field testing. In addition, various bearing capacity theories have been developed. In the past decades, the centrifuge test technique has been utilized to determine the bearing capacity of foundations. It is especially efficient to investigate the effect of foundation size. The limit equilibrium method assumes failure surfaces and seeks an approximate solution of failure loads; the method of characteristics is used for solving the equilibrium equations with the Coulomb yield criterion in the uncontained plastic zone under a footing; the upper-bound method derives the failure load by equating the external work done to the internal work dissipated in a kinematically admissible velocity field. These three numerical methods, assuming a rigid-perfect plasticity soil response, have been widely used in the development of classical bearing capacity theories. However, they can only be adopted in the cases of simple boundary and loading conditions. The finite element technique can model the elasto-plastic response of soil and can be applied to various boundary and loading conditions.

In this work, centrifuge tests of axially and eccentrically loaded ring footings on a dense sand are conducted to investigate the influence of footing size, ring shape and loading pattern on bearing capacity. The method of characteristics is employed for axially loaded circular footings to further study the footing size effect. The finite element approach is adopted for ring footings under axial loading conditions. A procedure for evaluating the bearing capacity of ring footings under vertical loads is developed.

Chapter 2

Fundamentals of Bearing Capacity: A Review

Foundations can be classified as shallow foundations (footings) and deep foundations. The design of a shallow foundation must take into consideration the requirements of tolerable deformation and safety against failure. The soil supporting the foundation should not undergo significant shear failure. During the performance of the foundation, the loading from superstructures should limit the corresponding displacement of the foundation to tolerable levels. The allowable bearing capacity of a foundation may be controlled by either the ultimate bearing capacity or the deformation.

This study deals primarily with the problem of ultimate bearing capacity; the term "bearing capacity" used herein refers to the ultimate bearing capacity. This chapter presents the theories and experimental observations of bearing capacity, most of which relate to strip footings under plane strain conditions. A good understanding of the behaviour of strip footings is essential to conducting this research on the bearing capacity of ring footings.

2.1 Failure Modes of Soil

A foundation subjected to an increased vertical loading tends to penetrate into the soil supporting it. When the loading is increased to such a value that the penetration is out of control or it exceeds an allowable value, the foundation is said to have failed. The behaviour of foundations indicates that the failure of foundations is usually due to insufficient shear strength of the soil. The three principal modes of such failure are general shear failure, local shear failure and punching shear failure (Vesic, 1973; and De Beer, 1987).

In the case of general shear failure, there usually exists a continuous slip failure surface from one edge of the footing to the ground surface. When the load applied to the foundation is increased to the failure load, the failure of the soil supporting the foundation is sudden and catastrophic under stress-controlled conditions. In strain-controlled conditions, a decrease of load with increasing settlement of the foundation can be observed after failure. The penetration of the foundation causes lateral and upward expulsion of soil and the soil adjacent to the foundation tends to heave. The ultimate bearing capacity (q_u) of this kind of failure is the maximum unit load applied.

In contrast to general shear failure, the punching shear failure is characterized by a failure pattern that is not distinct. The foundation penetrates due to the compression and shear distortion of the soil immediately beneath the foundation and the soil outside the immediate foundation is relatively less affected. The penetration increases as the loading is increased and there is no peak load.

Local shear failure is a transitional mode between general failure and punching failure. The failure pattern consists of a wedge and slip surfaces and is clearly defined only immediately beneath the foundation. There is a visible bulging of the soil adjacent to the foundation. The slip surfaces end in the soil mass; only under the condition of a substantial vertical settlement of the foundation may they appear at the ground surface. Using the load-settlement curve, the ultimate load can be determined at a point at which the slope of the curve first reaches a steady, minimum value (Vesic, 1973).

The failure mode of a foundation depends upon a number of factors, particularly upon the soil compressibility, stress state, foundation geometry and loading conditions. A strip footing on the surface of a very dense sand or stiff clay will fail in general shear. In contrast, this footing on the surface of a loose sand will fail in punching shear. However, soil compressibility alone can not determine the failure mode. For instance, the footing mentioned above on a dense sand may fail in punching shear if it is placed at a great depth (Vesic, 1963) or if it is subjected to a transient or dynamic load (Selig and McKee, 1961; and Vesic *et. al*, 1965). A footing resting on a saturated normally consolidated clay may fail in general shear if the loading is so rapid that no drainage of the clay can occur, while it will fail in punching shear if it is loaded so slow that the clay is sheared under drained condition. The failure mode depends also upon the shape and dimension of foundations. By increasing the dimension of a footing, the failure mode tends to move from general shear failure to punching shear failure (De Beer, 1987). Figure 2.1 presents the failure mode of foundations on sand, which is influenced by sand density, foundation dimension and depth.

There are no reliable numerical criteria for predicting the failure mode of soil supporting foundations. Vesic (1965, 1973) has proposed a rigidity index, I_r, for evaluating the relative compressibility of soil, expressed as

$$I_r = \frac{G}{c + q\tan\phi} \tag{2.1}$$

where G is the shear modulus of soil, c is the cohesion, q is the overburden pressure and ϕ is the friction angle. This rigidity index is associated with the assumption that the soil is of elastic-ideal plasticity. To take into consideration the average volumetric strain in the plastic zone (Δ), it is suggested (Vesic, 1973) that I_r is replaced by a

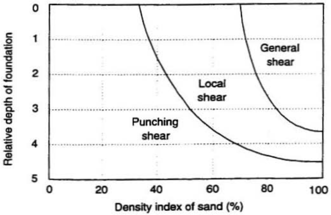

Figure 2.1: Effect of relative depth of foundation (D_f/B^*) and density of sand on failure mode (after Vesic, 1973: $B^* = B$ for square or circular footings; $B^* = 2BL/(B+L)$ for rectangular footings)

reduced rigidity index, I_{rr}, defined as

$$I_{rr} = \frac{I_r}{1 + I_r\Delta} \tag{2.2}$$

It is related to the stress level in the soil and the character of loading. A high value of I_{rr} (e.g. over 250) implies that the soil is relatively incompressible while when I_{rr} is small than 10, the compressibility of the soil is high. In practice it is inconvenient to use I_{rr} to evaluate the failure mode of soil, because it is difficult to estimate the value of the average volumetric strain Δ in the plastic zone.

2.2 Basic Methods for Bearing Capacity

Stability problems of soil mechanics deal with the conditions of ultimate failure of a soil mass, such as bearing capacity of foundations, stability of slopes and earth pressure on retaining walls. These problems are often solved by applying the theory of perfect plasticity. The main methods using rigid-perfect plasticity for bearing capacity problems are the method of characteristics, limit equilibrium method and limit analysis method. In the cases of elasto-plastic responses and under some loading conditions, the finite element method is usually applied.

2.2.1 Limit analysis method

A valid complete solution in mechanics of a soil mass requires three conditions: stress equilibrium equations, stress-strain relationships and compatibility equations of strains and displacements. To simplify the procedure of analysis, limit analysis method has been developed to bound the collapse load without carrying out full elasto-plastic analysis. The soil stress-strain relationship is idealized with rigid-perfect plasticity. Using this method, the lower and upper bounds of the collapse load may be obtained.

Upper-bound method:

An assumed velocity field (deformation mode) of a soil mass which satisfies: (1) the velocity boundary conditions; and (2) the strain and velocity compatibility conditions, is termed a kinematically admissible velocity field. The loads, determined by equating the external rate of work to the internal work rate of dissipation in a kinematically admissible velocity field, are not less than the actual collapse load. This upper-bound theorem states that if a kinematically admissible velocity field can be found, the uncontained plastic flow must impend or have taken place previously. Using the upper-bound technique, the stress distribution need not be in equilibrium.

Chen (1975) presents upper-bound solutions of a strip footing on a general c-ϕ-γ soil using the Prandtl mechanism and the Hill mechanism. In the Prandtl mechanism there is only one rigid wedge-shaped zone immediately under the footing while the Hill mechanism has two symmetrical rigid wedge-shaped zones. The Prandtl mechanism assumes that no sliding occurs between the footing and the soil; it does not take into account the effect of the footing base roughness. Solutions by the Prandtl mechanism are rigorous upper bounds for perfectly rough to perfectly smooth footings. For footings with small base friction, a better upper bound can be obtained using the Hill mechanism which permits sliding between footing base and soil and takes into account the energy dissipation due to the sliding. The analysis indicates that when both the soil internal friction angle (ϕ) and the friction angle between soil and footing base (δ) are greater than 15° , the Prandtl mechanism yields better (smaller) upper bound solutions; at smaller δ values, the Hill mechanism is better. When ϕ is no more than 15°, the Hill mechanism may control both smooth and rough footings. For a surface footing on a weightless soil, the Prandtl mechanism and the Hill mechanism ($\delta = 0$) yield the same bearing capacity factor N_c. The bearing capacity factor N_c due to soil cohesion and the factor N_q due to surcharge derived by Chen (1975) are identical to those obtained by Prandtl (1921) and Reissner (1924) respectively when the footing base is assumed to be perfectly rough. For a surface footing on cohesionless soil, the bearing capacity factor N_γ by Hill mechanism (smooth base) is only about one half of that by Prandtl mechanism, which is in accordance with the experimental results of Meyerhof (1955).

Lower-bound method:

The assumed stress distribution of a soil mass which satisfies: (1) the equilibrium equation; (2) the stress boundary conditions; and (3) nowhere violates the yield criterion, is termed a statically admissible stress field. The loads determined from such a stress field are not greater than the actual collapse load. This lower-bound theorem states that if a statically admissible stress field can be found, the uncontained plastic flow will not occur at a lower load. The lower-bound technique only gives consideration to equilibrium and yield. It does not consider the soil kinematics. Although Chen (1975) presents some lower-bound solutions of bearing capacity problems, the use of the lower-bound technique for bearing capacity evaluation in engineering practice is limited.

2.2.2 Limit equilibrium method

Terzaghi (1943). Taylor (1948) and Meyerhof (1951) present many examples of limit equilibrium method for obtaining the solutions of stability problems. This method is an approximate approach and generally assumes failure surfaces of various simple shapes: plane, circular or logspiral. With the assumption of failure surface, the approximate solution of a stability problem can be obtained by finding the most critical position of the failure surface and by finding an overall equilibrium of stress resultants of the soil mass inside the failure surface.

Using this method, the overall force equilibrium conditions are satisfied across the failure surface. It is not required that the stress distributions inside and outside the failure surface are in equilibrium or satisfy the yield condition. Meanwhile, although this technique assumes failure surface and seeks a least answer, it does not necessarily satisfy all the requirements of the upper-bound theorem. Therefore, the solution obtained using the limit equilibrium method is not necessarily a lower bound or an upper bound.

2.2.3 Method of characteristics

In the study of soil plasticity, the method of characteristics (slip-line method) is introduced to obtain a set of differential equations of plastic equilibrium and transform them to curvilinear coordinates (Sokolovskii, 1960; and Chen, 1975). At the instant of impending uncontained plastic flow, equilibrium, yield condition (normally Coulomb criterion) and stress boundary conditions are satisfied and a set of differential equations of plastic equilibrium can be established to investigate the stresses in the soil. For convenience, this set of equations is transformed to curvilinear coordinates whose directions at every point in the plastic zones coincide with the directions of slip plane. Using this method, many researchers obtained closed form solutions of some bearing capacity problems of footings on weightless soils, when at least one family of the slip-lines are straight (Chen, 1975). To take into account the soil weight, Sokolovskii (1965) adopted a finite difference approximation of the slip-line equations and solved a number of bearing capacity problems.

In the method of characteristics, the stress-strain relationship of rigid-perfect plasticity is assumed. The equilibrium, yield criterion and stress boundary conditions are satisfied only in the plastic zones. The stress field in the plastic zones determined from slip-line equations is termed partial stress field. The stress distribution outside this partial stress field region is not defined. The bearing capacity of a footing obtained from the method of characteristics is not necessarily a lower-bound or an upper-bound solution.

2.2.4 Finite element method

The aforementioned methods for bearing capacity can only be used in the cases of rigid-perfect plasticity under some simple boundary and loading conditions. To take into account the elasto-plastic response of soils and to solve bearing capacity problems of general boundary conditions and loading patterns, the finite element method has been employed (Chen, 1975; Christian, 1977; Griffith, 1982; and Britto and Gunn, 1987). The most important aspect in using finite element method to solve bearing capacity problems is to choose a rational constitutive model of soil.

2.3 Terzaghi's Bearing Capacity Theory

Terzaghi (1943) defined a shallow strip footing as one whose width, B, is equal to or greater than the embedment depth, D_f. With this condition, the shear resistance

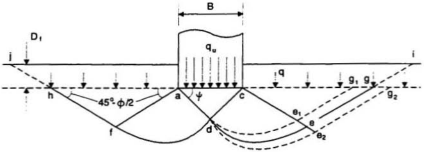

Figure 2.2: Bearing capacity failure in soil under a rigid strip footing

of the overburden soil located above the level of the footing base can be neglected and the overburden soil is replaced by an equivalent surcharge equal to

$$q = \gamma D_f \tag{2.3}$$

where γ is the unit weight of the soil. The error of this assumption is on the safe side.

The failure pattern of this footing is shown in Figure 2.2. The failure zone under the footing can be divided into three parts: (1) a wedge-shaped zone *acd* beneath the footing; (2) two radial shear zones *adf* and *cde*; and (3) two passive Rankine zones afh and *ceg*. Terzaghi (1943) indicates that the angle ψ of the wedge *adc* in Figure 2 depends on the roughness of the footing base; for a perfectly smooth base which eliminates completely the friction and adhesion between the base and the soil, the value of ψ is equal to $45° + \phi/2$; for a rough base, ψ can be assumed equal to the angle of internal friction of the soil, ϕ.

Assuming ψ=ϕ and the soil is perfectly rigid-plastic (general shear failure), the bearing capacity can be estimated using plasticity theory. The problem is solved in two steps: (1) assuming the soil is weightless to derive the bearing capacity due to soil cohesion (c) and surcharge (q); and (2) assuming the footing is resting on the surface of a cohesionless soil (c=0, q=0) to derive the bearing capacity due to the weight of the soil. The total bearing capacity is supposed to be the sum of the two cases.

For a weightless soil (γ=0), failure of the soil occurs along the surface of de_2g_2 in Figure 2.2. The curve de_2 is a logarithmic spiral whose center is at point c, expressed as

$$r = r_o e^{\theta \tan \phi} \tag{2.4}$$

where r_o represents the length of cd. The shape of the curve de_2 is related only to the value of ϕ. For ϕ=0, it becomes an arc of a circle. Using limit equilibrium method, the bearing capacity due to c and q is expressed as

$$q_{cq} = cN_c + qN_q \tag{2.5}$$

where

$$N_c = (N_q - 1)\cot\phi \tag{2.6}$$

$$N_q = \frac{e^{2(3\pi/4-\phi/2)\tan\phi}}{2\cos^2(\pi/4+\phi/2)} \tag{2.7}$$

When c=0, q=0 and γ is greater than zero, the failure surface is approximately along de_1g_1. The bearing capacity due to the soil weight is determined by

$$q_\gamma = \frac{1}{2}\gamma B N_\gamma \tag{2.8}$$

in which

$$N_\gamma = \frac{1}{2}\tan\phi(\frac{K_{P\gamma}}{\cos^2\phi} - 1) \tag{2.9}$$

where $K_{P\gamma}$ is the coefficient of passive earth pressure.

When the values of c, q and γ are greater than zero, the failure surface is along deg. The ultimate bearing capacity, q_u, due to c, q and γ is supposed to be the sum of q_{cq} and q_γ, expressed as

$$q_u = cN_c + qN_q + \frac{1}{2}\gamma B N_\gamma \tag{2.10}$$

where the bearing capacity factors N_c, N_q and N_γ are determined using Equations (2.6), (2.7) and (2.9) respectively. It can be seen that q_u increases with footing width B.

There exists an obvious error associated with Equation (2.10). As shown in Figure 2.2, the ultimate bearing capacity q_u due to c, q and γ corresponds to the failure surface deg while the bearing capacities q_{cq} due to c and q and q_γ due to γ correspond to de_2g_2 and de_1g_1 respectively. Terzaghi (1943) realized that the bearing capacity associated with the failure surface deg is greater than that determined by Equation (2.10). However, the difference is less than 10 per cent and the error is on the safe side.

Equation (2.10) can be modified for the estimation of bearing capacity of circular and square footings. Based on experimental data it is assumed that for square footing

$$q_u = 1.3cN_c + qN_q + 0.4\gamma BN_\gamma \tag{2.11}$$

and for circular footing

$$q_u = 1.3cN_c + qN_q + 0.3\gamma DN_\gamma \tag{2.12}$$

where B is the width of the square footing, D represents the diameter of the circular footing.

2.4 Development of Bearing Capacity Theories

In the past 50 years, the well known expression

$$q_u = cN_c + qN_q + \frac{1}{2}\gamma BN_\gamma \tag{2.13}$$

termed as Terzaghi's equation has been widely accepted as a basic formula for the estimation of bearing capacity. It has been demonstrated that the bearing capacity derived by superposition is conservative and the error is not more than 20% (Hansen, 1970; and Bolton and Lau, 1993). For cohesionless soils, Lundgren and Mortensen (1953) have proposed that the actual bearing capacity should be

$$q_u = \mu(\gamma D_f N_q + \frac{1}{2}\gamma B N_\gamma) \tag{2.14}$$

where $\mu \geq 1$ is a superposition factor related to footing depth. For surface ($D_f=0$) and very deep footings, $\mu=1$. Hansen and Christensen (1969) and Tan (1990) show that the maximum value of μ of up to 1.2 occurs when $B/(B+D_f)$ is approximately between 0.6 and 0.8.

Experimental data (Vesic, 1973) indicate that the value of ψ in Figure 2.2 is approximately equal to $45°+\phi/2$ rather than equal to ϕ as suggested by Terzaghi (1943). With the assumption of $\psi=45°+\phi/2$, Vesic (1973) recommends to use the bearing capacity factors

$$N_c = (N_q - 1)\cot\phi \tag{2.15}$$

$$N_q = e^{\pi \tan\phi}\tan^2(45° + \frac{\phi}{2}) \tag{2.16}$$

$$N_\gamma = 2(N_q + 1)\tan\phi \tag{2.17}$$

where N_c and N_q are the rigorous solutions for weightless soil by Prandtl (1921) and Reissner(1924) respectively, while N_γ is the numerical estimation by Caquot and Kerisel (1953) with an error on the safe side (less than 10%).

In the literature there are a variety of proposed solutions to the problem shown in Figure 2.2. Many researchers agree that the values of N_c and N_q can be represented by Equations (2.15) and (2.16) respectively (Meyerhof, 1963; Vesic, 1973; De Beer, 1987; and Das, 1990). The variations in the N_γ-values are, however, substantial. A closed analytical solution of N_γ has not yet been found. The values of N_γ by Meyerhof (1963) and Hansen (1970) are derived respectively from

$$N_\gamma = (N_q - 1)\tan(1.4\phi) \tag{2.18}$$

$$N_\gamma = 1.5(N_q - 1)\tan\phi \tag{2.19}$$

where N_q is defined by Equation (2.16). It should be mentioned herein that the Prandtl-Reissner and Caquot-Kerisel factors given by Equations (2.15), (2.16) and (2.17) are considered to be most reliable (Vesic, 1973). The variations of some important bearing capacity factors with soil friction angle (ϕ) are listed in Table 2.1.

It is very important to correctly assess the ϕ value of soils. There exist difficulties in selecting a representative value of ϕ for the computation of the ultimate bearing capacity. Soils supporting strip footings are essentially in plane strain conditions. The ϕ value is, however, usually determined by triaxial tests. Bishop (1961, 1966) found that the ϕ value of a sand in plane strain tests is approximately 10% greater than that found in triaxial compression tests. Although the bearing capacity factor N_γ of Terzaghi (1943) is considered to be conservative when ϕ is determined by triaxial testing, it becomes non-conservative when ϕ is determined by plain strain testing (Chen, 1975). Meyerhof (1963) and Hansen (1970) suggest that a ϕ value which is 10% greater than that obtained from triaxial tests should be used for the bearing capacity of strip footings. For a rectangular footing with width of B and length of L, Meyerhof (1963) suggests using

$$\phi = (1.1 - 0.1\frac{B}{L})\phi_{tr} \tag{2.20}$$

where ϕ_{tr} is the angle of internal friction found in triaxial testing.

Another argument is that in reality the shear failure of the footing in Figure 2.2 is the phenomenon of progressive rupture (Muhs, 1965; and Chen, 1975). The slip line *adeg* begins at point a and develops gradually to point g. Therefore when shear failure occurs the soil at g is just mobilized to its peak strength while the strength of the soil at a may be as low as the strength at critical state. In addition, the stress levels at different locations of the failure surface are different. To take into account the curvature of Mohr's envelope, it is suggested that the value of ϕ corresponding to the

Table 2.1: Bearing capacity factors

ϕ (degree)	N_c Prandtl (1921) Eq.(2.15)	N_q Reissner (1924) Eq.(2.16)	N_γ Caquot *et al.* (1953) Eq.(2.17)	N_γ Meyerhof (1963) Eq.(2.18)	N_γ Hansen (1970) Eq.(2.19)
0	5.14	1.00	0.00	0.00	0.00
2	5.63	1.20	0.15	0.01	0.01
4	6.19	1.43	0.34	0.04	0.05
6	6.81	1.72	0.57	0.11	0.11
8	7.53	2.06	0.86	0.21	0.22
10	8.35	2.47	1.22	0.37	0.39
12	9.28	2.97	1.69	0.60	0.63
14	10.37	3.59	2.29	0.92	0.97
16	11.63	4.34	3.06	1.37	1.43
18	13.10	5.26	4.07	2.00	2.08
20	14.83	6.40	5.39	2.87	2.95
21	15.82	7.07	6.20	3.42	3.50
22	16.88	7.82	7.13	4.07	4.13
23	18.05	8.66	8.20	4.82	4.88
24	19.32	9.60	9.44	5.72	5.75
25	20.72	10.66	10.88	6.77	6.76
26	22.25	11.85	12.54	8.00	7.94
27	23.94	13.20	14.47	9.46	9.32
28	25.80	14.72	16.72	11.19	10.94
29	27.86	16.44	19.34	13.24	12.84
30	30.14	18.40	22.40	15.67	15.07
31	32.67	20.63	25.99	18.56	17.69
32	35.49	23.18	30.21	22.03	20.79
33	38.64	26.09	35.19	26.17	24.44
34	42.16	29.44	41.06	31.15	28.77
35	46.12	33.30	48.03	37.15	33.92
36	50.59	37.75	56.31	44.43	40.05
37	55.63	42.92	66.19	53.27	47.38
38	61.35	48.93	78.02	64.07	56.17
39	67.87	55.96	92.25	77.33	66.76
40	75.31	64.20	109.4	93.69	79.54
42	93.71	85.37	155.5	139.3	114.0
44	118.4	115.3	224.6	211.4	165.6
45	133.9	134.9	271.7	262.7	200.8
46	152.1	158.5	330.3	328.7	244.6
48	199.3	222.3	496.0	526.5	368.7
50	266.9	319.1	762.9	873.9	568.6

mean value of normal stress (σ_m) along the failure surface should be used. Meyerhof (1950) suggests that

$$\sigma_m = \frac{q_u}{10} \tag{2.21}$$

while the value of σ_m proposed by De Beer (1965a) is

$$\sigma_m = \frac{q_u + 3q}{4}(1 - \sin\phi) \tag{2.22}$$

in which q represents the overburden pressure.

Equation (2.13) is for the evaluation of ultimate bearing capacity of strip footings under vertical loading, ignoring the shear resistance of overburden soil. To take into account the influences of the loading inclination, the shear strength of overburden soil and the footing shape, Meyerhof (1963) and Hansen (1970) introduce a general bearing capacity equation expressed as

$$q_u = cN_c s_c d_c i_c + qN_q s_q d_q i_q + \frac{1}{2}\gamma B N_\gamma s_\gamma d_\gamma i_\gamma \tag{2.23}$$

where s_c, s_q, s_γ are shape factors; d_c, d_q, d_γ are depth factors; and i_c, i_q, i_γ are load inclination factors. The bearing capacity factors N_c and N_q are determined by Equations (15) and (16) respectively while N_γ may be the solution of Caquot and Kerisel of Equation (17) or it may be the solutions of other researchers as described above.

The shape factors of rectangular foundations have been found by Meyerhof (1963) and De Beer (1970). Meyerhof's shape factors are given by

$$s_c = 1 + \frac{B}{L}\frac{N_q}{N_c} \tag{2.24}$$

$$s_q = s_c \tag{2.25}$$

$$s_\gamma = 1 - 0.4\frac{B}{L} \tag{2.26}$$

where L represents the length of rectangular foundations.

The depth factors have been proposed by Meyerhof (1963) and Hansen (1970). For shallow foundations, Hansen's depth factors are

$$d_c = 1 + 0.4\frac{D_f}{B} \tag{2.27}$$

$$d_q = 1 + 2\tan\phi(1 - \sin\phi)^2\frac{D_f}{B} \tag{2.28}$$

$$d_\gamma = 1 \tag{2.29}$$

The load inclination factors have been derived by Hansen (1970), Meyerhof (1963), and Hanna and Meyerhof (1981). The factors proposed by Meyerhof (1963) are expressed by

$$i_c = \left(1 - \frac{\beta}{90^\circ}\right)^2 \tag{2.30}$$

$$i_q = i_c \tag{2.31}$$

$$i_\gamma = \left(1 - \frac{\beta}{\phi}\right)^2 \tag{2.32}$$

where β is the inclination angle of load with respect to the vertical.

For a vertically loaded strip or circular footing resting on the surface of cohesionless soils, the bearing capacity is expressed as

$$q_u = \frac{1}{2}\gamma B N_\gamma s_\gamma \tag{2.33}$$

where B represents the width of a strip footing or the diameter of a circular footing, and s_γ is a shape factor. For a strip footing, s_γ=1. Terzaghi (1943) and Vesic (1973, 1975) proposed that s_γ=0.6 for circular footings. Using the method of characteristics, Tan (1990) obtained s_γ=0.63 when ϕ=30° is used for the circular footing and ϕ=33° (10% increase) for the strip footing. When ϕ=30° is used for both footings, s_γ=1.04. It is stressed that s_γ is not constant with ϕ.

2.5 Factors Affecting Bearing Capacity

2.5.1 Soil compressibility and footing scale

The aforementioned analyses of bearing capacity of foundations assume that soils are of rigid-perfect plasticity and general failure occurs. This assumption can only be most reasonably applied to dense sands or stiff clays. There is no rational method for computing the bearing capacity in the two other failure modes. To utilize the bearing capacity equation and factors in general shear failure for the evaluation of bearing capacity in local shear and punching shear modes, Terzaghi (1943) proposes to use reduced strength parameters ϕ^* and c^* defined by

$$\phi^* = \tan^{-1}(\frac{2}{3}\tan\phi) \tag{2.34}$$

$$c^* = \frac{2}{3}c \tag{2.35}$$

instead of ϕ and c. Although this approach is not always on the safe side (Vesic and Johnson, 1963), the reduction of ϕ of sand in the case of local or punch shear failure may be too conservative (Vesic, 1973). In addition, it leads to a jump in bearing capacity on transition from local failure to general failure.

Based on test results of small footings on sands, Vesic (1973) suggests that for the evaluation of bearing capacity of sand in local and punching shear failures, the value of ϕ^* should be expressed as

$$\phi^* = \tan^{-1}(I_c\tan\phi) \tag{2.36}$$

in which

$$I_c = 0.67 + I_D - 0.75I_D^2 \tag{2.37}$$

where I_D is density index in the range $0 \leq I_D \leq 0.67$.

Studies of De Beer (1965a) and Vesic (1965) indicate that the average shear strength mobilization along the failure surface of soil supporting a shallow foundation decreases with footing size. The decrease of the mobilized strength is due to the curvature of Mohr's strength envelope (Meyerhof, 1950; and De Beer, 1965a) and the progressive rupture along the failure surface (De Beer, 1965b; and Muhs, 1965). The relative compressibility of soils increases with footing size. Vesic (1969) shows that the values of N_γ of large footings may be much lower than those conventionally assumed and postulates that the bearing capacity of large surface footings could not be greater than that of deep footings on the same soil. This postulate suggests that very large footings should fail exclusively in punching shear mode.

2.5.2 Roughness of footing base

The failure pattern of soil supporting foundations relates to the roughness of the bases of the foundations (Terzaghi, 1943; and Meyerhof, 1955). It has been argued that the Prandtl mechanism requires perfectly rough foundation base; for smooth foundations, the Hill mechanism should be used. According to theoretical analyses and small scale footing tests, Meyerhof (1955) concludes that the bearing capacity of a perfectly smooth foundation on the surface of a sand is only one half of that of a rough foundation. Vesic (1973) indicates, however, that it is impossible to reproduce experimentally a two-wedge failure pattern suggested by Meyerhof (1955); the two-wedge pattern is fictitious and should not be used in bearing capacity evaluation. In reality there is no perfectly smooth footing used in any test. Upper-bound analysis of Chen (1975) shows that for a strip footing resting on a cohesionless soil with an internal friction angle (ϕ) greater than 18°, when the friction angle between the footing base and soil (δ) is greater than 15°, the bearing capacity obtained using the Prandtl mechanism is smaller (more reasonable) than that using the Hill mechanism. In engineering practice foundation bases are usually rough (Meyerhof, 1955). For vertically loaded foundations, the base roughness has little influence on the bearing capacity (Vesic, 1973).

2.5.3 Rate of loading

The preceding analysis of bearing capacity assumes that foundations are loaded so slowly that no viscous or inertia effects occur. Under these conditions, the bearing capacity may be affected by the rate of loading only due to the rate of drainage of excess pore pressure. However, the bearing capacity of foundations subjected to high-rate loading may be affected by the viscous, drainage and inertia effects induced in the soil supporting the foundations. Under impact loads, a foundation on both dense sand and stiff clay will fail in punching shear mode (Vesic *et. al*, 1965); the effect of soil inertia is similar to that of overburden pressure. Vesic (1973) indicates that foundations on stiff clay show an increase of bearing capacity with the rate of loading from static to impact loading conditions, while the bearing capacity of foundations on dense sand decreases first with loading rate to a minimum value and then increases with loading rate. The data of De Beer (1987) shows that for a footing with a width of 100 mm resting on a dense sand, the bearing capacity reaches the lowest value and does not change much when the loading rate is 0.01 to 1 mm per second.

2.6 Bearing Capacity in Practice

The aforementioned theories employ soil strength parameters for evaluating the bearing capacity by using the Equation (2.13) or a more general formula as given by Equation (2.23). In addition to the selection of soil strength parameters, the difference in the estimated bearing capacity usually results from the method for calculating N_γ, because it is widely recognized that the bearing capacity factors N_c and N_q should be calculated using Equation (2.15) and (2.16). Canadian Geotechnical Society (1992) has proposed using the bearing capacity factor N_γ of Hansen (1970) as expressed by Equation (2.19). In this case, a factor of safety of 3 should be selected for determining the allowable bearing capacity.

In practice, the bearing capacity of in situ soils is often derived from the results of field tests. The methods recommended by the Canadian Geotechnical Society (1992) for the evaluation of bearing capacity from the data of standard penetration tests (SPT), static cone penetration tests (CPT), pressuremeter tests and vane shear tests are described as follows.

The bearing capacity of a footing on sand can be estimated by means of the SPT blow count, N, defined as the required number of blows of a 63.5 kg weight having a free fall of 760 mm for driving a standardized split sampler 51 mm in diameter a distance of 300 mm into soil, after an initial penetration of 150 mm. Meyerhof (1956) has proposed the formulas for the allowable bearing capacity, q_a, of shallow strip footings as

$$q_a = 12NK_d, \quad B < 1.2m \tag{2.38}$$

$$q_a = 8NK_d\left(\frac{0.3+B}{B}\right)^2, \quad B \geq 1.2m \tag{2.39}$$

where q_a is in kPa, B is footing width in meter and K_d is a depth coefficient given by

$$K_d = 1 + \frac{D_f}{3B} \tag{2.40}$$

in which D_f is the embedment depth. It should be cautious against using SPT blow count for bearing capacity evaluation, because the SPT results are subject to many errors. The correlation between the SPT blow count and soil friction angle is very poor. It is considered that the SPT data are not suitable for the bearing capacity of cohesive soils.

In simple cases, the allowable bearing capacity of commonly used shallow footings with an embedment depth of about 1 m can be roughly estimated from cone penetration test (CPT) results using

$$q_a = 0.1q_c \tag{2.41}$$

where q_c is the cone tip resistance. Meyerhof (1956) presents a more detailed procedure for the bearing capacity from CPT data by considering the influence of footing width and depth. The allowable bearing capacity is about 1 to 10% of the cone tip resistance. Generally, CPT data are considered more reliable than SPT results. However, it is difficult to use CPT results for evaluating the bearing capacity of dense or mixed soil deposits.

The bearing capacity of foundations on clays is controlled by short-term stability conditions. The bearing capacity of rectangular foundations can be determined using vane shear results by

$$q_u = 5\mu\tau_u(1 + 0.2\frac{D_f}{B})(1 + 0.2\frac{B}{L}) + q \tag{2.42}$$

where B is the width of foundations, L is the length, q is the overburden pressure at the foundation level, τ_u is the undrained shear strength measured from in situ vane shear tests, and μ is a strength reduction factor. The value of μ given by Bjerrum (1973) is related to soil plasticity index (I_P). For I_P=20, μ is approximately 1.0; for I_P=80, μ is reduced to about 0.65.

The results of the Menard pressuremeter tests (Menard, 1965) can be used to estimate the bearing capacity of shallow foundations on soils. The bearing capacity is expressed as

$$q_u = K_g(p_l - p_o) + q \tag{2.43}$$

where p_l is the pressuremeter limit pressure at which the volume tends to increase rapidly with pressure , p_o is the total horizontal pressure at the foundation level, K_g is a capacity coefficient and q is the overburden pressure at foundation level. To obtain the allowable bearing capacity, a factor of safety of at least 3 should be applied to the term $K_g(p_l - p_o)$ called the net limit pressure. The capacity factor K_g is related to the width, length and depth of foundations and the type of soil. For shallow strip footings,

K_g ranges from 0.8 to about 1.5, increasing with soil strength and the value of a depth factor D_f/B.

Chapter 3

Soil Properties and Behaviour

This work presents a research on the bearing capacity of ring foundations on a dense sand. The behaviour and properties of the sand described in this chapter are used in the centrifuge modelling and numerical analysis of the ring footings in subsequent chapters. Triaxial compression, oedometer compression, direct shear, and other conventional laboratory tests are conducted to determine the soil parameters regarding the physical properties, friction angles, plasticity and elasticity, in situ stress conditions, and friction against an aluminum surface. Because the sand used in various tests and numerical analysis in this study is dry (drained conditions), all stress parameters used in this thesis refer to effective stresses.

3.1 Physical Properties

The soil used in this study was a clean silica sand named glass sand purchased from Shaw Resources in Nova Scotia. Conventional laboratory tests were conducted to determine the physical properties. The sand with little fines had a specific gravity of 2.66, a maximum void ratio of 1.06, a minimum void ratio of 0.65, a mean grain size of 0.22 mm, an effective grain size of 0.14 mm and a uniformity coefficient of 1.69. The main physical properties of the sand are summarized in Table 3.1 and the grain size distribution is shown in Figure 3.1.

With a mean grain size of 0.22 mm and a uniformity coefficient of 1.69. the soil is considered as a uniformly-graded medium sand.

Table 3.1: Soil physical properties

Parameter name:	Unit	Parameter value
Specific gravity, G_s:	1	2.66
Maximum dry unit weight, γ_{dmax}:	kN/m^3	15.8
Minimum dry unit weight, γ_{dmin}:	kN/m^3	12.7
Maximum void ratio, e_{max}:	1	1.06
Minimum void ratio, e_{min}:	1	0.65
Mean grain size, d_{50}:	mm	0.22
Effective grain size, d_{10}:	mm	0.14
Uniformity coefficient, C_u:	1	1.69

3.2 In situ Stress and Elasticity

3.2.1 In situ stresses

In a soil, which has not experienced lateral (horizontal) strain, the ratio of lateral stress, σ_h, to vertical stress, σ_v, is defined as the coefficient of earth pressure at rest, K_o, expressed as

$$K_o = \frac{\sigma_h}{\sigma_v} \tag{3.1}$$

K_o is related to soil physical properties (Andrawes and El-Sohby, 1973) and stress history (Brooker and Ireland, 1965; and Mayne and Kulhawy, 1982). Laboratory

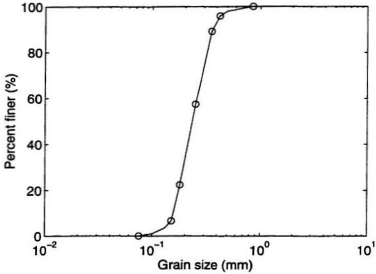

Figure 3.1: Grain size distribution of sand

investigations indicate that K_o of soils remains constant during loading and increases during unloading with increasing overconsolidation ratio (OCR). A widely accepted empirical relationship between K_o and the internal friction angle of soil proposed by Mayne and Kulhawy (1982) is

$$K_o = (1 - \sin\phi)(OCR)^{\sin\phi} \tag{3.2}$$

where ϕ is the peak friction angle. A difficulty in using this equation is how to properly select the peak friction angle (ϕ), because it decreases with stress level.

The in situ lateral stress of soil can be measured in the laboratory using triaxial cells or modified oedometer rings (Ofer, 1981). In this study an oedometer ring (Zhu *et al.*, 1995) was used. The oedometer ring had an inside diameter of 61.3 mm, an outside diameter of 94.0 mm and a height of 70.0 mm. The thickness of the thin wall was 1.5 mm. Strain gauges were cemented on the thin wall to measure the hoop strain

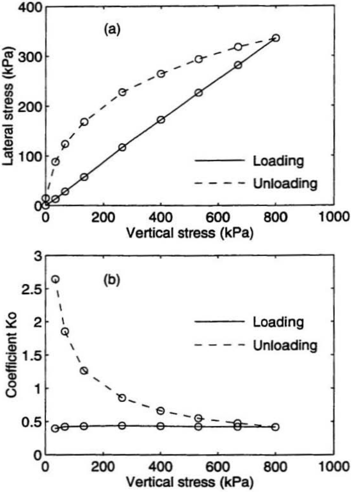

Figure 3.2: At rest lateral stress and K_o versus vertical stress

of the ring caused by the lateral stress in the sand. Dry sand samples in the oedometer were prepared using a raining technique resulting in a density index (I_D) of 90% (see chapter 4 for details).

The measured in situ lateral stress of the sand during loading and unloading are shown in Figure 3.2(a). The relationship between the vertical stress and the lateral stress is approximately linear during loading and the K_o in Figure 3.2(b) remains a constant value of 0.42. During unloading, the value of K_o increases with decreasing vertical stress. The value of K_o is about 2.7 when the vertical stress is reduced from 800 to 33 kPa. The K_o value of 0.42 during loading will be used to determine the initial stress conditions of soil for finite element analysis of ring foundations described in chapter 6.

3.2.2 Soil elastic moduli

The elastic moduli of soil can be described by Poisson's ratio (ν) and Young's modulus (E) or bulk modulus (K). Their relationship is in the form of

$$E = 3(1 - 2\nu)K \tag{3.3}$$

Under K_o conditions, the value of Poisson's ratio during initial loading can be derived using (Britto and Gunn, 1987)

$$\nu = \frac{K_o}{1 + K_o} \tag{3.4}$$

The measured K_o value of 0.42 results in ν=0.30 for the dense sand.

For the sand under K_o conditions, both the vertical stress, σ_v, and the lateral stress, σ_h, are principal stresses. The mean principal stress is given by

$$p = \frac{1}{3}(\sigma_v + 2\sigma_h) \tag{3.5}$$

The volumetric strain is

$$\varepsilon_v = \varepsilon_1 \tag{3.6}$$

in which ε_1 is the vertical strain.

Table 3.2: Stress and strain in sand under K_o conditions

Vertical stress σ_v (kPa)	Lateral stress σ_h (kPa)	Mean principal stress p (kPa)	Volumetric strain ε_v (%)
0	0.0	0.0	0.0
100	42.8	61.9	0.132
33	24.1	27.1	0.110
300	126	184	0.277
167	96.3	120	0.256
800	339	493	0.517
433	256	315	0.476
1600	661	974	0.764
1067	562	730	0.717

In order to measure the elastic modulus E or K, a sand sample in the oedometer ring with a density index of 90% was vertically loaded, unloaded and reloaded several times at different stress levels, while lateral stress and vertical deformation were measured. The vertical loading sequence was from 0, 100, 33, 300, 167, 800, 433, 1600 to 1067 kPa. During each loading or unloading, the load was increased or reduced in steps. The measured stresses and strains are listed in Table 3.2.

During each unloading, the change of strain is considered to be solely elastic. The bulk modulus can be obtained by

$$K = \frac{\delta p}{\delta \varepsilon_v^e} \tag{3.7}$$

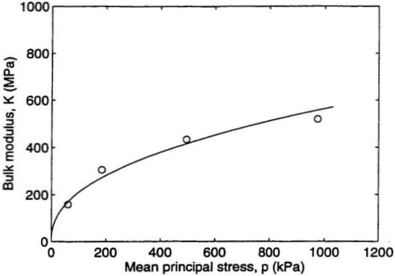

Figure 3.3: Elastic bulk modulus (K) versus mean principal stress (p)

where δp is the mean principal stress increment and $\delta\varepsilon_v^e$ is the volumetric strain increment during unloading.

Using Equation (3.7) and the data in Table 3.2, the calculated bulk modulus, K, increases with the level of principal stress which is the value of p immediately before unloading. When the values of p are 61.9, 184, 493 and 974 kPa, the values of K are 158, 305, 434 and 519 MPa respectively. As shown in Figure 3.3, the relationship between elastic bulk modulus, K, and mean principal stress, p, can be expressed as

$$K = 28.9p^{0.43} \tag{3.8}$$

and using Equation (3.3), the Young's modulus is given by

$$E = 34.7p^{0.43} \tag{3.9}$$

where p is in kPa, K and E are in MPa.

The elastic shear modulus (G) of soils is expressed in terms of Young's modulus and Poisson's ratio as

$$G = \frac{E}{2(1+\nu)} \tag{3.10}$$

Using Equation (3.9) and ν=0.30, the shear modulus of the dense sand in the present study is given by

$$G = 13.3p^{0.43} \tag{3.11}$$

where p is in kPa and G is in MPa.

An empirical equation proposed by Hardin and Richart (1963) for estimating the shear modulus of sands is

$$G = 3.27\frac{(2.97-e)^2}{1+e}p^{0.5} \tag{3.12}$$

where e is the void ratio of sands, p is in kPa and G is in MPa.

For the sand in this study, using the initial void ratio of 0.69 corresponding to I_D=90%, Equation (3.12) becomes

$$G = 10.1p^{0.5} \tag{3.13}$$

The values of G calculated using Equations (3.11) and (3.13) are given in Figure 3.4. The value of G obtained in the present study is close to that estimated by the empirical equation of Hardin and Richart (1963).

3.3 Triaxial Behaviour

Triaxial tests are often carried out for the determination of soil strength parameters, especially for measuring the friction angle (ϕ). Compared with direct shear box testing, triaxial testing has the following advantages: (1) the drainage conditions can be well controlled according to test purpose; (2) pore water pressure can be monitored in undrained tests; (3) volume change can be measured in drained tests; (4) back pressure

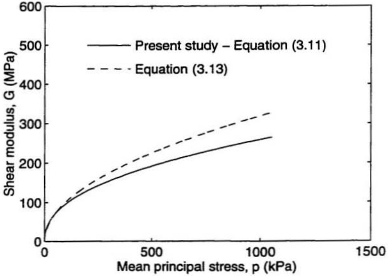

Figure 3.4: Comparison of the values of elastic shear modulus G

can be applied on soil samples to increase the degree of saturation; and (5) the stress and strain in a soil sample is more uniform and failure may occur in any plane depending on stress conditions.

In drained compression testing, the cell pressure (σ_3) is the minor principal stress; the axial stress (σ_1) is the major principal stress. The mean principal stress (p) and the deviator stress (q) are in the form of

$$p = \frac{1}{3}(\sigma_1 + 2\sigma_3) \tag{3.14}$$

$$q = \sigma_1 - \sigma_3 \tag{3.15}$$

For this work, triaxial tests of the silica sand described above were conducted under drained conditions, at cell pressures of up to 2500 kPa. Sand samples, with a density index of approximately 90%, were prepared using a raining technique similar to that described in Chapter 4. The height of the sand samples was typically 85 mm and the diameter was about 38 mm. The axial loading rate of each sample was 1 mm per minute.

3.3.1 Stress and strain

In the triaxial compression tests conducted, the stress-strain relationship and the volumetric behaviour are dependent on cell pressure, as typically shown in Figure 3.5. For the curve when σ_3=100 kPa, point M corresponds to the peak shear strength while point C to the critical state strength. The critical state is a condition under which the soil will continue to deform without further change in stresses and volume (Roscoe *et al.*, 1958; Schofield and Wroth, 1968; and Woods, 1990). It can be seen from Figure 3.5(a) that the deviator stress ratio

$$\frac{q}{\sigma_3} = \frac{\sigma_1 - \sigma_3}{\sigma_3} \tag{3.16}$$

of different samples at a given axial strain decreases with increasing cell pressure. The strain required to reach the peak strength as well as the critical state strength increases with stress level. Figure 3.5(b) indicates that the dilation of the sand during shearing decreases significantly with cell pressure. At a high pressure of σ_3=2500 kPa, the dilatant behaviour of the sand is suppressed.

3.3.2 Soil friction angles

For each sample of the dense sand under drained triaxial compression shearing, the shear stress increases with strain until a peak strength is reached. After the peak value, the shear stress decreases with shear strain. With the further increase of shear strain, the soil will reach the critical state where the shear stress keeps constant. For the sand sample with σ_3=100 kPa as shown in Figure 3.5, the peak friction angle (ϕ_{max}) and the critical state friction angle (ϕ_{cs}) can be derived using the stress parameters at points

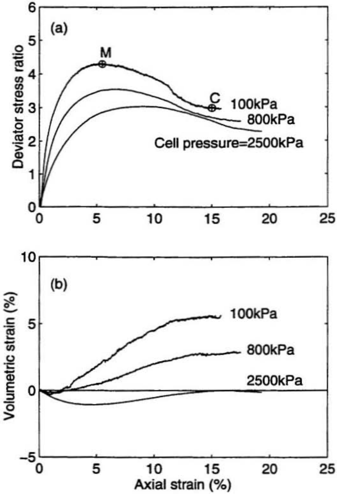

Figure 3.5: Drained triaxial compression: (a). Deviator stress ratio, $(\sigma_1\text{-}\sigma_3)/\sigma_3$, versus axial strain; (b). Volumetric strain versus axial strain

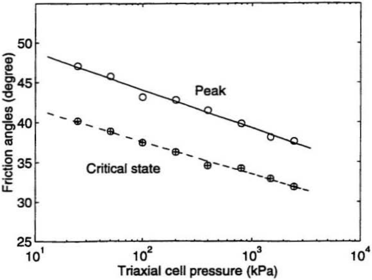

Figure 3.6: Peak and critical state friction angles versus cell pressure (σ_3)

M and C respectively. The friction angles obtained from test data of sand samples at cell pressures from 25 to 2500 kPa are given in Figure 3.6.

The peak friction angle decreases with stress level, which is in accordance with the test data reported by Meyerhof (1950), De Beer (1965a), Ladd *et al.* (1977) and Bolton (1986). When the cell pressure is increased from 25 to 2500 kPa, the peak friction angle is reduced from approximately 46.9 to 37.3°. This means that the Mohr's failure envelope is a curve rather than a straight line. Similar to the test results of Chu (1995), the critical state friction angle shown in Figure 3.6 also decreases with stress. The peak friction angle is expressed as

$$\phi_{max} = 53.6 - 4.78 \log_{10} \sigma_3 \tag{3.17}$$

while the critical state friction angle is

$$\phi_{cs} = 45.8 - 4.09 \log_{10} \sigma_3 \tag{3.18}$$

in which ϕ_{max} and ϕ_{cs} are in degrees; the cell pressure. σ_3 is in kPa.

The difference between the peak friction angle and the critical state friction angle can be written as

$$\delta\phi = \phi_{max} - \phi_{cs} = 7.8 - 0.69 \log_{10} \sigma_3 \tag{3.19}$$

which decreases slightly with stress level.

The peak and critical state friction angles can also be expressed in term of mean stress (s) as

$$\phi_{max} = 57.0 - 5.29 \log_{10} s \tag{3.20}$$

$$\phi_{cs} = 47.8 - 4.42 \log_{10} s \tag{3.21}$$

in which the mean stress, s, is in kPa and is in the form of

$$s = \frac{\sigma_1 + \sigma_3}{2} \tag{3.22}$$

The results indicate that the friction angle of the dense sand decreases linearly with stress in a semi-log scale diagram. For a log-cycle increase of stress, the soil friction angle is reduced by about 5 degrees.

3.3.3 Plastic volumetric strain

A sand sample with density index of 90% was isotropically compressed in the triaxial cell under drained conditions to observe the volumetric behaviour. At isotropic compression conditions, the mean principal stress is

$$p = \sigma_3 \tag{3.23}$$

where σ_3 is the cell pressure.

The sample was compressed from 10 kPa to 2500 kPa while the volume change was measured. The relationship between the plastic volumetric strain ε_v^p obtained and the mean principal stress is shown in Figure 3.7. The plastic volumetric strain at a given

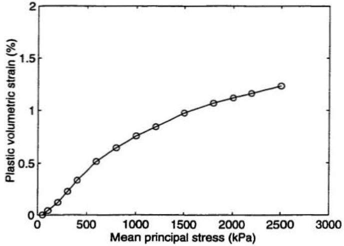

Figure 3.7: Plastic volumetric strain ε_v^p versus mean principal stress p in isotropic compression

pressure can be obtained by subtracting the elastic strain from the total volumetric strain measured. That is

$$\varepsilon_v^p = \varepsilon_v - \varepsilon_v^e \tag{3.24}$$

where ε_v is the total volumetric strain measured, and ε_v^e is the elastic volumetric strain corresponding to pressure p, given by

$$\varepsilon_v^e = \frac{p}{K} \tag{3.25}$$

in which the bulk modulus K can be calculated using Equation (3.8).

3.4 Friction between Sand and Footings

3.4.1 Test device

The proper estimation of friction between soils and construction materials is important in soil-structure interaction problems such as piles, footings and retaining walls.

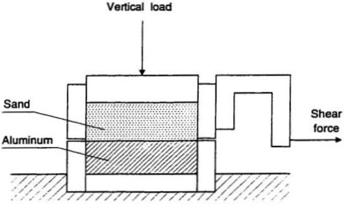

Figure 3.8: Direct shear apparatus for surface friction

Based on experimental results, Potyondy (1961) suggests that skin friction between soils and construction materials can be expressed in a sum of the cohesion and the normal stress-dependent component, similar to the Coulomb failure envelope of soils. In the measurement of the skin friction, the direct shear apparatus has been widely adopted (Potyondy, 1961; Feda, 1976; and Al-Hussaini and Perry, 1978). In addition, ring torsion apparatus has also been used (Yoshimi and Kishida, 1981), in order to overcome the disadvantages of direct shear apparatus, such as the non-uniform distributions of shear strain and stress over the contact surface.

A direct shear box, shown in Figure 3.8, was used in this study to measure the friction between the aluminum footings used in centrifuge tests and the dry silica sand with a density index of 90%. The sand samples had a diameter of 63.3 mm and a height of 20 mm. Shear force to the sample was applied by horizontally pushing the upper part of the shear box containing sand, while the lower part of the shear box holding

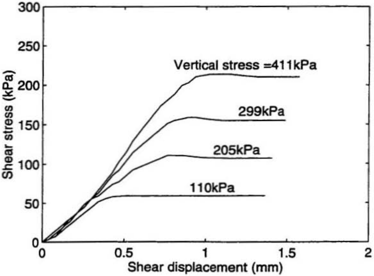

Figure 3.9: Shear stress (τ) versus displacement (χ)

the aluminum specimen was motionless. The horizontal shearing rate of the samples was 0.2 mm per minute.

3.4.2 Shear stress and displacement

It is observed that during shearing of each sample, shear stress increased with shear displacement when the vertical load was kept constant by applying a dead load of steel weights. When the displacement is increased to certain extent, slip between the sand surface and the aluminum surface occurs. Figure 3.9 shows the relationships between the average shear stress (τ) along the shear surface and shear displacement (χ) of 4 samples at normal (vertical) stresses of 110, 205, 299 and 411 kPa. It is seen that the pattern of shear stress-displacement changes with vertical stress. In the range of a small displacement, the 4 curves follow the same path. After the initial stage, they begin to diverge when the displacement is increased. The shear displacement required

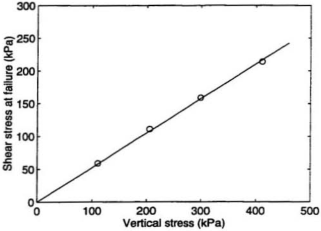

Figure 3.10: Shear stress at failure versus vertical stress

to reach failure (slip) increases with stress level.

3.4.3 Coefficient of skin friction

The relationship between vertical stress and shear stress at failure in Figure 3.10 is approximately linear. The coefficient of the skin friction is defined in terms of shear stress at failure (τ_f) and vertical stress (σ_v) as

$$\mu_f = \frac{\tau_f}{\sigma_v} \tag{3.26}$$

The data in Figure 3.10 result in μ_f=0.53. This is equivalent to a friction angle of 28° between the sand and the aluminum surface. Yoshima and Kishida (1981) state that the coefficient of friction between sand and steel surfaces of various roughness is typically from 0.3 to 0.7.

Chapter 4

Centrifuge Modelling of Ring Footings

4.1 Background and Principle

4.1.1 Introduction

Coulomb's model for soils is widely recognized by geotechnical engineers and researchers. The model treats soils as essentially frictional materials and reveals that the shear failure of soils is pressure-level dependent. This model is fundamental for developing the criteria of soil failure in modern soil mechanics. As a result frictional materials like soils are often termed Coulomb materials.

The geotechnical centrifuge technique has been aimed at dealing with the stress dependent behaviour of soils. In model tests of earth retaining structures, slopes and foundations, the scale of the model is a very important factor influencing the results. Large scale field tests are usually difficult or even impossible to perform and they are costly. Laboratory tests, on the other hand, are easy to operate and the test conditions can be well controlled (Mikasa and Takada, 1973). However, under normal gravity, the stress level in small scale models due to self-weight is much less than that in the prototype. Therefore the stress-strain behaviour and the patterns of deformations will be quite different in the two cases. For model tests concerning soil strength, a key issue is to achieve the stress similarity between the model and the prototype. An efficient way to do this is to use the centrifuge technique. In centrifuge modelling, the self-weight stress distribution of the model can be simulated by applying a centrifugal acceleration to simulate the stress conditions in the prototype.

In 1868, Edouard Phillips, an engineer in France, presented the idea of centrifuge modelling and its possible use in bridge engineering (Craig, 1989). In the 1930's, researchers in the United States and the former Soviet Union adopted this technique to geotechnical engineering (Rowe, 1975). A paper in 1936 (Craig, 1989) related to centrifuge work was presented by Pokorovskii and Fiodorov on the first International Conference on Soil Mechanics and Foundation Engineering (ICSMFE). Papers regarding centrifuge tests presented to the *7th* ICSMFE held in Mexico in 1969 and to the *8th* ICSMFE in Moscow in 1973 brought wide recognization of centrifuge modelling as an effective research tool. In the 1960's and 70's, important development of the centrifuge technique for geotechnical applications was made at the University of Manchester and the University of Cambrige in the United Kingdom (Rowe, 1975; Schofield, 1980). There are currently about 80 geotechnical centrifuge facilities in the USA, United Kingdom, Russia, France, Japan, Canada, China and some other countries. The centrifuge technique has been effectively used for studies of soil consolidations (Kimura *et al.*, 1985), earth retaining structures (Schcherbina, 1988), embankments (Lee and Schofield, 1988; Feng and Hu, 1988), foundations (Kutter *et al.*, 1988), cone penetration tests (Ferguson and Ko, 1985) and soil liquefaction potential (Hushmand *et al.*, 1988).

4.1.2 Principle and scaling law

In centrifuge testing, acceleration is applied to the soil model by spinning the model in a centrifuge normally in a horizontal plane at a prescribed angular velocity. As

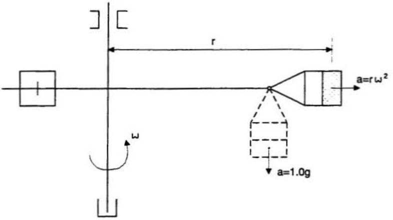

Figure 4.1: Principle of centrifuge modelling

illustrated in Figure 4.1, at a centrifuge radius r, the acceleration, a, that the model experiences is

$$a = r\omega^2 \tag{4.1}$$

where ω is the angular velocity of the centrifuge.

For a 1/N scale soil model subjected to a centrifuge acceleration of N times of gravitational acceleration (g), that is

$$a = Ng \tag{4.2}$$

the self-weight stress distribution in this model is similar to that of the soil prototype under gravitational acceleration, as shown in Figure 4.2. In this case, the acceleration scale is given by

$$\frac{a_m}{a_p} = N \tag{4.3}$$

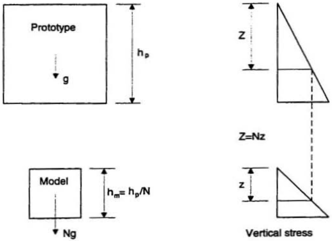

Figure 4.2: Stress distribution in prototype and centrifuge model

where subscripts m and p represent model and prototype respectively. The geometric scale is

$$\frac{L_m}{L_p} = \frac{1}{N} \tag{4.4}$$

where L is geometric dimension. If the same material is used in the model and the prototype, the soil unit weight scale is

$$\frac{\gamma_m}{\gamma_p} = N \tag{4.5}$$

where γ is unit weight. The centrifuge technique aims at obtaining the same mechanical behaviour of a small-scale soil model as that of a large-scale prototype. A summary of the scaling laws after Lee (1985) is presented in Table 4.1.

4.1.3 Effectiveness and accuracy of centrifuge modelling

A model test is designed to investigate the behaviour of a prototype. It is usually inevitable that the prototype can not be exactly and accurately modelled. The

Table 4.1: Scaling laws in centrifuge tests

Parameter Modelled	Scale factor (Prototype : Model at Ng)
Acceleration	$1 : N$
Model dimension	$1: 1/N$
Soil density	$1 : 1$
Soil unit weight	$1 : N$
Force	$1 : 1/N^2$
Stress	$1 : 1$
Strain	$1 : 1$
Displacement	$1 : 1/N$
Void ratio	$1 : 1$
Degree of saturation	$1 : 1$
Time (Inertial events)	$1 : 1/N$
Time (Consolidation and diffusion)	$1 : 1/N^2$
Time (Viscous flow)	$1 : 1$

fundamental considerations for the design of models are that (1) all significant effects should be modelled in similarity; (2) all effects not modelled in similarity should be considered; and (3) any unknown influence should be revealed by experimental results. In centrifuge tests, there also exist inaccuracies and errors. The main scale effects and errors involved in centrifuge modelling are discussed as follows.

Acceleration field

The major consideration in centrifuge tests is the similarity of self-weight vertical stress between the model and the prototype. As illustrated in Figure 4.1, the radial acceleration field in the centrifuge model is not uniform; the acceleration increases linearly with the centrifuge radius. In contrast to the linear increase of vertical stress with depth in the prototype as shown in Figure 4.3, the slight variation of the acceleration results in a nonlinear change of vertical stress (in radial direction in the centrifuge) in the model, expressed as

$$\sigma_{vm} = \int_{r_t}^{r_t+z} \rho\omega^2 r dr = \rho\omega^2 z(r_t + \frac{1}{2}z) \tag{4.6}$$

where ρ is the density of the model material, z is the depth and r_t is the centrifuge radius at the top surface of the model. The stress distribution in the prototype is

$$\sigma_{vp} = \rho g N z \tag{4.7}$$

In order to minimize the difference of stress between the model and the prototype, Schofield (1980) employed a rule that the under-stress ratio at the top portion of the model should be equal to the over-stressed ratio at the bottom. Under this rule, the vertical stress in the model is exact at two-thirds depth of interest in the model. The angular velocity, ω, during the operation of centrifuge test should be calculated using

$$Ng = (r_t + \frac{1}{3}h)\omega^2 \tag{4.8}$$

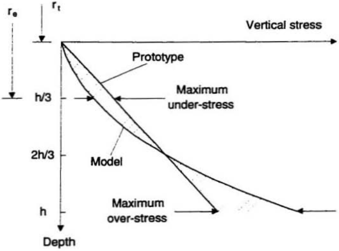

Figure 4.3: Vertical stress with depth in prototype and centrifuge model

where h is the depth of interest in the model. In this case, the maximum error of stress in the model can be estimated by

$$R_s = \frac{h}{6r_e} \tag{4.9}$$

where r_e is the centrifuge radius at one-third depth of the model. For $h/r_e \leq 0.1$, the stress error is less than 1.7%.

In addition to the slight variation of acceleration with depth in a centrifuge model, there is a change of acceleration in the horizontal plane. The horizontal acceleration in the plane is

$$a_h = a_v \frac{b}{r} \tag{4.10}$$

where a_v is the vertical acceleration, r is the centrifuge radius at the center of the plane and b represents the distance from the center of the plane. The horizontal acceleration, which is in the direction against the center of the model, may be significant if there is a large area of activity. One way to eliminate the influence of the horizontal acceleration is to shape the surface of a model to take consideration of the radius nature of the acceleration. This is, however, not the usual way in reality. A good practice is to make major test events take place in the central part of a model where the horizontal acceleration is small.

Another factor causing error is the so-called Coriolis acceleration in the horizontal direction due to the vertical movement of a particle in a model. The Coriolis acceleration is represented by

$$a_c = 2\omega v \tag{4.11}$$

where v is the vertical velocity of the particle relative to the model. Coriolis effect may be significant in the centrifuge modelling of some dynamic events.

The effect of earth gravity in some centrifuges has been discussed in detail by Phillips (1995). For fixed and restained platform centrifuges, the resultant acceleration is inclined to the platform at n:1, where n is the centrifuge acceleration. For the swinging platform centrifuges, the resultant acceleration is always normal to the platform surface, provided the hinge is frictionless.

Scale effect:

In centrifuge tests, a prototype of 5 m in size may be simulated, for instance, by a model of 0.5 m at 10 g or a model of 0.05 m at 100 g. It is important that a proper scale factor should be selected to obtain reliable results at a low cost. In practice, the scale factor should be kept as low as possible, subjected to the limitation of the size of the model due to payload capacity and the dimension of the centrifuge. The results from a small model will be more sensitive to the presence of instrumentation and the manner of model preparation. The selection of model size should also take into account the effect of soil particle size.

The effectiveness of centrifuge modelling of an event and the appropriateness of a scale factor in centrifuge modelling can be verified using the technique of modelling of models (Schofield, 1980). To check the validity of using the model test results for the prediction of a prototype behaviour, two model tests with different dimensions, namely L_1 and L_2, are repeated at two different acceleration levels of a_1 and a_2 respectively. If the product of dimension times acceleration is identical, that is

$$a_1 L_1 = a_2 L_2 \tag{4.12}$$

the same phenomenon is expected in the two tests when the models are well established.

Soil particle size:

In geotechnical centrifuge tests, the size of soil particles is not modelled in similarity. It is commonly questioned if there is anything wrong when the particle size is not reduced by a scale factor of N. If the similarity law were employed for particle size, a clay in a model at 100 g would be representing a fine sand. This is obviously flawed because the stress-strain and permeability behaviour of a clay are quite different from that of a fine sand.

Therefore the size of particles is a parameter which can not normally be scaled down for similarity. The same material is often used in the centrifuge model as the prototype. In the selection of the scale factor, the value of the ratio of a major dimension, l_m, of the model to the mean particle size, d_{50}, of soil should be large enough to eliminate the effect of particle size on test results. The particle size effect has been discussed by a number of researchers and some critical values of l_m/d_{50} are listed in Table 4.2.

4.1.4 Testing of foundations in centrifuge

In the past, due to the high cost and the difficulty of controlling testing conditions of large scale in-situ tests, most of the tests for bearing capacity of foundations were carried out in laboratories at normal gravity conditions or in fields using small bearing

Table 4.2: Critical ratio of model dimension and particle size

Reference	Critical l_m/d_{50}	Type of research
Mikasa & Takada (1973)	25	Strip footings on sand
Ovesen (1979)	15	Circular footing on sand
Gemperline & Ko (1984)	25	Strip footings on sand slope
Phillips (1995)	30	General summary
Fuglsang & Oveson (1988)	30	Footing on sand

plates. These small-scale tests have played important roles in the development of bearing capacity theories (Terzaghi, 1943; Meyerhof, 1951; De Beer, 1965a; and Vesic, 1973). It is realized, however, that the bearing capacity factor N_γ of footings on sand decreases with footing size, partly due to the fact that the internal friction angle of soils decreases with stress level (De Beer, 1965a; Kutter *et al.*, 1988; and Lau, 1988). Therefore, bearing capacity tests modelling large-scale foundations become very important in engineering practice. Centrifuge technique is considered to be an efficient method for modelling large-scale foundations in the laboratory under well controlled test conditions. In the past, this technique has been widely used for bearing capacity studies (Kimura *et al.*, 1985; Pu and Ko, 1988; and Bakir and Gainier, 1994). The work of some researchers is briefly introduced below.

Aiban and Znidarcic (1991):

In this work, 30g centrifuge tests were carried on a dense silica sand (I_D=88%, d_{50}=0.18 mm, C_u=1.7) to examine the effect of load eccentricity and inclination and initial embedment of footing under plane strain conditions. Sand was glued to the bottom to simulate rough base conditions. Grooves in the footing were made so that rotation of the footing is possible. The sand was pluviated using a hopper from a height of about 760 mm. It was observed that under vertical central loading, a major sliding wedge was formed and the failure surfaces were not symmetrical in both sides. Increase in load eccentricity or inclination decreases both the width and depth of the failure zone.

The effect of initial embedment was examined by the tests. For obtaining N_q and N_γ, it is important to correct for settlement at peak load using a normalized form

$$\frac{q_u}{\gamma B} = \frac{D_f + s}{B} N_q + \frac{1}{2} N_\gamma \tag{4.13}$$

where B is footing width, D_f is embedment depth and s represents settlement. The test results are in good agreement with the theoretical values of Vesic (1975), Meyerhof (1963) and Hansen (1970), with the best agreement with Meyerhof's results.

Under eccentric loading, tests were conducted with e/B values of 1/12, 1/6 and 1/4. The results indicate that the effective width method does not represent the behaviour of the footing. A better agreement is achieved using the Meyerhof's reduction factor method. The factor which fits the results is expressed as

$$R_e = 1 - (e/B)^{0.42} \tag{4.14}$$

The results also indicate that assuming a linear distribution of pressure is a good approximation for footings under eccentric loading.

Bakir and Garnier (1994):

Sand density is the most important factor affecting footing test results. Therefore, an extensive study of the homogeneity of pluviated samples using an automatic raining hopper was performed. In addition, handling of sand may cause a decrease of ϕ; care must be taken in re-using the same material in successive samples.

For dense sand, the peak load is the ultimate bearing capacity corresponding to a settlement of s_r; s_r/B increases with N_γ. The link between the loading device and the footing must be rigorously controlled, especially when the test results are compared with numerical calculations. To allow the footing to move horizontally and rotate freely so as to avoid moment and eccentricity of the load, two ball links were used, one was on the footing and the other was on the top of the loading rod.

Corte *et al.* (1988):

Three laboratories were involved in a test program to evaluate the variability of centrifuge test results. The reference tests were axially loaded circular shallow footings on a saturated silica sand (d_{50}=0.17 mm, C_u=1.47); the footing with diameter of 56.6 mm was tested at 28.2g when I_D=86%. A thin layer of sand was glued onto the base so that the base was rough. The loading was so slow that no excess pore pressure was generated. It is found that loading rate did not have a large effect on results. The main cause of the resulting scatter appears to be the imperfections in the layering procedures. Specimen preparation and density control are very important. The influence of other factors, such as footing size, loading rate and proximity of boundaries, may be masked by a small difference in density. CPT tests appear highly desirable to assess the model state.

Gainier and Canepa (1991):

For the relatively undisturbed sand, 24 centrifuge tests at 14.5g of shallow foundations 50 mm square were performed, up to an embedment depth of $D_f=2B$. Loads were applied by shifting a mass. There was a ball joint at the top of the footing for loading. When $0 \leq D_f/B \leq 0.5$, there is a large increase in bearing capacity with D_f, followed by a slower increase up to $D_f/B=2$. The effect of lateral friction of embedded foundations was investigated when $D_f/B=2$. The tip bearing capacity and the lateral friction were measured separately. It is concluded that the increase of total bearing capacity in the case of rough footings is due to the lateral friction.

James and Shi (1988):

Centrifuge tests were performed on a dry coarse sand to study the behaviour of spud-can type footings under vertical, horizontal and moment loads. The footing with a small cone tip was 700mm in diameter. A horizontal load was applied above the footing surface at a given height. The sand was poured from a hopper. The sample density indixes (I_D) were 95.4% and 46.2%. The loading system consisted of one main jack for vertical load and two sub-jacks for horizontal load. The tests were conducted at 60 g and were stress controlled. By means of yield locus, the influence of horizontal load on the vertical bearing capacity may be described by a simple mathematical expression.

Kimura *et al.* (1985):

The work presents the research of Tokyo Institute of Technology Soil Mechanics group on shallow foundations in dense sand. Tests were conducted to explain De Beer's scale effect and to investigate the effects of base roughness, soil anisotropy, embedment and soil slopes. Radiographs were used to detect the slip surfaces. Progressive failure is associated with wider footings, which is the main scale effect. A smooth footing yielded two symmetrical wedges and smaller bearing capacity. A simple expression for predicting the embedment effect is deduced. The results indicate that the bearing capacity was virtually not affected by particle sizes in these three groups of test conditions.

For De Beer's scale effect, tests were performed for rough footings with widths (B) of 20, 30 and 40mm, depth (D_f) of 0, 0.5B and 1.0B and accelerations of 1, 10, 20 and 40g. The bearing capacity factor is defined by

$$N_{\gamma q} = \frac{q_{max}}{\gamma B_N/2} \tag{4.15}$$

and a parameter

$$\beta = \frac{\gamma B_N}{E_q} \tag{4.16}$$

where q_{max} and B_N denote the bearing capacity and width in prototype scale, E_q is the Young's modulus of the parent rock of the sand (De Beer, 1965a). Test results show that $N_{\gamma q}$ decreases with β and that De Beer's scale effect becomes less marked with a decrease of I_D. The mechanism of the scale effect can be explained by the observed shear strain distribution at the four stages of the footing settlement. For smaller footings, the shear strain along the slip surface at failure is smaller.

Meyerhof (1951) extended the two-wedge failure mechanism of Hill (1950) and suggested that the bearing capacity of a smooth footing be one half that of a rough footing. Test results of this study confirm that smooth footing does yield two symmetrical wedges and yield smaller bearing capacity. However the difference becomes smaller as width increases.

Okamura *et al.* (1997):

Centrifuge tests using a circular footing and rectangular footings with various aspect ratio (L/B) values from 1.0 to 7.5 were conducted on a dense sand with relative density of 85%. The acceleration levels were from 15 to 100 gravities, resulting in prototype footing dimensions of up to 3.0 m. The results show that the normalized bearing capacity decreases with footing size but increases with aspect ratio. It was found that the shape factor, s_γ, of rectangular footings increases with both aspect ratio and footing width. The finite element analysis carried out assuming elasto-perfect plasticity indicates that the soil friction angle (ϕ) from triaxial test is valid for calculating the bearing capacity of circular footings.

Oveson (1975):

The tests of footings on sands were done at University of Florida. The centrifuge had a radius of 1m and could hold a soil mass of 28 kg and produce an acceleration of 85g. The load was applied by mercury fed into a load container. The diameters of the circular footings were 1.57cm, 2.47cm and 4.12cm while N values were 79. 51 and 30 respectively. The results of this study as well as of Mikasa and Takada (1973) indicate that (1) A footing on sand with length scale $1/N_1$ and subjected to acceleration N_1g yields the same bearing capacity as a footing on sand with length scale $1/N_2$ and subjected to acceleration N_2g, at least for $1 \leq N_1/N_2 \leq 3$; (2) The ϕ value is not a constant, it decreases with increasing stress level.

Pu and Ko (1988):

These tests were to investigate the influence of footing size, shape and depth and sand density on bearing capacity. There were three aluminum footings: square (2.54×2.54 cm), strip (2.54×15.24 cm) and rectangular (2.54×7.62 cm). The sand had parameters as: d_{50} of 0.39 mm, C_u of 1.68, I_D of 41 to 92% and ϕ of 33.2 to 38.5°.

For the strip footing on the surface of dense sand, the failure modes were general shear at 25g, local shear at 50g and punching shear at 75g. For the dense sand (I_D=92%) at 25g, a surface strip footing failed in general shear while the square and the rectangular footings failed in local shear or punching. The bearing capacity is proportional to the depth. The summary of the influence of sand density, acceleration and depth on failure mode indicates that the credibility of small model tests at 1g conditions becomes questionable.

Tan (1990):

Conical and spud model footings of 28.3 mm in diameter were tested on sand at an acceleration of 56.6 gravities to investigate the effect of footing roughness and cone angle on bearing capacity. The test results indicate that the increase in footing roughness is to increase the bearing capacity, especially when the footing roughness becomes greater. Within a particular value of cone angle between (25° to 45°). the increase of cone angle will decrease the bearing capacity of semi-rough footings; this effect is not significant for rough footings. Further increase in cone angle beyond this particular value tends to increase the bearing capacity for both semi-rough and rough footings.

Ueno *et al.* (1994):

The anisotropic initial stress condition is usually represented by K_o. In the tests. the centrifuge radius was 1.18 m. The dry sand was pluviated from a height of 0.9 m. The initial density index was about 81%. The steel circular footing was 30 mm in diameter and 40 mm in thickness. The footing was solidly fixed to the jack driven by a motor. The settlement of sand surface was measured to obtain void ratio change. The test results show that a noticeable void ratio change due to centrifuge acceleration was observed. It is observed that the bearing capacity increases with increasing K_o.

4.2 Preparation of Sand Samples

4.2.1 Introduction

Sand samples for centrifuge tests can be prepared by tamping or raining (pluviation). The tamping technique often results in nonuniform density sample (Corte *et al.*, 1988; and Phillips, 1995). High quality samples are essential to obtain reliable test results of bearing capacity of footings on sands, because a slight variation in sand density will cause a significant change in the bearing capacity (Corte *et al.*, 1988). Therefore, the raining method was used for this work in preparation of dry sand samples for centrifuge modelling. This technique was also employed for the small sample preparation for the triaxial and lateral stress tests introduced in Chapter 3.

Almost half a century ago Kolbuszewski (1948a, b) introduced the raining method for preparing sand samples. Since then this technique has been widely used. A review of the development of this method has been presented by Eid (1987). The raining method not only provides reasonably homogeneous samples with desired density but also closely simulates the fabric of in situ soils formed by sedimentation. Other advantages of the raining method are its simplicity, its flexibility and the fact that it can be employed for making large or small samples with equal effectiveness. The principle of the raining technique is schematically shown in Figure 4.4.

The basic equipment consists of a sand container above the shutter, a diffuser and a sand collector. The shutter has distributed holes and the diffuser usually consists of two or more sieves. The sand falling through the shutter is dispersed by the diffuser and is evenly distributed on the surface of the sand in the sand collector. As discussed by Rad and Tumay (1987), factors affecting the density of rained sand include deposition intensity, falling height, diffuser sieve size and the shutter-hole pattern. The deposition intensity, defined as the weight of sand rained per unit area per unit time, is a dominating factor. The influence of falling height, the diffuser sieve size and shutter-hole pattern is limited under certain conditions selected. The influence of the distance between the diffuser sieves, the distance between the shutter and the diffuser, and the sand height in the top container on sand density is relatively negligible.

The sand rainers described by Eid (1987) and Rad and Tumay (1987) were used for relative small sample preparation; the sand was rained over the whole area of the sand collector in the same time. In this study, as the tub for holding the sand samples was as large as 1180 mm in length and 940 mm in width, constructing a rainer covering the whole tub was difficult. The raining technique in this work was a modified one from those employed by the researchers mentioned above.

4.2.2 Equipment

As shown by the photograph in Figure 4.5, the equipment for preparing the cen-

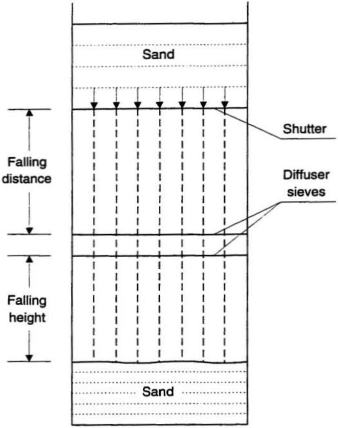

Figure 4.4: Principle of raining technique

trifuge sand model by raining consisted of a sand hopper, a plastic bucket with holes on the bottom and three sieves attached to the bottom of the bucket. The hopper could hold sand of up to 0.11 m^3. The bottom of the plastic bucket is used as a shutter. Different patterns of holes of the shutter were tried in tests in order to obtain designated sand density of about 90%. The selected pattern of the holes is shown in Figure 4.6. There were 19 holes distributed on the shutter. The diameter of the holes was 4.2 mm. The shutter porosity, defined as the ratio of the total area of the holes to the area of raining, was 0.84%.

The three sieves under the shutter were used as a diffuser. In a downward sequence, they were No. 10, No. 14 and No. 18 standard sieves with apertures of 2.00, 1.40 and 1.00 mm respectively. The diameter of the sieves was 200 mm. The height between the shutter and the top sieve was 100 mm and the distance between two adjacent sieves was 50 mm. To achieve the best diffusing result, each two adjacent sieves were turned 45° horizontally with each other as suggested by Eid (1987) and Rad and Tumay (1987). The shutter and the sieves were positioned horizontally parallel during sand raining.

4.2.3 Preparing sand samples

As indicated by Rad and Tumay (1987), the density of rained sand decreases significantly with increasing deposition intensity. For the selected shutter-hole pattern in Figure 4.6, the rate of sand falling through shutter was 1.95 kilograms per minute. As the diameter of the sieves was 200 mm, the deposition intensity of the sand was about 0.103 g/cm^2 per second. At this deposition intensity, the density of sand increased with falling height between the bottom sieve and the surface of the rained sand, as shown in Figure 4.7. The data in the figure were obtained when a circular container 250 in diameter and 310 mm in height and a density cup 100 cm^3 in volume were used as sand collectors. It can be seen that when the falling height is small the sand density

Figure 4.5: Equipment for raining sand

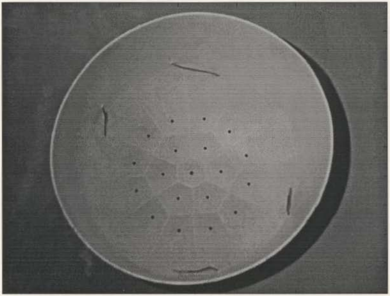

Figure 4.6: Shutter-hole pattern for raining sand

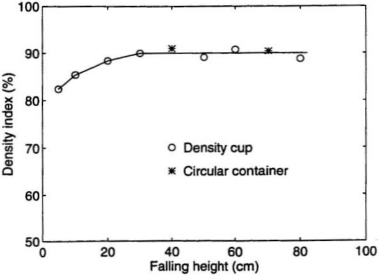

Figure 4.7: Sand density versus falling height

increases with falling height. When the falling height is greater than 30 cm, the density index reaches a constant value of approximately 90%. This tendency is in accordance with the observation of Rad and Tumay (1987). Accordingly, the falling height was kept at a constant value of 50 cm to obtain dense sand samples in the containers for centrifuge tests with a density index of about 90%.

In preparing the soil models, a container (tub) was put on a pallet cart. The cart could be moved on the ground horizontally in any direction. It can also be used to lift and lower the soil tub vertically in a range of about 11 cm. During raining, the rainer (hopper, shutter and diffuser) was fixed in place. The falling height was kept about 50 cm. By moving the tub on the pallet cart horizontally, sand was rained into the tub layer by layer of which the thickness was about 10 mm each. When the sand level in the tub was arising, the tub was being lowered using the pallet cart to keep the constant falling height of 50 cm. A thin string hung from the side of the diffuser to about 20 mm from the sand surface in the tub was used to control the falling height.

When the sand rained in tub was about 20 mm thicker than required, the raining of sand was stopped. The extra sand was removed by a vacuum cleaner. Vacuuming was applied to the sand through a small tube about 12 mm in diameter guided by two cross beams positioned on the tub. The vacuum tube was flattened at the end in order that the sand surface was smooth after the vacuuming. The thickness of the sand samples was from 250 mm to 300 mm.

For a sample of about 430 kilograms in weight, it usually took 4 hours raining the sand. The total time for preparing a sample, including equipment preparation, sand raining and sample surface treatment by vacuuming was 7 to 9 hours.

4.2.4 Verification of sample quality

The density of the samples rained in the tubs was estimated by weighing the sand and by measuring the volume of the samples. The density index of the dry sand samples ranged from 88% to 91%, while the average density index was 90%. It has been evaluated that the error caused in weighing the sand and calculating the volume of the samples for the density estimation was less than 1%. This means that the raining technique developed for this investigation is effective and reliable. The repeatability of obtaining uniform and dense sand samples is very good.

The quality of the sand samples was also verified by cone penetration testing (CPT) during centrifuge flight. Typical cone tip resistances in centrifuge at 40 g and 100 g are shown in Figure 4.8. CPT is a technique for the measurement of soil properties by pushing an instrumented cone into soils at a constant rate. The main applications of CPT are to determine the soil profile and identify soils and to evaluate soil engineering parameters. In some cases, CPTs may be accompanied by borings to achieve more reliable test results. The CPT can provide continuous measurement of ground conditions;

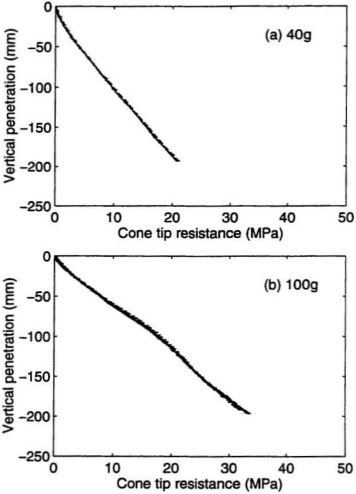

Figure 4.8: Cone tip resistance of sand in centrifuge at 40 and 100 gravities

it also causes less disturbance of soil layers associated with boring and sampling. The CPT technique has been widely used in research and engineering practice. Because of the complex changes of stress, strain and pore pressure during the cone penetration test, it is difficult to make a comprehensive theoretical analysis. In engineering practice, the analysis of CPT is highly empirical (Meigh, 1987).

CPT data can be used for estimation of the relative density of normally consolidated sand (Jamiolkowski, 1985) and overconsolidated sand (Schmertmann. 1975). sand strength (Durgunoglu and Mitchell, 1975) and other parameters (Meigh. 1987). Also, extensive investigations have been carried out for determining the properties of clays using CPT, including undrained shear strength of normally consolidated clays (Lunne and Kleven, 1981) and overconsolidated clays (Marsland and Quarterman, 1982), and deformability of clays (Meigh, 1987). In addition, CPT has also been used for the estimation of pile bearing capacity (Meigh, 1987), for the control of ground improvement (Juilie and Sherwood, 1983) and for the determination of liquefaction potential of sand layers (Zhou, 1980). Centrifuge cone penetration tests have been conducted by a number of researchers (Corte *et al.*, 1988, 1991; and Lin, 1995). The CPT technique is an effective way to measure the strength of sand in centrifuge flight. Ferguson and Ko (1985) used centrifuge CPT data to determine the internal friction angle of sand.

The cone penetration tests during centrifuge flight for this study were conducted using a cone penetrometer apparatus developed by C-CORE (Cunard, 1993). This apparatus is capable of moving at a constant speed to different positions along a fixed direction through a horizontal driving system. It is fixed on the top of the tub at the required position before the centrifuge testing is started. The penetrometer used has a cross-sectional area of 1.0 cm^2 with an apex angle of 60°. It measures tip resistance, q_c, through strain gauges mounted behind the cone tip. During centrifuge flight, the cone penetrometer was pushed vertically into the sand at a rate of 3 mm per second and the response of the strain gauges was recorded by the data acquisition system. Movement of the cone during the test can be observed through the camera mounted inside the swinging basket.

In this study, the CPT technique is used to determine the quality (uniformity) of sand samples prepared by the raining method. Cone penetration tests in centrifuge from 10 g to 160 g were conducted. For each sand sample, two cone tests were conducted at different locations. It has been observed that the tip resistances of the two tests for each sample are virtually identical. The cone penetration data, as typically shown in Figure 4.8 indicate that the density of the samples were very uniform.

4.3 Test Program and Procedure

4.3.1 Centrifuge facilities

The footing tests for this study were undertaken in C-CORE Centrifuge Centre located at Memorial University of Newfoundland. The centre houses an Acutronic 680-2 centrifuge made in France. The centrifuge can carry masses of up to 22,000 kilograms to 100 gravities or 650 kilograms to 200 gravities. The maximum centrifugal rotational speed is 189 r.p.m. while the maximum acceleration at an effective radius of 5.0 m is 200 gravities. The data acquisition system can provide 78 channels for data sampling of electrical signals from transducers during tests. Figure 4.9 shows a view of the C-CORE geotechnical centrifuge. The specifications of the centrifuge are listed in Table 4.3.

4.3.2 Test program

The tests were for footings on the surface of dense sand (I_D=90%). Most of the centrifuge tests were conducted using a set of model ring footings with a constant area

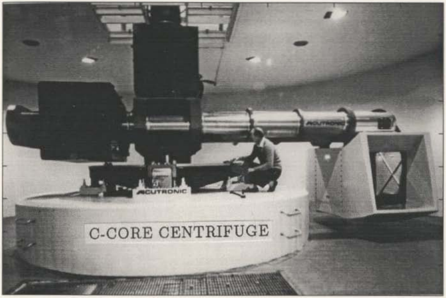

Figure 4.9: C-CORE geotechnical centrifuge

Table 4.3: C-CORE centrifuge specification

Machine	Acutronic 680-2
Platform radius	5.5 m
Nominal radius	5.0 m
Acceleration range	10 - 200 g
Acceleration accuracy	0.5%
Maximum speed	189 rpm
Payload at 100 g	22000 kg
Payload at 200 g	650 kg
Platform width	1.1 m
Platform depth	1.4 m
Container height	1.1 m
Maximum usable height	1.5 m
Sliprings	78
Fluid joints	6
Installed power	800 kVA
Maximum imbalance	100 kN

of 15 cm^2; when the ring radii ratio were 0, 0.2, 0.35, 0.5, 0.7, 0.8 and 0.9, the outside diameters of the model rings were 43.7, 44.6, 46.7, 50.5, 61.2, 72.8 and 100.3 mm respectively. Table 4.4 shows the tests of ring (and circular) footings conducted under axial load conditions. Test No. A1 to A23 were for the examination of variation of bearing capacity of constant area footings with ring radii ratio at different acceleration levels (namely 10, 40, 100 and 160 gravities). Test No. A24 to No. A27 were for the study of modelling of models. Test No. A28 to A30, together with A1, A8, A13, A18, A24 and A25 were for the investigation of the effect of footing size on bearing capacity. In Table 4.4, A_m is the area of the model footings, D_m is the outside diameter of the model footings, n is the ring radii ratio and D_p represents the outside diameter of the prototype footings. It can be seen that the maximum outside diameters of the prototype footings modelled are 7.0, 7.1, 7.5, 8.1, 9.8 and 11.6 m when the ring radii ratio of the constant area footings are 0, 0.2, 0.35, 0.5, 0.7 and 0.8 respectively. The bearing capacity of each footing obtained from centrifuge test is also given on the table.

In addition to the axially loaded footing tests aforementioned, 15 tests of footings under eccentric loading listed in Table 4.5 were carried out at an acceleration level of 100 g, numbered E1 to E15. The model footings also had a constant area of 15 cm^2. The tests were divided into 5 groups with ring radii ratio of 0, 0.35, 0.5, 0.7 and 0.9 respectively. The eccentricity of loading, e, represents the distance between the centre of a footing and the point where the concentrated vertical load was applied. The loading eccentricity ratio is defined as a ratio of the eccentricity (e) to the outside diameter of a ring footing (D), written as

$$r_e = \frac{e}{D} \tag{4.17}$$

For different ring footings, tests were conducted at eccentricity ratios of 0, 0.075, 0.15, 0.25 and 0.375 to investigate the effect on bearing capacity.

Table 4.4: Tests of ring footings under axial loading

No.	A_m (cm^2)	D_m (mm)	n	Gravity (g)	D_p (m)	q_u (kPa)
A1	15	43.7	0	10	0.437	820
A2		44.6	0.2		0.446	930
A3		46.7	0.35		0.467	1000
A4		50.5	0.5		0.505	820
A5		61.2	0.7		0.612	650
A6		72.8	0.8		0.728	570
A7		100.3	0.9		1.003	470
A8	15	43.7	0	40	1.748	2260
A9		46.7	0.35		1.868	2650
A10		50.5	0.5		2.020	2350
A11		61.2	0.7		2.448	1740
A12		100.3	0.9		4.006	1170
A13	15	43.7	0	100	4.37	4250
A14		46.7	0.35		4.67	4700
A15		50.5	0.5		5.05	4190
A16		61.2	0.7		6.12	3320
A17		100.3	0.9		10.03	2160
A18	15	43.7	0	160	6.99	6150
A19		44.6	0.2		7.14	6710
A20		46.7	0.35		7.47	6890
A21		50.5	0.5		8.08	5780
A22		61.2	0.7		9.79	4350
A23		72.8	0.8		11.6	3660
A24	44.18	75.0	0	20	1.50	1960
A25	11.04	37.5	0	40	1.50	1920
A26	33.14	75.0	0.5	20	1.50	1340
A27	8.28	37.5	0.5	40	1.50	1310
A28	15	43.7	0	1	0.0437	160
A29	44.18	75.0	0	1	0.075	220
A30	3.14	20.0	0	10	0.200	480

4.3.3 Test equipment and procedure

The equipment for the footing tests in centrifuge includes soil containers, load cells for measuring the load applied on the footing, load actuator and the supporting parts, and transducers for measuring footing displacement and the deformation of soil during testing. The test setup is shown by the photograph on Figure 4.10.

Two tubs were used in the centrifuge tests as soil containers: an aluminum rectangular tub and a steel circular tub. The rectangular tub was 1180 mm in length, 940 mm in width and 400 mm in depth. The circular tub had a diameter of 900 mm and a depth of 500 mm. The tubs were stiff enough that the soil samples contained were considered at K_o conditions.

The vertical load on the footing was applied by a 10 kN actuator. Two load cells made of 6061-T6 aluminum were manufactured and used. Their load capacities were 8 kN and 15 kN. The smaller load cell was used for tests at low gravities while the other was used at high gravities. The model footings listed in Table 4.4 and 4.5 were also made of aluminum. The footings were vertically loaded at a rate of 0.1 mm per second. A steel ball was positioned on the footing to transfer load from the load cell so that the footing could rotate during loading. Three linear displacement transducers (LDTs) were used at three points on the footing to measure the vertical and rotational displacements of the footing. In addition, two other LDTs were used to monitor the settlement of the surface of the sand samples during centrifuge flight and testing. For each tub of sand sample, a maximum number of 9 footing tests could be carried out. In order to reduce the influence of repeated centrifuge flights on tests results, each sample was cyclically accelerated between 10 g and the required test acceleration 3 times before the first footing test was conducted. During test, signals from the load

Table 4.5: Tests of eccentrically loaded ring footings at 100 gravities

Test No.	A_m (cm^2)	$D_m (mm)$	n	e/D_m	D_p (m)	q_u (kPa)
A13	15	43.7	0	0	4.37	4250
E1				0.075		3250
E2				0.15		2600
E3				0.25		2250
E4				0.375		1690
A14	15	46.7	0.35	0	4.67	4700
E5				0.075		3760
E6				0.375		1820
A15	15	50.5	0.5	0	5.05	4190
E7				0.075		3100
E8				0.15		2450
E9				0.375		1610
A16	15	61.2	0.7	0	6.12	3320
E10				0.15		2220
E11				0.375		1330
A17	15	100.3	0.9	0	10.0	2160
E12				0.075		1650
E13				0.15		1430
E14				0.25		1130
E15				0.375		940

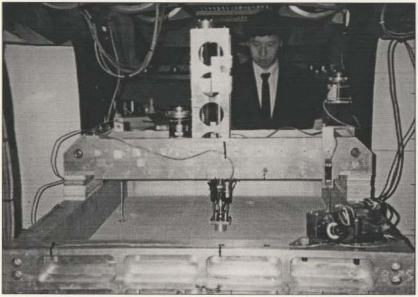

Figure 4.10: Equipment for footing tests in centrifuge

cell and the LDTs were sampled at a frequency of 5 Hz by a personal computer data acquisition system.

4.3.4 Model test verification

In order to check the validity of the centrifuge modelling of footings, the principle of modeling of models, as introduced previously, is employed. To model the models, two groups of tests have been carried out: (a) the ring radii ratio (n) was equal to zero; and (b) n was 0.5. There are two tests in each group; the first test was conducted when the centrifuge acceleration, a, was 20g and the footing outside diameter, D, was 75.0mm, while the second test was carried out when a was 40g and D was 37.5mm. The relationships between the loading and the relative settlement of the footings are shown in Figure 4.11, where s represents the vertical settlement of the footings. In Figure 4.11(a), the bearing capacities of the two circular footings (n=0) are virtually identical, the difference between the relative settlements is also very small; the relative settlements are 10 to 15 percent when the vertical load s reach the maximum values. In Figure 4.11(b), the peak vertical loads (bearing capacities) of the two ring footings with a ring radii ratio (n) of 0.5 are approximately the same. Before the peak loads, the relative settlements of the two footings are very close. After the peak loads, the difference between the relative settlements becomes greater, while the behavior of the footings after the peak loads is considered less important.

The results in Figure 4.11 indicate the validity of centrifuge modeling of the bearing capacity of the circular and ring footings. The relative settlements of the footings can also be well modeled, especially before the peak loads.

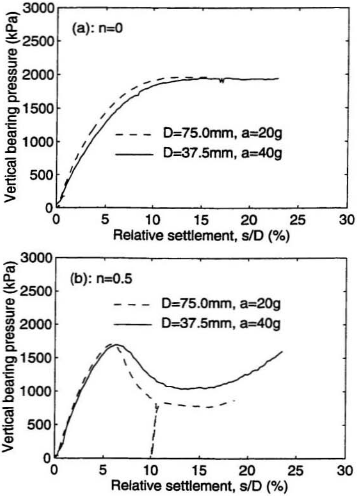

Figure 4.11: Modelling of model footings

4.4 Effect of Footing Size

4.4.1 Load, settlement and failure mode

There are three failure modes of soil supporting foundations: general shear failure, local shear failure and punching shear failure (Vesic, 1973). In the case of general shear failure, there usually exists a continuous failure surface from one edge of the footing to the ground surface. The ultimate bearing capacity (q_u) is the peak load applied. In contrast, the punching shear failure is characterized by a failure pattern that is not obvious. The foundation penetrates due to the compression of the soil immediately beneath the foundation. The penetration increases as the loading is increased and there is no peak load. Local shear failure is a transitional mode between general failure and punching failure. There is a visible bulging of the soil adjacent to the foundation. The failure surfaces usually end in the soil. The failure mode of a foundation depends upon soil compressibility, foundation size and depth. By increasing the dimension of a footing on dense sand, the failure mode tends to move from general shear failure to punching shear failure.

Figure 4.12 shows the normalized pressure with the relative settlement of a model footing 43.7 mm in diameter tested at accelerations of 1, 10, 40 and 160g, corresponding to prototype footing diameters of 0.044, 0.44, 1.75 and 7.0 m respectively. In the figure, s represents the settlement of the footings, and the loading ratio, R_p, is given by

$$R_p = \frac{p}{\gamma D} \tag{4.18}$$

in which p is the averaged pressure applied, γ is the unit weight of soil and D represents the diameter of circular footings.

It is obvious that the failure mode of the 0.044 m footing is general shear; the load reaches the maximum at a relative settlement of about 7%. It was observed that the failure surface of approximately 18 cm in diameter in the centrifuge model extended

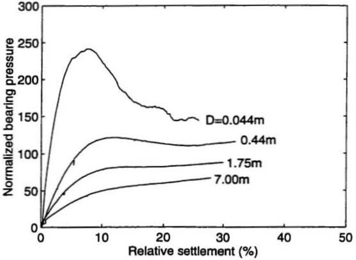

Figure 4.12: Normalized pressure (R_p) versus relative settlement (s/D) of circular footings

to the surface of the soil. For the 0.44 m footing, the load reaches the peak value at a relative settlement of 10%; in the centrifuge model, there was a visible but not very obvious failure surface of about 20 cm in diameter around the footing at the top of the soil. The failure mode of this footing is also general shear failure. For the 1.75 m footing, the load becomes relatively constant after a relative settlement of about 12%. A failure surface was not observed in the centrifuge model, but an obvious bulging of soil around the footing was seen. The failure mode in this case is approaching local shear failure. For the 7.0 m footing, the loads increase with settlement; there are no peak loads; the failure mode is local shear failure. There was soil heave in the centrifuge model but the range was difficult to identify. The increase of footing diameter leads the failure pattern to change from general shear mode to local shear mode.

It is seen from Figure 4.12 that when the footing diameters are 0.044, 0.44, 1.75 and 7.0 m, the normalized footing pressures (R_p) at failure are approximately 240, 120, 80 and 60 respectively, decreasing with footing size. The slope of the curves before failure decreases with footing dimension. This means that the relative compressibility of soil is increased by the increase of footing size. It can also be seen that the relative settlement (s/D) at which the failure load is reached increases with footing size. When D changes from 0.044 to 7.0 m, the relative settlement at failure load is increased from about 7 to 15%.

Comparison of the footing test results in Figure 4.12 and the data of triaxial tests of the same sand in Figure 3.5 will provide a further understanding of the failure mode feature. In the triaxial tests, the sand dilated significantly during shearing at low stress level. At high confining pressure of 2500kPa, the dilation phenomenon disappeared. Both the relative compressibility of the sand and the strain at peak load increase with stress level. For the small footing, since the stress level in the soil is low, the movement and heave of soil around the footing is caused by both the dilation of soil during shearing and the expulsion of soil due to the penetration of the footing. Because of the high dilatancy and the low strain at failure of dense sand at low stress, the strength mobilization at points A, B and C in Figure 4.13 along the failure surface of a small footing is more uniform and the footing fails in general failure mode. The increase of footing size results in the increase of stress level in the soil. The dilation of the soil becomes smaller and the strain at failure becomes higher. To mobilize the strength along the failure surface in the soil, larger displacement of the footing is required and failure mode becomes less general. It should be emphasized that the volume change of soil under footings must also be an important factor affecting the failure mode.

4.4.2 Bearing capacity of circular footings

The well known Terzaghi's equation, accepted widely as a basic formula for the

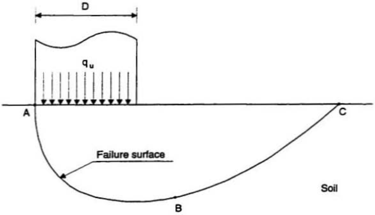

Figure 4.13: Failure pattern of foundation

bearing capacity of strip foundations, is given by

$$q_u = cN_c + qN_q + \frac{1}{2}\gamma BN_\gamma \tag{4.19}$$

where q_u is the ultimate bearing capacity, c is soil cohesion, q is overburden pressure, γ is soil unit weight, B is the width of foundations, and N_c, N_q and N_γ are bearing capacity factors. In the literature there are a variety of bearing capacity theories. While the bearing capacity factors N_c and N_q proposed by Prandtl (1921) and Reissner (1924) are widely accepted, the variation in N_γ is substantial (Terzaghi, 1943; Caquot and Kerisel, 1953; Meyerhof, 1963; and Hansen, 1970). For strip foundations resting on the surface of cohesionless soil, Equation (4.19) becomes

$$q_u = \frac{1}{2}\gamma BN_\gamma \tag{4.20}$$

and for circular foundations, the bearing capacity is expressed by (Terzaghi, 1943)

$$q_u = 0.3\gamma DN_\gamma \tag{4.21}$$

where D is the diameter of a circular foundation. In using the equations mentioned above it is usually assumed that the value of N_γ is constant and independent of footing size. For a constant N_γ, the bearing capacity expressed by Equations (4.19) to (4.21) increases linearly with foundation dimension.

Experimental data collected by De Beer (1965a), however, show that the bearing capacity factor N_γ decreases with foundation size. Centrifuge test results (Clark, 1998; Zhu *et al.*, 1996; and Kusakabe *et al.*, 1991) indicate that the bearing capacity increases in proportion with foundation size when plotted on a log-log scale diagram. This suggests that N_γ decreases linearly with footing size on a double-log scale diagram. Studies of the effect of footing size by De Beer (1965a) and Vesic (1965) suggest that the average shear strength mobilization along the failure surface of soil supporting a shallow foundation decreases with footing size. The decrease of the mobilized strength is due to the curvature of Mohr's strength envelope (Meyerhof, 1950; and De Beer, 1965a) and the progressive rupture along the failure surface (De Beer, 1965b; and Muhs, 1965). The relative compressibility of soils increases with footing size.

To illustrate the effect of footing size on bearing capacity, test results of 9 circular footings (n=0) listed in Table 4.4 are analyzed herein. For the footings tested, the prototype diameters are 0.044, 0.075, 0.20, 0.44, 1.50, 1.50, 1.75, 4.37 and 7.0 m; the bearing capacities are 160, 220, 480, 820, 1920, 1960, 2260, 4250 and 6150 kPa accordingly. The relationship between the bearing capacity and footing diameter is shown in Figure 4.14 and can be expressed by the equation of

$$q_u = 1480D^{0.72} \tag{4.22}$$

in which q_u is in kPa and D is in meters. The figure also presents the centrifuge test data of Kusakabe *et al.* (1991). Their values are smaller than those of the present study. This may be due to the fact that their experiments were carried out in sand at a lower density index of 82%.

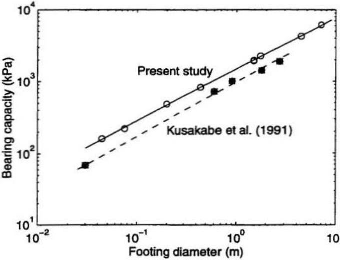

Figure 4.14: Bearing capacity versus circular footing diameter

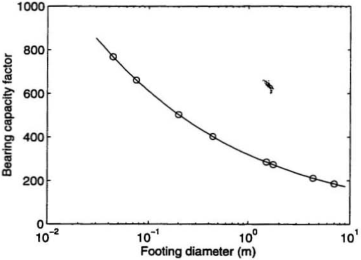

Figure 4.15: Bearing capacity factor (N_γ) versus circular footing diameter

Using Equation (4.21) and (4.22) and the test data in Figure 4.14, the calculated values of bearing capacity factor N_γ of the sand with a unit weight of $\gamma = 15.4$ kN/m^3 are given in Figure 4.15. The relationship between N_γ and D is

$$N_\gamma = 320D^{-0.28} \tag{4.23}$$

in which D is in meter. It can be seen that the value of N_γ decreases significantly with D, due mainly to the decrease of soil friction angle (ϕ) with increasing stress level and the phenomenon of progressive failure of soil.

In Figure 3.6, both the peak friction angle (ϕ_{max}) and the critical state friction angle (ϕ_{cs}) of the sand from triaxial shearing decrease with stress level. Their relationships with the mean stress

$$s = \frac{1}{2}(\sigma_1 + \sigma_3) \tag{4.24}$$

are given by Equations (3.22) and (3.23), respectively.

With the increase of footing size, the stress level in the soil supporting the footing increases. The stress level increase leads to a decrease of soil friction angle and the bearing capacity factor N_γ will be reduced. In order to take into account the curvature of the Mohr's envelope of failure, Meyerhof (1950) and De Beer (1965a) suggest that the value of ϕ corresponding to the mean normal stress along the failure surface should be used. For surface footings, Meyerhof (1950) suggests

$$\sigma_m = \frac{q_u}{10} \tag{4.25}$$

where σ_m is the mean normal stress along the failure surface. Using the above equation and the relationship among σ_m, σ_1 and σ_3 in the diagram of Mohr's envelope, the average value of s along the failure surface can be given roughly by

$$s = \frac{1}{2}(\sigma_1 + \sigma_3) = \frac{q_u(1 + \tan^2 \phi)}{10} \tag{4.26}$$

where ϕ is the average mobilized friction angle.

Table 4.6: Effect of footing size on values of average mobilized friction angle (ϕ)

D (m)	0.1	0.2	0.5	1.0	2.0	5.0	10.0
q_u (kPa)	282	465	899	1480	2440	4720	7770
ϕ_{max} (degree)	47.5	46.5	45.1	44.0	42.9	41.5	40.5
ϕ_{cs} (degree)	40.4	39.5	38.3	37.4	36.4	35.2	34.3

A rough quantitative evaluation of the effect of footing size on bearing capacity is shown in Table 4.6. When the diameter of a footing is given, the bearing capacity q_u can be calculated by Equation (4.22). Then using Equation (3.22) and (3.23) for friction angles, together with Equation (4.26) for estimating the mean stress level along the failure surface, the average ϕ_{max} and ϕ_{cs} corresponding to the mean stress level can be obtained, as in Table 4.6. When the footing diameter increases from 0.1 m to 10.0 m, the value of the mobilized peak friction angle (ϕ_{max}) decreases from 47.5° to 40.5° while the critical state friction angle (ϕ_{cs}) decreases from 40.4° to 34.3°. This is due to the increase of stress level in the soil. For a log-cycle increase of footing size, the friction angle of the sand is reduced by about 3 to 3.5°. This reduction of ϕ will lead to a decrease of N_γ by about 50%, if the theories for N_γ as listed in Table 2.1 are adopted. Therefore, the selection of the value of ϕ according to footing size (or stress level) is critical to evaluate the bearing capacity in practice.

In addition to stress level in soil, the phenomenon of progressive failure should also significantly affect the bearing capacity. In the classic bearing theories (Terzaghi, 1943; Meyerhof, 1950; and Sokolovski, 1960), in which soil is assumed to be rigid-perfectly plastic, the mobilization of shear strength along the failure surface is uniform. The soil elements at points A, B, and C (Figure 4.13) fail simultaneously when the foundation collapses. In reality, because soil is elasto-plastic, the failure of soil along the failure surface is a progressive process (Muhs, 1965; and De Beer, 1965b). The failure surface begins at point A and develops gradually to point C. The mobilization of shear strength is not uniform. When the foundation fails, the soil at C is just mobilized to its peak strength while the strength of the soil at A may be as low as the critical state strength. The average strength mobilization should be between the peak and the critical state values. The influence of progressive failure on the bearing capacity depends on the deformation before failure and will be more prominent when the settlement is large. When the size of a footing is given and the mean stress level has been estimated, the difference between the values of bearing capacity from ϕ_{max} and ϕ_{cs} will be very large.

It should be mentioned herein that the values of ϕ_{max} and ϕ_{cs} in Table 4.6 are only rough estimations. The purpose of the quantitative analysis above is intended to provide a clearer understanding of the influence of footing size and stress level on bearing capacity. In engineering practice, the engineer must be very careful to select soil strength parameter ϕ. The error caused by improper selection of ϕ in estimating the bearing capacity may be very serious.

It is difficult to conduct bearing capacity tests of very large foundations. As seen in Figure 4.14, the bearing capacity increases with foundation size. Conducting bearing capacity tests for very large foundations is also very costly. To the best knowledge of the author, only a few test results of ultimate bearing capacity of foundations with dimensions over 7 m are available in the literature. If Equation (4.22) obtained from the test data in Figure 4.14 is used for very large footings, the roughly estimated bearing capacities will be 7.8, 12.8, 17.1 and 24.7 MPa when the footing diameters are 10, 20, 30 and 50 m respectively. Therefore, for conducting bearing capacity test of a foundation with a dimension of over, say, 20 m: (1) It is difficult to apply and/or react the huge load to cause the foundation to fail, even in a centrifuge at 160g; (2)

Because of the high pressure in the soil under the foundation, soil particles will be crushed (Hardin, 1985; and Lade and Yamamuro, 1996) and will behave differently; (3) As the failure mode tends to move from general shear failure to punching shear failure with the increase of foundation size, the relative settlement of foundations at failure increases with foundation size. For very large foundations, the ultimate bearing capacity may not be a problem; the settlement may control the design.

4.5 Axially Loaded Ring Footings

The geometry of a ring footing (Figure 1.1) can be defined by the outside diameter (D) and the inside diameter (d), or by the outside diameter and the ring radii ratio (n). Therefore, the behaviour of the footing depends on the combination of its geometric parameters D and n and the value of vertical load, Q.

4.5.1 Load and settlement

In order to study the bearing capacity of ring footings, centrifuge tests at accelerations of 10, 40, 100 and 160g were conducted using 7 model rings with a constant area of 15.0 cm^2. The ring radii ratios (n) were 0, 0.2, 0.35, 0.5, 0.7, 0.8 and 0.9, and the outside diameters of the model footings were 43.7, 44.6, 46.7, 50.5, 61.2, 72.8 and 100.3 mm respectively. For n=0, the prototype diameters (D) of the circular footings were 0.44, 1.75, 4.37 and 7.0 m when the centrifuge accelerations were 10, 40, 100 and 160g respectively. Figures 4.16 to 4.19 present the relationships between the load and the settlement of the constant area footings with various n tested at the aforementioned acceleration levels.

At an acceleration of 10g, each curve in Figure 4.16 has a peak load; all the footings at various values of n have failed in general shear. The failure load increases when n changes from 0 to 0.35. After the maximum value at n=0.35, the failure load decreases.

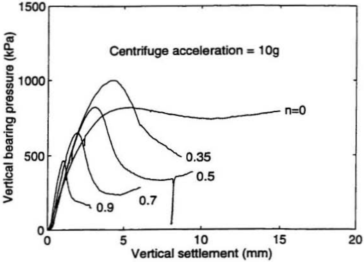

Figure 4.16: Load versus settlement of ring footings of 15 cm^2 in area at 10 gravities

It is also seen that the settlement required to reach the failure load decreases with increasing ring radii ratio. The failure mode becomes more and more general when the value of n is increased. Those features of the influence of n on the behaviour of load, settlement and failure mode are also observed at acceleration levels of 40, 100 and 160g as shown in Figure 4.17 to 4.19.

The failure mode is also affected by the level of acceleration (or footing size). For the circular footings (n=0), the failure mode of the footing at 10g was general shear; for the footings at 40, 100 and 160g, the failure mode is considered local shear failure. For n=0.2, the footing at 10g fails in general shear (there is a peak load) while the footing at 160g is in local shear failure. When the value of n is from 0.35 to 0.9, all the footings are in general shear failure mode, regardless of the acceleration level. At each value of n, the failure mode is more general for a footing at a smaller acceleration level.

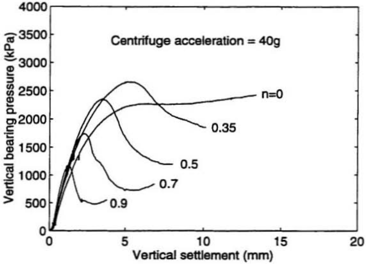

Figure 4.17: Load versus settlement of ring footings of 15 cm^2 in area at 40 gravities

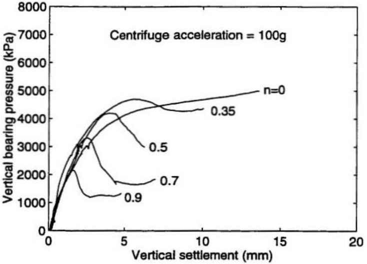

Figure 4.18: Load versus settlement of ring footings of 15 cm^2 in area at 100 gravities

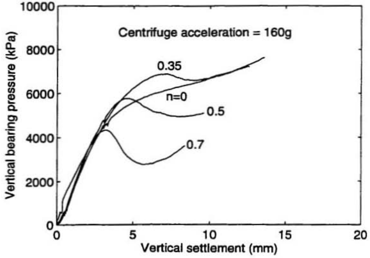

Figure 4.19: Load versus settlement of ring footings of 15 cm^2 in area at 160 gravities

4.5.2 Bearing capacity with ring radii ratio

The bearing capacity of the ring footings with a constant area of 15 cm^2 at different acceleration levels are shown in Figure 4.20. It is observed that the bearing capacity increases with acceleration level (footing size). At each acceleration level, the bearing capacity increases with ring radii ratio until n reaches a value of approximately 0.35. After this point, the bearing capacity decreases with n. It is noted that the bearing capacity of a ring footing with n=0.9 is about one half of that of a circular footing with the same area.

The increase of bearing capacity in small n cases is believed to be due to the effect of soil arching under the center part of a footing. When n is very small, the footing with the soil in the center region behaves like a solid footing with a size equivalent to the outside diameter of the ring footing. Hence the bearing capacity is increased. With the increase of the ring radii ratio, the effect of arching is reduced and finally

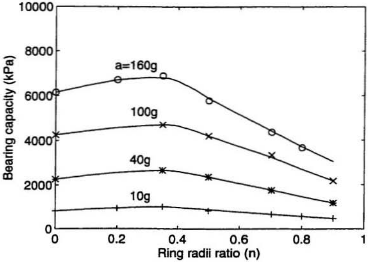

Figure 4.20: Bearing capacity versus ring radii ratio

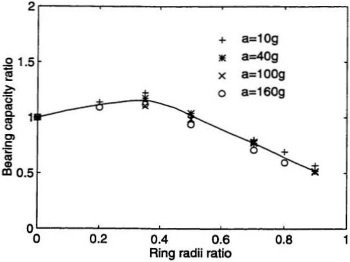

Figure 4.21: Bearing capacity ratio versus ring radii ratio

Table 4.7: Bearing capacity ratio of constant area ring footings

Ring radii ratio, n	0	0.2	0.35	0.4	0.5	0.6	0.7	0.8	0.9
Bearing capacity ratio, B_r	1.0	1.11	1.15	1.13	1.02	0.90	0.77	0.64	0.52

disappeared when n is increased to a certain extent. Therefore, the bearing capacity becomes smaller.

The bearing capacity of a ring footing can be represented by a bearing capacity ratio, B_r, defined as

$$B_r = \frac{q_u}{q_{uc}} \tag{4.27}$$

where q_u is the bearing capacity of a ring footing and q_{uc} is the bearing capacity of a circular footing with the same area. For a circular footing (n=0), B_r=1.

Values of B_r of constant area ring footings plotted against ring radii ratio are presented in Figure 4.21. They are also listed in Table 4.7 for convenience of use. It is observed that the variation of B_r at different acceleration levels is very small. This suggests that B_r is independent of acceleration level (or prototype size of footings). The bearing capacity ratio has a maximum value of about 1.15 (average) when n is approximately 0.35. At n=0.9, B_r is about 0.52. Using the curve shown in Figure 4.21, the B_r value can be estimated according to the n value of a ring footing. The bearing capacity of a ring footing can thus be calculated using Equation (4.27), once the bearing capacity of the circular footing with the same area is known. This procedure for estimating the bearing capacity of ring footings is practical because the bearing capacity of circular footings can be obtained using generally accepted experimental data and theories available in the literature.

4.6 Eccentrically Loaded Ring Footings

4.6.1 Background and theory

For a strip footing subjected to a vertical load with an eccentricity of e, when the pressure distribution is assumed to be linear, the maximum and minimum normal pressures on the footing (Das, 1990) are in the forms of

$$p_{max} = \frac{Q}{B}\left(1 + \frac{6e}{B}\right) \tag{4.28}$$

$$p_{min} = \frac{Q}{B}\left(1 - \frac{6e}{B}\right) \tag{4.29}$$

where B is the footing width, Q is the load applied on a unit length, and e is load eccentricity.

It is noticed that when e is equal to $B/6$, p_{min} becomes zero. When e is greater than $B/6$, p_{min} will be negative. There will be a separation between the footing and the soil because soil cannot take significant tension. In such a case, the maximum pressure is calculated from

$$p_{max} = \frac{4Q}{3(B - 2e)} \tag{4.30}$$

and p_{min} is assumed to be zero in the area where p_{min} obtained using Equation (4.29) is negative.

The bearing capacity of an eccentrically loaded strip footing can be estimated by a so-called effective width method (Meyerhof, 1953). The effective width of the footing is

$$B' = B - 2e \tag{4.31}$$

Using B' instead of B in Equation (2.23), the bearing capacity of the footing can be obtained (in calculating d_c, d_q and d_γ, B should be used). Theoretical and experimental studies indicate that this method for taking into account load eccentricity is on the safe side for bearing capacity estimation (Vesic, 1975). However, the effective width method is widely accepted in practice.

Another way to account for the eccentricity is to use Meyerhof's reduction factor method. The bearing capacity reduction factor (R_e) is defined as

$$R_e = \frac{q_u}{q_{uo}} \tag{4.32}$$

where q_u is the averaged bearing capacity of an eccentrically loaded footing, and q_{uo} is the bearing capacity of the same footing under axial loading. The relationship between R_e and eccentricity (e) can be expressed as

$$R_e = 1 - (e/B)^m \tag{4.33}$$

where B represents the width of a strip footing or the diameter of a circular footing; m is a constant having a value of about 0.5. For a strip footing on a dense sand, Aiban and Znidarcic (1991) obtained m=0.42. It can be deduced that the effective width method is equivalent to a reduction factor method when the value of R_e is equal to (1-2e/B). The reduction factor method is more suitable to fit experimental data. It will be used in the following analysis.

4.6.2 Loading and settlement

When a footing on soil is loaded eccentrically, the footing will develop a vertical displacement (s) at the loading point and a rotation angle (θ), as shown in Figure 4.22. With the eccentric loading of the footing, the rotation angle is expected to increase.

Figures A.1 to A.20 in Appendix A show the the average vertical loading pressure and the rotation angle with settlement of eccentrically as well as axially loaded ring footings with a constant area of 15cm^2, tested in centrifuge at 100 gravities. It can be seen that all the axially loaded footings (e=0) with ring radii ratios (n) of 0, 0.35, 0.5,

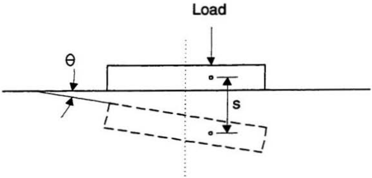

Figure 4.22: Deformation pattern of eccentrically loaded footing

0.7 and 0.9 have not rotated during loading; the rotation angles are about zero. The footings were penetrated into sand without rotation.

For the footings with eccentricity ratios (e/D) of 0.075, 0.15, 0.25 and 0.375, the rotation angles increase with the penetration of the footings into sand. For most of the footings, the rate of the increase of rotation angle is increased after the points where the failure loads are approached. It can be seen that the footing rotation angle at failure increases slightly with eccentricity. For n=0, the rotation angles are about 6, 7, 7 and 10 degrees when the eccentricity ratios are 0.075, 0.15, 0.25 and 0.375 respectively. The effect of ring radii ratio on the rotation angle is more significant. The average rotation angles at failure loads are roughly 8, 6, 3, 2 and 1 degrees for the footings with ring radii ratios of 0, 0.35, 0.5, 0.7 and 0.9 respectively. When the value of n is greater than 0.5, the rotation angle of eccentrically loaded ring footings at failure is small.

The influence of eccentricity on the relationship between the average vertical loading

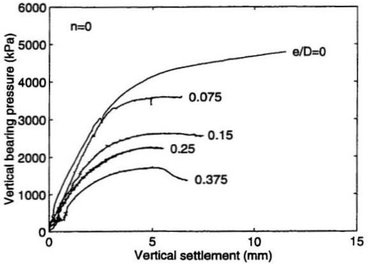

Figure 4.23: Load and settlement of eccentrically loaded footings (n=0)

and the settlement is presented in Figure 4.23 to 4.25 when the ring radii ratios are 0, 0.5 and 0.9. It can be seen that for each n value, the vertical bearing capacity of footings decreases significantly with increasing eccentricity. In Figure 4.23 where n=0, the slope of the loading-settlement curves is reduced when the eccentricity is increased from 0 to 0.375, while the bearing capacity has changed from approximately 4250 to 1700 kPa. The settlement required to reach the failure load decreases from about 6 to 3 mm. With the increase of eccentricity, the failure mode moves towards general shear failure.

In Figure 4.24 when n=0.5, the loading-settlement curves approximately follow the sample path at the initial stage of loading. They begin to diverge when failure occurs. The settlements at failure decrease from about 4 to 2 mm when the eccentricity ratio (e/D) is increased from 0 to 0.375. In Figure 4.25 for n=0.9, the loading-settlement pattern is also different. For e/D=0.075, 0.15, 0.25 and 0.375, the footings fail at a

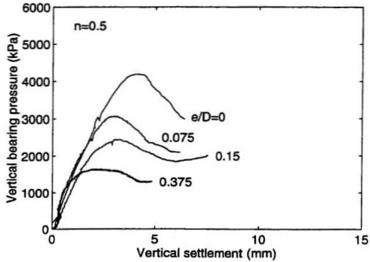

Figure 4.24: Load and settlement of eccentrically loaded footings (n=0.5)

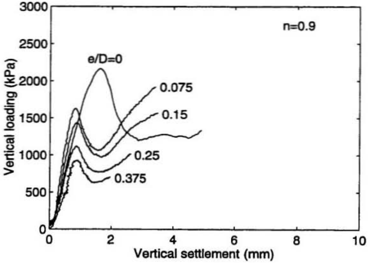

Figure 4.25: Load and settlement of eccentrically loaded footings (n=0.9)

same settlement of about 0.7 mm, while the footing with e/D=0 fails at a settlement of about 1.7 mm. The loading-settlement pattern is influenced by the eccentricity of loads and the ring radii ratio of footings.

4.6.3 Bearing capacity with eccentricity

Figures 4.23 to 4.25 indicate that the bearing capacity of ring footings decreases with increasing ring radii ratio and increasing loading eccentricity. The variations of bearing capacities of 20 footings listed in Table 4.5 with eccentricity at ring radii ratios of 0, 0.35, 0.5, 0.7 and 0.9 are presented in Figure 4.26. Analysis of the data in this figure indicates that the relationship of the bearing capacity and the eccentricity of the ring footings can be well expressed using the reduction factor method. The bearing capacity reduction factor (R_e) calculated using Equation (4.32) at different values of ring radii ratio (n) is shown in Figure 4.27. It can be seen that the relationship between the reduction factor and the loading eccentricity ratio (e/D) is independent of n. By linear regression of the data in the figure, the reduction factor can be written as

$$R_e = 1 - (e/D)^{0.53} \tag{4.34}$$

for all footings with different ring radii ratio, where D represents the outside diameter of a ring footing (a circular footing is treated as a special ring footing with n=0). As seen in Figure 4.27, the reduction factor for the ring footings is slightly greater than that obtained by Aiban and Znidarcic (1995) for strip footings.

Using the bearing capacity ratio (B_r), the reduction factor (R_e), the bearing capacity of an eccentrically loaded footing on the dense sand with a given ring radii ratio (n) can be evaluated. Using Equation (4.32), the bearing capacity of an eccentrically loaded footing is given by

$$q_u = R_e q_{uo} \tag{4.35}$$

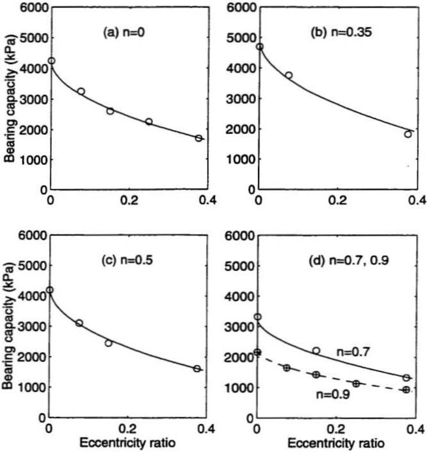

Figure 4.26: Bearing capacity versus eccentricity ratio (e/D) of constant area ring footings

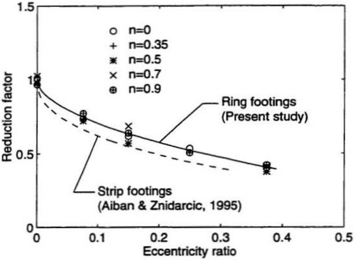

Figure 4.27: Bearing capacity reduction factor (R_e) versus eccentricity ratio (e/D) of constant area ring footings

where R_e is the reduction factor calculated by Equation (4.34) with a given (e/D); q_{uo} is the bearing capacity of the ring footing under axial loading, which is given, using Equation (4.27), by

$$q_{uo} = B_r q_{uc} \tag{4.36}$$

A combination of the above two equations yields the bearing capacity of an eccentrically loaded ring footing as

$$q_u = R_e B_r q_{uc} \tag{4.37}$$

in which the bearing capacity ratio (B_r), depending on the value of n, is shown in Figure 4.21; q_{uc} is the bearing capacity of an axially loaded circular footing with the same area, which can be obtained using Equation (4.22). The procedure for estimating the bearing capacity of a ring footing under eccentric loads using R_e, B_r and q_{uc} is very convenient and practical.

4.7 Concluding Remarks

This chapter has introduced the background and principle of centrifuge modelling for geotechnical application. The centrifuge test equipment and procedure have been presented. A raining technique for the preparation of sand samples has been developed and used in tests, resulting in a density index of 90%. The quality of sand samples has been monitored by centrifuge cone penetration tests. Over 40 footing tests in centrifuge with accelerations of up to 160 gravities have been conducted to investigate the effect of footing size, ring radii ratio and loading eccentricity on bearing capacity. Model tests have been verified using the principle of modelling of models.

For circular footings, the bearing capacity increases linearly with prototype footing size in a double-log scale diagram. For a tested footing with a prototype diameter of 7.0 m, the measured bearing capacity is as high as 6150 kPa. It is found that the bearing capacity factor N_γ decreases with footing size, due to the effect of progressive failure and the reduction of soil friction angle with stress level. When the footing diameter is increased from 0.1 to 10 m, the estimated value of N_γ is reduced from about 610 to 170. For a log-cycle increase of footing size, the estimated reduction of average mobilized soil friction angle is approximately 3 to 3.5°. It is observed that with the increase of footing size, the failure mode of footings tends to move from general shear failure to local shear failure.

Constant area ring footings, with ring radii ratios of 0, 0.2, 0.35, 0.5, 0.7, 0.8 and 0.9, have been tested in centrifuge at accelerations of 10, 40, 100 and 160 gravities. For the axially loaded footings, the bearing capacity increases with prototype footing size. At a certain acceleration level, the bearing capacity increase slightly with ring radii ratio (n) when n is from 0 to about 0.35, due to the arching effect of soil under the footing. When n is greater than 0.35, the bearing capacity decreases significantly with the ring radii ratio. For a footing with n=0.9, the bearing capacity is about 52% of that of a circular footing with the same area. It is shown that the bearing of a ring footing can be related to the bearing capacity of a corresponding circular footing with the same area by using a bearing capacity ratio (B_r). The value of B_r is related only to the ring radii ratio, independent of footing size. Using the bearing capacity ratio, it is very convenient to estimate the bearing capacity of a ring footing, because the bearing capacity of a circular footing can be obtained using the available experimental data and bearing capacity theories.

For the eccentrically loaded footings, the bearing capacity decreases with loading eccentricity. It is shown that the bearing capacity of an eccentrically loaded ring footing can be expressed in terms of a reduction factor and the bearing capacity of the footing under axial loading. The bearing capacity reduction factor (R_e) has been obtained by analyzing the test data of footings loaded with eccentricities of 0, 0.075, 0.15, 0.25 and 0.375 at various ring radii ratios. It is found that the value of R_e is related only to loading eccentricity, independent of the ring radii ratio of footings.

It is shown that the bearing capacity of an eccentrically loaded ring footing can be estimated using a reduction factor (R_e), a bearing capacity ratio (B_r) and the bearing capacity of an axially loaded circular footing. This procedure is very practical. The centrifuge test results are considered very satisfactory.

Chapter 5

Analysis of Footing Size Effect using Method of Characteristics

5.1 Introduction

Using the method of characteristics (slip-line method) for bearing capacity, equilibrium equations with yield condition (usually Mohr-Coulomb criterion) and stress boundary conditions are satisfied in the soil domain of uncontained plastic flow near a footing. A set of differential equations of plastic equilibrium is established to investigate the stresses in the soil at the instant of impending failure. The equations can be solved by finite difference approximation. The bearing capacity obtained is the average vertical pressure acting on the footing.

Sokolovskii (1960) used the method of characteristics for the solution of bearing capacity of a strip footing. Shield (1955) extended this technique for an axisymmetric footing on a Tresca material. Cox *et al.* (1961) applied it for a smooth, rigid footing on weightless Mohr-Coulomb materials. Cox (1962) used this technique for a circular footing on soils with weight, by putting $c^{*} = c + \sigma_o \tan\phi$ (σ_o is the atmospheric pressure) and introducing a dimensionless parameter $G = \gamma B/(2c^{*})$. The average bearing capacity pressure is a function of both G and ϕ. The solution of Cox (1962) can directly account for the soil cohesion, self-weight and surcharge without superposition.

The unusual assumption of applying the atmospheric pressure as a surcharge to the soil surface may be due to the misunderstanding of the principle of effective stress. However, the formulation for the solution is mathematically correct.

Larkin (1968) presents a detailed formulation of the method of characteristics for the bearing capacity of very shallow circular and strip footings, in which the frictional effect of the soil above the footing base has been taken into account. The stress variables are normalized by $0.5B\gamma$ and the co-ordinates by $0.5B$ for both plane strain and axisymmetric cases. Since the footings are assumed to be frictionless, the characteristics lines are extended to the footing bases. The failure pattern is similar to Hill's mechanism. The values of N_γ of a surface strip footing are 15.7 and 87 when the ϕ is equal to 30° and 40° respectively. The calculated bearing capacity of footings on cohesionless soils is very sensitive to the embedment depth. For a circular footing, an embedment depth of 0.09 to 0.13 of the footing diameter will result in a bearing capacity increase of 100%. However, the calculated results of Graham and Stuart (1971) show a much smaller increase of bearing capacity with depth. They considered that neglecting the shear resistance of sand above the footing base would not cause a significant error for very shallow footings. Analysis of Hansen and Christensen (1969) also showed an increase of bearing capacity with depth, but not as large as that indicated by Larkin (1968).

When a footing base is rough (δ=ϕ), experimental evidence (Biarez *et al.*, 1961; Gorbunov-Possadov, 1965; Ko and Davidson, 1973) shows that there is a wedge-shaped rigid (elastic) zone of soil under the footing. In the characteristics analysis, Graham and Stuart (1971) define the rigid wedge after Terzaghi (1943); the edge of the wedge is straight and inclined at ϕ to the horizontal. The results agree with those of Meyerhof (1955). When ϕ=35°, the value of N_γ is 54.7. A similar rigid wedge is also assumed by Graham and Hoven (1986) in their footing analysis using a critical state model.

For a rough strip footing, Lundgren and Mortensen (1953) present the solution of N_γ using a one-wedge failure mechanism. The α-line bounding the rigid wedge is tangential to the base at the footing edge. For ϕ=30°, the calculated N_γ is 14.8. A similar rigid wedge was assumed by Gorbunov-Possadov (1965) and an N_γ value of 192 was derived for ϕ=40°. The failure mechanism of Lundgren and Mortensen (1953) has been employed by Hansen (1970) to derive the formula for N_γ as expressed by Equation (2.19).

Based on the principle presented by Lundgren and Mortensen (1953), Hansen and Christensen (1969) investigated the effect of base friction on N_γ for surface strip footings. The value of N_γ increases with base friction angle (δ); for a certain ϕ, N_γ of a smooth footing ($\delta = 0$) is half of N_γ of a fully rough footing ($\delta = \phi$). When $\phi = 30°$, N_γ is 15 for a rough footing. For $\phi \leq 45°$, if $\delta \geq 20°$ a footing can be assumed to be rough for deriving N_γ.

A more recent investigation of the bearing capacity of strip and circular footings using the method of characteristics was carried out by Bolton and Lau (1993). For a rough footing, a trapped rigid wedge underneath the footing is assumed; the wedge angle with the horizontal footing base is taken as $(\pi/4 + \phi/2)$. With this assumption, the resultant stress at the tip of the wedge is always vertical and symmetry at the centerline is conserved. For ϕ=30°, the value of N_γ is 23.6 for a strip footing and is 31.9 for a circular footing. N_γ is higher for circular footings than for strip footings when $\phi \geq 20°$. For smooth footings, N_γ of circular footings is greater when ϕ is greater than 33°.

The method of characteristics can obtain the combined bearing capacity factor $N_{\gamma q}$ due to the contributions of surcharge (q) and soil weight. For a strip footing, $N_{\gamma q}$ can be expressed as

$$N_{\gamma q} = \frac{q_u}{0.5\gamma B(1+\bar{q})} = \frac{\bar{q}N_q + N_\gamma}{1+\bar{q}} \tag{5.1}$$

where

$$\bar{q} = \frac{q}{0.5\gamma B} \tag{5.2}$$

A finite surcharge must be applied in analysis for Mohr-Coulomb material with no cohesion (Graham, 1968; and Lau, 1988), because the condition of zero surcharge causes some difficulties at the singularity at the footing edge (Graham and Hoven. 1986). The computation for N_γ is started by assuming a constant surcharge at the footing base level. As described by Graham and Stuart (1971), a solution for N_γ is obtained by increasing the footing size until the surcharge has no significant effect on the calculated bearing capacity. It is shown that when $\bar{q}$ is smaller than 0.001, $N_{\gamma q}$ converges to N_γ (Graham and Stuart, 1971; Bolton and Lau, 1993). In contrast, N_q is obtained for $\bar{q}$ values exceeding 1000.

This chapter presents a study of the effect of footing size on the bearing capacity of circular footings on a dense sand using the method of characteristics. The analysis will be carried out using both variable friction angles and an equivalent constant friction angle for each footing.

5.2 Governing Equations and Formulation

5.2.1 Basic equations

In the case of axisymmetry about the z-axis in an r-z-θ coordinate system, the stress components are σ_r, σ_θ, σ_z and τ_{rz}. The circumferential stress σ_θ is a principal stress. The other two principal stresses (compression is positive) are

$$\sigma_1 = \frac{1}{2}(\sigma_r + \sigma_z) + [\frac{1}{4}(\sigma_r - \sigma_z)^2 + \tau_{rz}^2]^{1/2} \tag{5.3}$$

$$\sigma_3 = \frac{1}{2}(\sigma_r + \sigma_z) - [\frac{1}{4}(\sigma_r - \sigma_z)^2 + \tau_{rz}^2]^{1/2} \tag{5.4}$$

Haar and Von Karman assumed that σ_θ is equal to one of the other two principal stresses (Chen, 1975). This assumption is safe (Lau, 1988). Cox *et al.* (1961) pointed out that the Haar and Von Karman hypothesis is quite general and applicable. The value of σ_θ is herein taken equal to the smaller principal stress, that is

$$\sigma_\theta = \sigma_3 < \sigma_1 \tag{5.5}$$

The Coulomb yield criterion and the two equilibrium equations are given by

$$\sigma_1 - \sigma_3 = 2c\cos\phi + (\sigma_1 + \sigma_3)\sin\phi \tag{5.6}$$

$$\frac{\partial \sigma_r}{\partial r} + \frac{\partial \tau_{rz}}{\partial z} + m\frac{\sigma_r - \sigma_\theta}{r} = 0 \tag{5.7}$$

$$\frac{\partial \tau_{rz}}{\partial r} + \frac{\partial \sigma_z}{\partial z} + m\frac{\tau_{rz}}{r} = \gamma \tag{5.8}$$

in which $m = 1$ is for circular footing and $m = 0$ is for strip footing. Equations (5.5)-(5.8) provide four equations for the four unknown stresses so that the problem is statically determinate.

Using the Coulomb yield criterion and Haar and Von Karman hypothesis, the four stresses are expressed as (Tan, 1990)

$$\sigma_r = \sigma(1 - \sin\phi\cos 2\psi) - \sigma_c \tag{5.9}$$

$$\sigma_z = \sigma(1 + \sin\phi\cos 2\psi) - \sigma_c \tag{5.10}$$

$$\tau_{zr} = \sigma\sin\phi\sin 2\psi \tag{5.11}$$

$$\sigma_\theta = \sigma_3 = \sigma(1 - \sin\phi) - \sigma_c \tag{5.12}$$

where ψ is the inclination of the direction of σ_1 from the z-axis, as shown in Figure 5.1; σ and σ_c are defined by

$$\sigma = \frac{\sigma_1 + \sigma_3}{2} + \sigma_c \tag{5.13}$$

$$\sigma_c = \frac{c}{\tan\phi} \tag{5.14}$$

Differentiating Equations (5.9)-(5.12) yields

$$\frac{\partial \sigma_r}{\partial r} = (1 - \sin\phi\cos 2\psi)\frac{\partial \sigma}{\partial r} + 2\sigma\sin\phi\sin 2\psi\frac{\partial \psi}{\partial r} \tag{5.15}$$

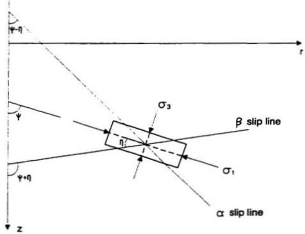

Figure 5.1: Direction of principal stresses

$$\frac{\partial \sigma_z}{\partial z} = (1 + \sin\phi \cos 2\psi)\frac{\partial \sigma}{\partial z} - 2\sigma \sin\phi \sin 2\psi \frac{\partial \psi}{\partial z} \tag{5.16}$$

$$\frac{\partial \tau_{rz}}{\partial r} = \sin\phi \sin 2\psi \frac{\partial \sigma}{\partial r} + 2\sigma \sin\phi \cos 2\psi \frac{\partial \psi}{\partial r} \tag{5.17}$$

$$\frac{\partial \tau_{rz}}{\partial z} = \sin\phi \sin 2\psi \frac{\partial \sigma}{\partial z} + 2\sigma \sin\phi \cos 2\psi \frac{\partial \psi}{\partial z} \tag{5.18}$$

Substituting the above equations into the two equilibrium equations results in a system of governing equations in terms of r, z, σ and ψ,

$$\begin{aligned}(1 - \sin\phi \cos 2\psi)\frac{\partial \sigma}{\partial r} + 2\sigma \sin\phi \sin 2\psi \frac{\partial \psi}{\partial r} + \sin\phi \sin 2\psi \frac{\partial \sigma}{\partial z} \\ + 2\sigma \sin\phi \cos 2\psi \frac{\partial \psi}{\partial z} + m\frac{\sigma}{r} \sin\phi (1 - \cos 2\psi) = 0\end{aligned} \tag{5.19}$$

$$\begin{aligned}\sin\phi \sin 2\psi \frac{\partial \sigma}{\partial r} + 2\sigma \sin\phi \cos 2\psi \frac{\partial \psi}{\partial r} + (1 + \sin\phi \cos 2\psi)\frac{\partial \sigma}{\partial z} \\ - 2\sigma \sin\phi \sin 2\psi \frac{\partial \psi}{\partial z} + m\frac{\sigma}{r} \sin\phi \sin 2\psi = \gamma\end{aligned} \tag{5.20}$$

These are two nonlinear differential equations. Under given stress boundary conditions, the equations can be solved for bearing capacity using finite difference techniques.

In Equations (5.19) and (5.20), σ and ψ are functions of r and z. Therefore, the variation equations of σ and ψ can also be expressed as

$$d\sigma = \frac{\partial \sigma}{\partial r} dr + \frac{\partial \sigma}{\partial z} dz \tag{5.21}$$

$$d\psi = \frac{\partial \psi}{\partial r} dr + \frac{\partial \psi}{\partial z} dz \tag{5.22}$$

Equations (5.19)-(5.22) can be written in matrix form as

$$\underline{A}\,\underline{x} = \underline{b} \tag{5.23}$$

where matrixes $\underline{A}$, $\underline{x}$ and $\underline{b}$ are in the forms

$$\underline{A} = \begin{pmatrix} 1 - \sin\phi\cos 2\psi & 2\sigma\sin\phi\sin 2\psi & \sin\phi\sin 2\psi & 2\sigma\sin\phi\cos 2\psi \\ \sin\phi\sin 2\psi & 2\sigma\sin\phi\cos 2\psi & 1 + \sin\phi\cos 2\psi & -2\sigma\sin\phi\sin 2\psi \\ dr & 0 & dz & 0 \\ 0 & dr & 0 & dz \end{pmatrix} \tag{5.24}$$

$$\underline{x} = \begin{pmatrix} \partial\sigma/\partial r \\ \partial\psi/\partial r \\ \partial\sigma/\partial z \\ \partial\psi/\partial z \end{pmatrix} \tag{5.25}$$

$$\underline{b} = \begin{pmatrix} -m\sin\phi(1 - \cos 2\psi)\sigma/r \\ \gamma - m(\sin\phi\sin 2\psi)\sigma/r \\ d\sigma \\ d\psi \end{pmatrix} \tag{5.26}$$

As these equations are hyperbolic, the solution for $\underline{x}$ is not unique; the determinant of $\underline{A}$ is zero. By using $\det\underline{A} = 0$, two families of characteristic lines can be obtained as

α-characteristics:

$$\frac{dr}{dz} = \tan(\psi + \eta) \tag{5.27}$$

β-characteristics:

$$\frac{dr}{dz} = \tan(\psi - \eta) \tag{5.28}$$

where $\eta = \pi/4 - \phi/2$.

Along the two families of characteristics, the governing equations (5.19) and (5.20) become two ordinary differential equations, which can be obtained by replacing a column of $\underline{A}$ by $\underline{b}$ and setting the determinant to zero (Tan, 1990). Therefore the relationships of σ and ψ along the characteristics are expressed as

$$d\sigma + 2\sigma \tan\phi d\psi + m\frac{\sigma}{r}[\sin\phi dr + \tan\phi(\sin\phi - 1)dz] = \gamma(dz - \tan\phi dr) \qquad (5.29)$$

along an α-characteristics; and

$$d\sigma - 2\sigma \tan\phi d\psi + m\frac{\sigma}{r}[\sin\phi dr - \tan\phi(\sin\phi - 1)dz] = \gamma(dz + \tan\phi dr) \qquad (5.30)$$

along a β-characteristics.

5.2.2 Computation procedure

For the convenience of computation as adopted by Larkin (1968), the variables σ, r and z are normalized as

$$\bar{\sigma} = \frac{\sigma}{0.5\gamma B}, \quad \bar{r} = \frac{r}{0.5B}, \quad \bar{z} = \frac{z}{0.5B} \qquad (5.31)$$

where γ is soil unit weight, B represents the width of a strip footing or the diameter of a circular footing.

In Figure 5.2, if the variables $\bar{r}_i$, $\bar{z}_i$, $\bar{\sigma}_i$ and ψ_i at point i and $\bar{r}_j$, $\bar{z}_j$, $\bar{\sigma}_j$ and ψ_j at point j are known, the variables $\bar{r}$, $\bar{z}$, $\bar{\sigma}$ and ψ at point w can be approximately determined using Equations (5.27)-(5.30). Equations (5.27) and (5.28) can be rewritten as

$$\bar{r} - \bar{r}_i = (\bar{z} - \bar{z}_i)\tan(\psi_i + \eta) \qquad (5.32)$$

$$\bar{r} - \bar{r}_j = (\bar{z} - \bar{z}_j)\tan(\psi_j - \eta) \qquad (5.33)$$

and Equations (5.29) and (5.30) can be rewritten as

$$\bar{\sigma} - \bar{\sigma}_i + 2\bar{\sigma}_i \tan\phi(\psi - \psi_i) = \bar{z} - \bar{z}_i - \tan\phi(\bar{r} - \bar{r}_i)$$

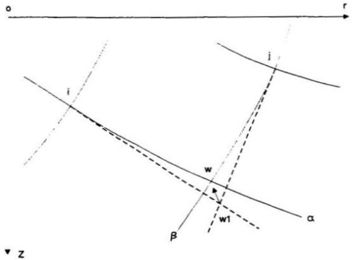

Figure 5.2: Computation scheme of point w from known points i and j

$$- m\frac{2\bar{\sigma}_i}{\bar{r}+\bar{r}_i}[\sin\phi(\bar{r}-\bar{r}_i) + \tan\phi(\sin\phi - 1)(\bar{z}-\bar{z}_i)] \tag{5.34}$$

$$\bar{\sigma} - \bar{\sigma}_j - 2\bar{\sigma}_j \tan\phi(\psi - \psi_j) = \bar{z} - \bar{z}_j + \tan\phi(\bar{r} - \bar{r}_j)$$
$$- m\frac{2\bar{\sigma}_j}{\bar{r}+\bar{r}_j}[\sin\phi(\bar{r}-\bar{r}_j) - \tan\phi(\sin\phi - 1)(\bar{z}-\bar{z}_j)] \tag{5.35}$$

From Equations (5.32) and (5.33), the variables $\bar{r}$ and $\bar{z}$ at point w can be approximately determined as

$$\bar{r} = \frac{(\bar{z}_i - \bar{z}_j)\tan(\psi_i + \eta)\tan(\psi_j - \eta) - \bar{r}_i \tan(\psi_j - \eta) + \bar{r}_j \tan(\psi_i + \eta)}{\tan(\psi_i + \eta) - \tan(\psi_j - \eta)} \tag{5.36}$$

$$\bar{z} = \frac{\bar{z}_i \tan(\psi_i + \eta) - \bar{z}_j \tan(\psi_j - \eta) - \bar{r}_i + \bar{r}_j}{\tan(\psi_i + \eta) - \tan(\psi_j - \eta)} \tag{5.37}$$

and Equation (5.34) and (5.35) can be solved for $\bar{\sigma}$ and ψ as

$$\bar{\sigma} = \frac{a_1\bar{\sigma}_j + a_2\bar{\sigma}_i}{\bar{\sigma}_i + \bar{\sigma}_j} \tag{5.38}$$

$$\psi = \frac{a_1 - a_2}{2(\bar{\sigma}_i + \bar{\sigma}_j)\tan\phi} \tag{5.39}$$

where the parameters a_1 and a_2 are expressed as

$$\begin{aligned} a_1 = \bar{z} - \bar{z}_i - \tan\phi(\bar{r} - \bar{r}_i) + \bar{\sigma}_i(1 + 2\psi_i \tan\phi) \\ - m\frac{2\bar{\sigma}_i}{\bar{r} + \bar{r}_i}[\sin\phi(\bar{r} - \bar{r}_i) + \tan\phi(\sin\phi - 1)(\bar{z} - \bar{z}_i)] \end{aligned} \tag{5.40}$$

$$\begin{aligned} a_2 = \bar{z} - \bar{z}_j + \tan\phi(\bar{r} - \bar{r}_j) + \bar{\sigma}_j(1 - 2\psi_j \tan\phi) \\ - m\frac{2\bar{\sigma}_j}{\bar{r} + \bar{r}_j}[\sin\phi(\bar{r} - \bar{r}_j) - \tan\phi(\sin\phi - 1)(\bar{z} - \bar{z}_j)] \end{aligned} \tag{5.41}$$

Because the characteristics are usually curved, the solution can be improved using iteration technique by putting $\psi_i = (\psi + \psi_i)/2$ and $\psi_j = (\psi + \psi_j)/2$ in calculating $\bar{r}$ and $\bar{z}$. By repeating the process, ψ and $\bar{\sigma}$ will converge to ψ_w and $\bar{\sigma}_w$ as the number of iterations increases (Sokolovskii, 1960).

5.3 Boundary Conditions

5.3.1 Smooth footings

The boundary conditions for the method of characteristics are related to the roughness of the footing bases. A perfectly smooth footing as shown in Figure 5.3, fails in Hill mechanism. As there is no horizontal shear stress between the footing and the soil, the vertical stress in soil along the footing base is a major principal stress (the angle between the z-axis and the direction of the major principal stress ψ=0). The zone *oba* is called an active zone. In Zone *acd*, the horizontal stress is a major principal stress; it is called a passive zone. Along soil surface the stress boundary conditions are known, and

$$\bar{\sigma} = \frac{\bar{q}}{1 - \sin\phi} \tag{5.42}$$

where the normalized surcharge is expressed by

$$\bar{q} = \frac{q}{0.5\gamma B} \tag{5.43}$$

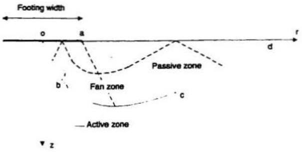

Figure 5.3: Failure pattern and failure zones of smooth footings

Between the passive zone and the active zone, there is a fan zone *abc*. The three zones share the same point, a, termed a singularity point at which the stress field makes the transitions between the extreme cases. At point a which is treated as a degenerate of a β-characteristics, ψ is 90° for the passive zone and is 180° for the active zone; the rotation angle of principal stresses in the fan zone at the singularity is $\Theta = 90°$. Bolton and Lau (1993) introduces at this point an exponential stress increase with rotation angle. Before rotation starting from the passive zone, ψ and $\bar{\sigma}$ are known. When the principal stress at a rotates by a value of θ, the boundary conditions become

$$\psi_\theta = \psi + \theta \tag{5.44}$$

$$\bar{\sigma}_\theta = \bar{\sigma} e^{2\theta \tan\phi} \tag{5.45}$$

The problem can be solved using the known parameters ψ, $\bar{\sigma}$, $\bar{r}$ and $\bar{z}$ along the soil surface *ad*, and the known ψ and $\bar{z}$ along the footing base. Starting from the soil surface *ad* with known stress boundary conditions, the stress field within *obcd* can be determined. The line *ad* is divided into several equally spaced points. The position of point d can be adjusted during iteration until the β-characteristic starting at d finally finishes at o with a required accuracy. When the variables at points along oa are known, the bearing pressure σ_z can be obtained using Mohr's circle as

$$\sigma_z = 0.5\gamma B\bar{\sigma}(1+\sin\phi) \tag{5.46}$$

The mean bearing capacity q_u of the footing can be determined by integrating σ_z numerically over the whole footing base. Lau (1988) carried out the analysis of strip and circular footings using a mesh of 96 β-characteristics and 220 α-characteristics and a rotation step in the fan zone of 3°.

5.3.2 Rough footings

In reality footings are usually rough and the failure pattern is not so simple. If the friction angle (δ) between soil and base is fully mobilized and the problem is solved by a direct extension of smooth footing solution, the characteristics will curve back along the footing base. For a fully mobilized δ, the angle between the direction of the major principal stress and the normal of the footing base, Γ, is given by (Graham and Stuart, 1971; and Tan, 1990)

$$\Gamma = 0.5\left[\delta + arc\sin\left(\frac{\sin\delta}{\sin\phi}\right)\right] \tag{5.47}$$

The main problem in this method results from the fact that symmetry at the centerline is violated, because the principal stress at the centerline is not vertical.

When no slip occurs between a rough footing base and soil, a wider rigid (elastic) wedge-zone extended to the edge of the footing can be assumed in analysis, as shown in Figure 5.4. The wedge surface is assumed to be perfectly rough; the friction angle with soil is δ=ϕ. Using the equation above, the angle between the direction of the major principal stress and the normal of the footing base is given by

$$\psi_1 = \Gamma - \alpha = 45° + \frac{\phi}{2} - \alpha \tag{5.48}$$

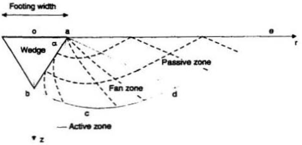

Figure 5.4: Rigid wedge and failure zones of rough footings

Graham and Stuart (1971) suggests that the wedge angle α is equal to soil friction angle ϕ for bearing capacity of footings. The calculated values of N_γ agree closely with those obtained by Hansen and Christensen (1969). However, this approach also violates the symmetry criterion at the wedge tip. To eliminate the error of non-symmetry at the tip, Bolton and Lau (1993) assumes α=45°+$\phi/2$ for strip and circular footings, so that the major principal stress at every point on the edge is vertical and symmetry is conserved at the tip. The wedge surface mobilizes ϕ and acts as the last characteristic in the marching solutions. However, this assumption of Prandtl failure mechanism is strictly correct only for footings on weightless material. The calculation results of Bolton and Lau (1993) indicate that the value of N_γ increases from smooth footing to rough footing by a factor of about 3 for strip footings and about 4 for circular footings.

A method for rough strip footings, in which the rigid wedge as shown in Figure 5.5 is naturally bounded by α-characteristics and symmetry is conserved at the tip, has been presented by Lundgren and Mortensen (1953) and later used by Hansen and

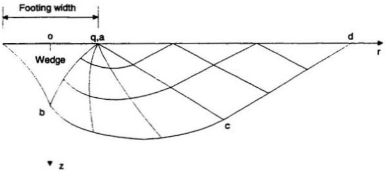

Figure 5.5: Failure pattern of rough footing with wedge bounded by α-characteristics

Christensen (1969), Steenfelt (1977) and Bonding (1977). Tan (1990) also used this technique for strip and circular footings with variable roughness. As shown in the figure, the shape of the wedge is related to the relative magnitude of surcharge and the friction mobilized between the soil and footing base. When the surcharge is high and no slip occurs between footing base and soil, the first α-line (ac) to the last α-line all pass through the singularity point a; the mobilized friction angle δ at point a can be assumed to be equal to or less than ϕ. Lundgren and Mortensen (1953) found that for ϕ=30°, all the α-lines pass through a only when $\gamma B/q$ is less than 11.4.

For very shallow footings with low surcharge, slip may occur near footing edges. The rigid wedge zone becomes smaller. In this case, only the first α-line (ac) passes through the singularity point a; all other α-lines to the left of ac reach the base at some distances from the footing edge. The size of the wedge is reduced with decreasing δ. When the footing is perfectly rough (δ=ϕ), all α-lines leaving the footing are tangential to the base. When δ is less than ϕ, the α-lines are no longer tangential to the base;

from a to q along the base near the edge, the angle between the direction of the major principal stress and the normal of the base is Γ, given by Equation (5.47). The rotation angle of principal stress in the fan zone at the singularity is

$$\Theta = 90^\circ + \Gamma \tag{5.49}$$

For $\delta = \phi$, $\Gamma = 45^\circ + \phi/2$, $\Theta = 135^\circ + \phi/2$. For ϕ=δ=30°, the results of Lundgren and Mortensen (1953) have given aq=0.104(0.5B).

5.3.3 Boundary conditions of analysis

In this study, the friction angle between the glass sand and the aluminum footings is about 28° (see Chapter 3). This value is much higher than the value of friction angle required for a rough footing, which is about 15° to 20° (Hansen and Christian, 1969; and Chen, 1975). Therefore, the footings in this analysis are all assumed to be rough, which will fail in Prandtl mechanism. An rigid wedge failure mechanism is used in the analysis.

Graham and Stuart (1971) assumed that the wedge angle is α=ϕ. Bolton and Lau (1993) used $\alpha = 45^\circ + \phi/2$ so that symmetry is conserved at the wedge tip. The assumption of Bolton and Lau is only appropriate for N_q at very large surcharge; the values of N_γ are much higher than those reported in the literature. It is desirable to combine the techniques adopted by Graham and Stuart (1971) and Bolton and Lau (1993). One way to do this is to use the logarithmic curve acb in Figure 5.6 as the boundary of the rigid zone. The inclination angle of the curve is ϕ at the footing edge and is $45^\circ + \phi/2$ at the tip. It is demonstrated, however, that with the increase of stress level from points a to b through c, the α-lines starting after the point c at some place between a and b will extend into the rigid zone. This would result in error in the analysis. In order to eliminate the error and to simplify the analysis, an rigid wedge is formed by linking points a and b using a straight line. The wedge angle α for this

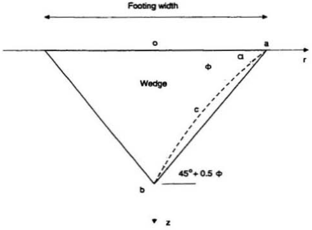

Figure 5.6: Assumed rigid wedge of rough footings in analysis

Table 5.1: Soil friction angle ϕ and wedge angle α

ϕ	30	35	40	45	50
α	48.6	51.5	54.4	58.1	60.9

work, as shown in Figure 5.6, is related to soil friction angle. The relationship between α and ϕ is listed in Table 5.1 and is also shown graphically in Figure 5.7.

5.4 Implementation of Analysis

5.4.1 Consideration of variable ϕ

It is well recognized that the Mohr's failure envelope of sand is usually curved (Hill, 1950) and the soil friction angle decreases with mean effective principal stress.

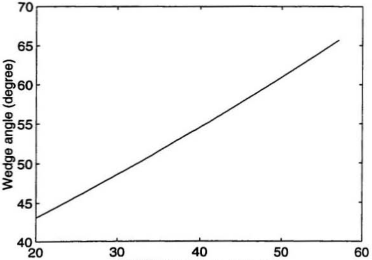

Figure 5.7: Wedge angle α versus soil friction angle ϕ

During drained shearing, soil may dilate or contract depending on the initial density and stress level (Rowe, 1962, 1969; De Josselin de Jong, 1976). Bolton (1986) suggests that for a sand under drained conditions, the peak secant triaxial friction angle ϕ can be expressed as

$$\phi = \phi_o - k \ln s \tag{5.50}$$

in which

$$s = \frac{1}{2}(\sigma_1 + \sigma_3) \tag{5.51}$$

where ϕ_o and k are soil constants. Bolton and Lau (1993) used $\phi = 30°$ in the highly stressed region and $\phi = 57°$ near the soil surface.

Bolton (1986) assumes that the critical state friction angle (ϕ_{cs}) is a function of soil mineralogy and independent of stress level. The triaxial results presented in Chapter 3 and the data given by Chu (1995) suggest that both the peak friction angle and critical state friction angle of sands decrease with confining pressure. According to the results given in Chapter 3 of the triaxial compression tests of the dense glass sand (I_D=90%) under drained conditions, the variation of the peak friction angle with stress level is given by Equation (3.20). The triaxial test results indicate that the peak friction angle of the sand dropped from about 46.9 to 37.3° when the confining pressure is increased from 25 to 2500 kPa.

As adopted by Graham and Stuart (1971) and Graham and Hoven (1986), ϕ is incorporated as a stress dependent variable in the characteristics analysis of this study and the value of ϕ is updated according to stress level during computation. The same governing equations are used as formulated for the cases of constant ϕ. During calculation, the value of ϕ corresponds to the average stress level at the two previously known points and the new point.

5.4.2 Implementation of computation

A code in the C programming language has been developed in a UNIX system to implement the analysis of the bearing capacity of circular and strip footings. The analysis starts from the soil surface where the stress conditions are known, and then advances to the passive zone, the fan zone, the active zone and the wedge surface, which are shown in Figure 5.4. The bearing capacity obtained for a footing is the average vertical pressure acting on the wedge surface. In the analysis, the following parameters are inputed to the program:

(1). The number of β-characteristics lines including the singularity point is 101 for all analyses. The mesh is equally spaced along the soil surface. The number of α-characteristics lines in the fan zone is also 101.

(2). For each point during iteration, the convergence criterion of stress is $\partial s/s =$ 0.0001.

Table 5.2: Comparison of N_γ of rough strip footings

ϕ (degree)	30	35	40	45
N_γ (this study)	19.4	40.8	88.9	203
N_γ (Larkin, 1968)	15.7	40.8	87	-
N_γ (Hansen, 1970)	15.7	33.9	79.5	201
N_γ (Graham & Stuart, 1971)	-	54.7	-	-
N_γ (Bolton & Lau, 1993)	23.6	-	121	324

(3). N_γ is obtained by applying a surcharge $\bar{q}$ $=q/(0.5\gamma B) = 0.001$, in order to simulate a surface footing; N_q is derived by applying $\bar{q}$=1000.

(4). The friction angle (ϕ) in the soil domain of analysis is related to stress level using Equation (3.20) obtained from triaxial tests. For the calculation of a new point, ϕ is corresponding to the average stress level of the new point and the two known points. At the soil surface, the maximum friction angle is ϕ=57°. In highly stressed regions, the lower limit of the friction angle is assumed to be 30°.

(5). The wedge angle α shown in Figure 5.6 is determined using a ϕ value corresponding to the mean stress level of points along the wedge surface. At the beginning of analysis, an initial value of the wedge angle α is assumed. Iteration was continued until the accuracy of α is less than or equal to 0.01°.

The program is verified for strip footings under constant ϕ conditions. The values of N_γ obtained for this study are compared with those in the literature, as shown in Table 5.2. It can be seen that the N_γ values of this study are reasonable compared with others; they are especially close to those of Hansen (1970) and Larkin (1968). It is obvious that the N_γ values obtained by Bolton and Lau (1993) are much higher than those of other researchers. The program has also been checked by calculating the value of N_q when the wedge angle is defined by α=45° + $\phi/2$. For ϕ=30°, the calculated N_q is 18.1, which is very close to the exact solution of 18.4 derived by Reissner (1924).

5.5 Analytical Results of Circular Footings

5.5.1 Bearing capacity from variable friction angle ϕ

Analysis of circular footings on the surface of the dense sand with a dry unit weight of 15.4 kN/cm^3 has been carried out using the method of characteristics described above. The stress-dependent peak ϕ value, calculated by Equation (3.20) is used in the analysis. When the footing diameter increases from 0.1 m to 10 m, the calculated bearing capacity (q_u) is increased from 292 to 6740 kPa; The bearing capacity factor N_γ is reduced from 632 to 146, due to the decrease of soil friction angle with stress level. With the increase of footing size, the wedge angle α is decreased from 57.9° to 52.2°.

The relationship between the calculated bearing capacity and footing diameter is illustrated in Figure 5.8. It is seen that the bearing capacity increases linearly with footing diameter in the double-log plot. The calculated bearing capacity (q_u) can be expressed in terms of footing diameter (D) as

$$q_u = 1400D^{0.69} \tag{5.52}$$

where q_u is in kPa and D is in meters. To make a comparison, the bearing capacity from centrifuge tests given by Equation (4.22) is also shown in the figure, as represented by the dotted line. The bearing capacity calculated by the method of characteristics is very close to that obtained from centrifuge tests. The differences, increasing with footing size, are 1.4, 5.4 and 11.7% when the footing diameters are 0.1, 1.0 and 10.0 m

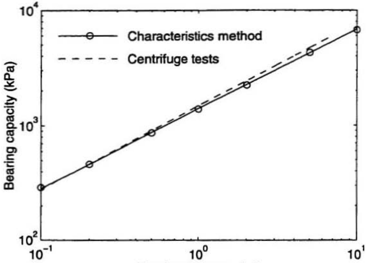

Figure 5.8: Calculated bearing capacity of circular footings

respectively.

5.5.2 Bearing capacity from equivalent friction angle ϕ_{eq}

The analysis above shows that when a variable ϕ corresponding to different stress level is used, the bearing capacity of footings can be well modelled by the method of characteristics. It is, however, desirable that an equivalent friction angle ϕ_{eq} of a footing with a certain dimension can be found so that the bearing capacity can be calculated using the constant ϕ_{eq}. Meyerhof (1950) and De Beer (1965a) suggest that ϕ_{eq} should correspond to the mean value of normal stress along the failure surface (σ_m). Meyerhof (1950) has proposed that

$$\sigma_m = \frac{q_u}{10} \tag{5.53}$$

where q_u is the bearing capacity. Using the above equation and Mohr's circle, the value

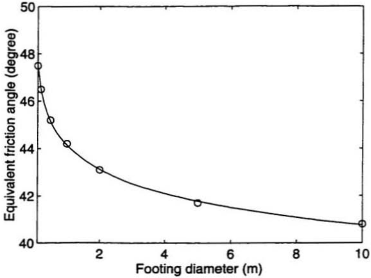

Figure 5.9: Equivalent friction angle ϕ_{eq} versus footing diameter

of s corresponding to ϕ_{eq} can be calculated by

$$s = \frac{\sigma_1 + \sigma_3}{2} = \frac{q_u(1 + \tan^2 \phi_{eq})}{10} \tag{5.54}$$

Then ϕ_{eq} can be obtained using Equation (3.20) by iteration. At the beginning of analysis, an initial bearing capacity of a footing is assumed to calculate the value of ϕ_{eq} and then a new bearing capacity can be obtained. Using the updated bearing capacity, the process of calculation can be repeated until a prescribed accuracy of bearing capacity of 0.1% is reached.

The calculated equivalent friction angle (ϕ_{eq}) and the bearing capacity (q_{ueq}) from ϕ_{eq} are shown in Figure 5.9 and 5.10. When the footing diameter increases from 0.1 to 10 m, ϕ_{eq} is decreased from 47.5 to 40.8°; for a log-cycle increase of footing size, ϕ_{eq} is reduced by about 3.5°.

The calculated bearing capacity (q_{ueq}) in Figure 5.10 from equivalent friction angle

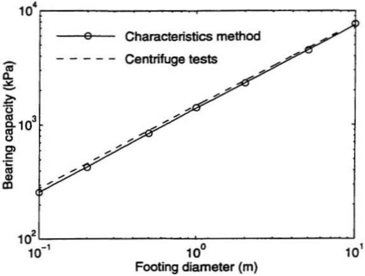

Figure 5.10: Bearing capacity from equivalent friction angle ϕ_{eq}

ϕ_{eq}, which is constant for a certain footing, increases linearly with footing diameter in a double-log diagram. The relationship is written as

$$q_{ueq} = 1400D^{0.73} \tag{5.55}$$

where q_{ueq} is in kPa and D is in meter. It can be seen from the figure that the bearing capacity calculated from ϕ_{eq} using the method of characteristics is very close to that obtained from centrifuge experiment. The differences are 7.6, 5.4 and 3.2% when the footing diameters are 0.1, 1.0 and 10.0 m respectively.

5.6 Summary

This chapter presents the basic equations and formulation of the method of characteristics for the bearing capacity of foundations. A detailed discussion regarding the effect of boundary conditions on the failure mechanism and bearing capacity of foundations is presented. Analysis has been carried out to investigate the size effect of circular footings. A rigid wedge under a rough footing is assumed for analysis. The wedge angle α can be derived from a soil friction angle corresponding to the average stress level along the wedge surface. The effect of footing size on bearing capacity due to the stress dependence of soil friction angle has been well modelled. A program written in the C programming language has been developed to implement the analysis.

The effect of footing size on bearing capacity can be modelled by taking into consideration the stress dependence of soil friction angle. During calculation for a point, the value of ϕ corresponding to the average stress level of the two previously known points and the new point is used. The peak friction angle of the sand obtained from triaxial tests is used. The calculated bearing capacity of circular footings increases linearly with footing diameter in a double-log scale diagram. It is very close to the bearing capacity obtained from centrifuge tests. The wedge angle is reduced by the increase of footing size, due to the decrease of soil friction angle with stress level.

The bearing capacity can also be estimated using a constant friction angle ϕ_{eq} for each footing corresponding to the mean normal stress along the failure surface. The mean normal stress can be related to the bearing capacity using Meyerhof's formula. Using the friction angle ϕ_{eq}, the effect of footing size on bearing capacity can also be well simulated. This procedure provides a basis for the finite element analysis of bearing capacity using a constant friction angle for each footing, as presented in the next chapter.

Chapter 6

Finite Element Analysis of Axially Loaded Ring Footings

6.1 Introduction

6.1.1 Finite element method

The finite element (FE) method, originally developed in the 1940s in structural engineering (Hrennikoff, 1941; and McHenry, 1943), is a numerical method for solving engineering and mathematical problems such as structural analysis, heat transfer, fluid flow and electro-magnetic potential. The finite element technique has been used in geotechnical engineering for various purposes, including settlement and consolidation of soils, embankments and excavations, earth retaining structures and foundation analysis (Desai and Christian, 1977). For many problems in which the analytical solutions are not available, the finite element technique can be employed for dealing with complicated conditions of geometries, loads and materials. For structural problems, the displacement (or stiffness) method is usually adopted. The procedure of the finite analysis mainly includes discretizing the body into small finite elements, defining the strain-displacement and stress-strain relationships according to the selected displacement function and material properties, deriving the element stiffness matrix and equations, assembling the element equations to obtain global equations, introducing boundary conditions and solving the equations for unknowns.

For nonlinear elasto-plastic materials like soils, of which the solution is load path dependent, an incremental method is essential for the solution of the finite element equations. The load is divided into a number of small increments and the solution at the end of an increment is the summation of the solutions of all previous increments. Using this method, the complete load-displacement history can be defined.

The equilibrium equations of the incremental analysis can be derived by applying the principle of virtual work, which is stated as follows (Logan, 1992):

> "If a deformable body in equilibrium is subjected to arbitrary virtual (imaginary) displacements associated with a compatible deformation of the body, the virtual work of external forces is equal to the virtual strain energy of the internal stresses."

For a finite element with a volume of V and a surface of S, the matrix of the displacement functions ($\{\psi\}$) is related to the matrix of nodal displacements ($\{d\}$) by

$$\{\psi\} = [N]\{d\} \tag{6.1}$$

where matrix $[N]$ represents the shape functions. The strain matrix ($\{\varepsilon\}$) and stress matrix ($\{\sigma\}$) are expressed as

$$\{\varepsilon\} = [B]\{d\} \tag{6.2}$$

$$\{\sigma\} = [D]\{\varepsilon\} \tag{6.3}$$

in which $[D]$ is a material stiffness matrix, $[B]$ is a matrix derived from $[N]$.

The internal virtual strain energy of a finite element is

$$\delta U = \int_V \{\delta\varepsilon\}^T\{\sigma\}dV \tag{6.4}$$

and the external work is in the form of

$$\delta W = \{\delta d\}^T\{P\} + \int_S \{\delta\psi\}^T\{T\}dS + \int_V \{\delta\psi\}^T\{X\}dV \tag{6.5}$$

where $\{\delta d\}$ is the vector of virtual nodal displacements, $\{\delta\psi\}$ is the vector of virtual displacement functions, $\{P\}$ is the nodal load matrix, $\{T\}$ is the matrix surface forces and $\{X\}$ is the matrix of body forces.

Combining the above equations and using the principle of virtual work expressed as

$$\delta U = \delta W \tag{6.6}$$

yield

$$\int_V \{\delta d\}[B]^T[D]dV\{d\} = \{\delta d\}^T\{P\} + \{\delta d\}^T \int_S [N]^T\{T\}dS + \{\delta d\}^T \int_V [N]^T\{X\}dV \tag{6.7}$$

That is

$$[k]\{d\} = \{P\} + \{f_s\} + \{f_b\} \tag{6.8}$$

in which

$$[k] = \int_V [B]^T[D][B]dV \tag{6.9}$$

$$\{f_s\} = \int_S [N]^T\{T\}dS \tag{6.10}$$

$$\{f_b\} = \int_V [N]^T\{X\}dV \tag{6.11}$$

Equation (6.8) is the equilibrium equation of the finite element. It can be assembled to the global equilibrium equations of the problem. By introducing boundary conditions the equations may be solved for unknowns. For the foundation analysis in the present study, due to the presences of soil nonlinearity, large soil deformation and complicated boundary conditions, the global equilibrium equations should be solved by incremental procedure. A general purpose finite element computer code ABAQUS will be used to implement the analysis.

6.1.2 Modelling of foundations

The finite element method associated with soil plasticity theories has been used to investigate the bearing capacity of foundations on cohesive soils (Davidson and Chen, 1976; Zienkiewicz *et al.*, 1975; Zienkiewicz *et al.*, 1978). Relative few finite element solutions of bearing capacity of cohesionless soils are available.

Griffiths (1982) carried out finite element analysis of strip footings on frictional materials, separately assessing N_c due to soil cohesion c, N_q due to overburden pressure q and N_γ of cohesionless soil with weight. The Mohr-Coulomb failure criterion with a flow rule of zero plastic volumetric strain was employed. The elastic modulus $E=2\times10^5$ kPa and Poisson's ratio $\nu=0.35$ were used. Perfect plasticity was implemented using the visco-plastic technique (Zienkiewicz and Cormeau, 1972, 1974). Eight-node quadrilateral, isoparametric elements were adopted. A footing was modelled by applying a prescribed vertical displacement on nodes of soil contacting with the footing. For a smooth footing ($\delta=0$) the nodes could freely move horizontally; for a rough footing ($\delta \geq \phi$) horizontal restraints to the nodes were added. This simplicity can avoid the convergence problem associated with the use of interface elements (Griffiths, 1982).

The results presented by Griffiths (1982) suggest that the finite element method can be used with confidence to estimate the bearing capacity factors N_c and N_q. Good results of N_γ have been obtained. The dependence of N_γ on footing roughness is confirmed. The calculated values of N_γ decrease with footing size, which is thought to be due partly to the non-linear stress distribution beneath the footing. In computing N_γ, convergence was very slow using the displacement control technique, due to the shear concentration at the footing edge. The convergence rate decreases with increasing ϕ. A ϕ value of 35° seemed to be the limit to obtain a reasonable N_γ using the raw visco-plastic technique.

Desai (1968, 1971) and Desai and Reese (1970) performed finite element analyses of bearing capacity of footings on clays. A footing was modelled by either a uniform pressure or a rigid displacement. The finite element method has given satisfactory results for predicting the stresses and deformations of footings. It is shown that the average bearing pressure obtained by applying a uniform pressure is very close to that by applying a rigid displacement. Griffiths (1982) indicated that applying a uniform pressure on the surface of cohesionless soil is unrealistic because the soil at the footing edge can not sustain normal stress. In such a case, the pressure at the edge must be zero. Analysis of strip loads on elasto-plastic soil was also carried out by Hoeg *et al.* (1968).

Christian (1977) also introduced the use of finite element technique for bearing capacity. It is stated that in using the incremental procedure for soil nonlinearity, solution accuracy and cost depend on many factors such as the number of elements, element type and the size of load increments. It is concluded that reducing the size of load increments can obtain the most benefit. The most popularly used isoparametric elements are good for nonfrictional materials. They may result in much greater ultimate loads than those estimated by bearing capacity theory.

Chen (1975) presented an example of finite element analysis of a rigid strip footing on a c-ϕ weightless soil using the Drucker-Prager elasto-perfectly-plastic model. The effects of mesh size and displacement increment size are studied. It is found that the finest mesh results in softest response (smallest load). The smallest increment size of loading yields lowest bearing pressure.

In summary, effort in using the finite element method for the bearing capacity of foundations has been made in the past decades. Compared with other methods such as the characteristics analysis and the limit equilibrium approach, the finite element technique for bearing capacity is far from mature and its application is limited. It seems that satisfactory results have been obtained only for foundations on cohesive soils. For foundations on sands, very few good data have been reported. It is believed that the difficulty results from the complexity of soil behaviour, rather than due to the finite element technique itself or the capacity of today's computers. The bottleneck in the finite element application to bearing capacity problems is how to select proper constitutive models for soils.

6.2 Soil Plasticity and Incremental Modelling

The stress-strain constitutive relation of soil is complicated because of the following features of soils: (1) The stress-strain relationship is nonlinear; even at very low strain, plastic deformation occurs. (2) Soils are frictional materials; the strength and stress-strain relation are pressure dependent. (3) Soils exhibit volumetric change when sheared; during drained shearing, a 'loose' soil tends to contract and a 'dense' soil tends to dilate.

The strain of a soil includes two parts: elastic strain and plastic strain. A constitutive model describing the elasto-plastic response of the soil must include four aspects: (1) the elastic deformation behaviour; (2) a yield surface in the stress space within which the soil deforms elastically; (3) a plastic potential defining the mode of plastic deformation when the soil is yielding; and (4) a hardening rule describing the expansion of the yield surface during plastic deformation. The increment of plastic strain during yielding is normal to the plastic potential. When the plastic potential is identical to the yield surface, the flow rule is termed associated, otherwise nonassociated.

For a soil, the total increment of strain matrix ($\{d\varepsilon\}$) is the sum of increment of elastic strain matrix ($\{d\varepsilon^e\}$) and the increment of plastic strain matrix ($\{d\varepsilon^p\}$), that is

$$\{d\varepsilon\} = \{d\varepsilon^e\} + \{d\varepsilon^p\} \tag{6.12}$$

The yield surface is assumed to be

$$f(\sigma, \kappa) = 0 \tag{6.13}$$

and the plastic potential is

$$g(\sigma, \xi) = 0 \tag{6.14}$$

where σ represents the stresses, κ is a parameter describing the hardening rule and ξ is a soil parameter. The increment of plastic strain is given by the flow rule as

$$\{d\varepsilon^p\} = \lambda \left\{ \frac{\partial g}{\partial \sigma} \right\}, \quad \lambda \geq 0 \tag{6.15}$$

The increment of stress matrix ($\{d\sigma\}$) is related to the increment of elastic strain matrix by

$$\{d\sigma\} = [D^e]\{d\varepsilon^e\} \tag{6.16}$$

where $[D^e]$ is the elastic stiffness matrix. Using Equation (6.12) and (6.15), the above equation is expressed as

$$\{d\sigma\} = [D^e]\{d\varepsilon\} - [D^e]\lambda \left\{ \frac{\partial g}{\partial \sigma} \right\} \tag{6.17}$$

Differentiation of Equation (6.13) results in

$$df = \left\{ \frac{\partial f}{\partial \sigma} \right\}^T \{d\sigma\} + \frac{\partial f}{\partial \kappa} d\kappa = 0 \tag{6.18}$$

The hardening parameter (κ) is a function of plastic strain. Therefore,

$$d\kappa = \left\{ \frac{\partial \kappa}{\partial \varepsilon^p} \right\}^T \{d\varepsilon^p\} = \left\{ \frac{\partial \kappa}{\partial \varepsilon^p} \right\}^T \lambda \left\{ \frac{\partial g}{\partial \sigma} \right\} \tag{6.19}$$

Combination of the above three equations yields

$$\lambda = \frac{\left\{ \frac{\partial f}{\partial \sigma} \right\}^T [D^e]\{d\varepsilon\}}{\left\{ \frac{\partial f}{\partial \sigma} \right\}^T [D^e] - \frac{\partial f}{\partial \kappa} \left\{ \frac{\partial \kappa}{\partial \varepsilon^p} \right\}^T \left\{ \frac{\partial g}{\partial \sigma} \right\}} \tag{6.20}$$

By substituting the above equation to Equation (6.17), the relationship between stress increment and the strain increment can be obtained in the form of

$$\{d\sigma\} = [D^{ep}]\{d\varepsilon\} \tag{6.21}$$

where the elasto-plastic stiffness matrix ($[D^{ep}]$) is

$$[D^{ep}] = [D^e] - \frac{[D^e]\left\{\frac{\partial g}{\partial \sigma}\right\}\left\{\frac{\partial f}{\partial \sigma}\right\}^T[D^e]}{\left\{\frac{\partial f}{\partial \sigma}\right\}^T[D^e] - \frac{\partial f}{\partial \kappa}\left\{\frac{\partial \kappa}{\partial \varepsilon^p}\right\}^T\left\{\frac{\partial g}{\partial \sigma}\right\}} \tag{6.22}$$

What is discussed above is a general procedure for the elasto-plastic incremental analysis. A particular model, Cam-clay, will be introduced in the following for a further discussion and a better understanding of the elasto-plastic behaviour of soil.

The Cam-clay model was originally proposed by Roscoe and Schofield (1963) for describing the elasto-plastic behaviour of clay. A modified version was presented by Roscoe and Burland (1968) and discussed in detail by Wood (1990). The model includes an elastic theory, a yield surface, a flow rule and a hardening law. The parameters for the model can be determined by triaxial compression tests. Cam-clay is widely recognized in both practice and academic circles because of its simplicity and satisfactory accuracy compared with more realistic models. A good comprehension of Cam-clay, a pedagogic model, is very beneficial to understanding fundamental soil behaviour and the feature of other particular models for soil.

The model is described in a three dimensional space, as shown in Figure 6.1, consisting of two effective stress invariants (p and q) and the specific volume of soil defined as

$$v = 1 + e \tag{6.23}$$

where e is soil void ratio. The mean principal stress p and the deviator stress q are expressed as

$$p = \frac{1}{3}(\sigma_1 + \sigma_2 + \sigma_3) \tag{6.24}$$

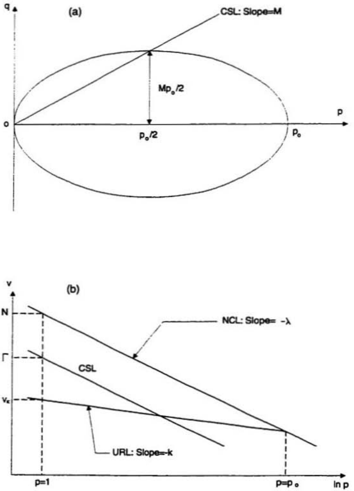

Figure 6.1: Cam-clay: (a) Yield locus and critical state line (CSL); (b) Normal compression line (NCL), unloading-reloading line (URL) and critical state line

$$q = \sqrt{\frac{1}{2}[(\sigma_1 - \sigma_2)^2 + (\sigma_2 - \sigma_3)^2 + (\sigma_3 - \sigma_1)^2]} \tag{6.25}$$

where σ_1, σ_2 and σ_3 are the major, intermediate and minor effective principal stresses respectively.

An important embodyment in Cam-clay is the critical state line (Schofield and Wroth, 1968), which is the locus of shear failure points. At critical state, a soil develops shear deformation without change in stress and volumetric strain, that is

$$\frac{\partial p}{\partial \varepsilon_q} = \frac{\partial q}{\partial \varepsilon_q} = \frac{\partial v}{\partial \varepsilon_q} = 0 \tag{6.26}$$

where ε_q represents the deviator (shear) strain.

The critical state line (CSL) in the p-q space is taken as a straight line through the origin. The relationship between the mean principal stress p and deviator stress q at critical state is

$$\frac{q}{p} = M \tag{6.27}$$

where M is a strength parameter, representing the slope of the critical state line.

As shown in Figure 6.1(b), the increment of elastic volumetric strain (ε_p^e) along the unloading-reloading line is given by

$$\delta\varepsilon_p^e = \kappa \frac{\delta p}{vp} \tag{6.28}$$

where δp is the increment of p, and κ is the slope of unloading-reloading line (URL) in the $\ln p$-v space. For finite element analyses the increment of elastic deviator strain is assumed to be

$$\delta\varepsilon_q^e = \frac{\delta q}{3G} \tag{6.29}$$

in which δq is the increment of q, and G is the elastic shear modulus of soil. In analysis, a constant Poisson's ratio can be assumed (Britto and Gunn, 1987; and Wood, 1990).

The current yield surface of Cam-clay is an ellipse on the p-q space. The equation of the ellipse is

$$f = q^2 - M^2 p(p_o - p) = 0 \tag{6.30}$$

where p_o is the preconsolidation pressure of isotropic normal compression, which controls the size of the yield surface; M is the slope of the critical state line. Another form of the equation for the yield locus is

$$\frac{p}{p_o} = \frac{M^2}{M^2 + \eta^2} \tag{6.31}$$

in which the stress ratio η is in the form of

$$\eta = \frac{q}{p} \tag{6.32}$$

At critical state, $\eta = M$ and $p = p_o/2$.

In Cam-clay, the flow rule is assumed to be associated; the soil obeys the normality condition. The plastic potential is identical to the yield surface, expressed as

$$g = f = q^2 - M^2 p(p_o - p) = 0 \tag{6.33}$$

where g is plastic potential. The vector of plastic strain increments is in the direction outward normal to the yield surface. Therefore,

$$\frac{\delta \varepsilon_p^p}{\delta \varepsilon_q^p} = \frac{\partial g/\partial p}{\partial g/\partial q} = \frac{M^2 - \eta^2}{2\eta} \tag{6.34}$$

where $\delta \varepsilon_p^p$ is the increment of plastic volumetric strain, $\delta \varepsilon_q^p$ is the increment of plastic deviator strain.

The size of the yield loci is controlled by p_o at a constant shape factor M. The soil hardening is related to isotropic compression. The change of yield loci is supposed to be related to plastic strain increments, that is

$$\delta p_o = \frac{\partial p_o}{\partial \varepsilon_p^p} \delta \varepsilon_p^p + \frac{\partial p_o}{\partial \varepsilon_q^p} \delta \varepsilon_q^p \tag{6.35}$$

Figure 6.1(b) suggests that the specific volume of soil under isotropic normal compression is

$$v = N - \lambda \ln p_o \tag{6.36}$$

where N is the specific volume when p_o=1, λ is the slope of the isotropic normal compression line (NCL) in the $\ln p$-v space. Then, the increment of the plastic volumetric strain is given by

$$\delta \varepsilon_p^p = \frac{(\lambda - \kappa)\delta p_o}{v p_o} \tag{6.37}$$

Comparing Equation (6.35) with Equation (6.37) yields the hardening law as

$$\frac{\partial p_o}{\partial \varepsilon_p^p} = \frac{v p_o}{\lambda - \kappa} \tag{6.38}$$

$$\frac{\partial p_o}{\partial \varepsilon_q^p} = 0 \tag{6.39}$$

This means that the hardening of soil depends only on plastic volumetric strain, independent of plastic shear strain.

Cam-clay has been adopted in computer codes for finite element analysis of geotechnical problems (Britto and Gunn, 1987; and Hibbitt *et al.*, 1994). The model is considered to be suitable for describing the elasto-plastic behaviour of clays, especially for normally consolidated or lightly overconsolidated clays. For sands, plastic deformation is due mainly to the deviator stress; high mean principal stress is required to produce significant plastic deformation in isotropic compression (Tatuoka and Ishihara, 1974; Lade and Duncan, 1975; Poorooshasb *et al.*, 1967; and Wood, 1990). For granular materials like sands, the Drucker-Prager model can be employed.

6.3 Modified Drucker-Prager/Cap Model

The Drucker-Prager model (extended Von Mises criterion) was originally proposed by Drucker and Prager (1952). The modified Drucker-Prager/Cap model in ABAQUS

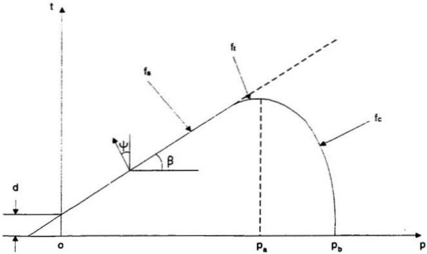

Figure 6.2: Yield surfaces of modified Drucker-Prager/Cap model

(Hibbitt *et al.*, 1994) will be used for the analysis of foundations on sand in this study. The purposes of adding the cap yielding surface to the extended Drucker-Prager model are to provide a plastic hardening mechanism and to control the volumetric dilation when the soil yields during shearing. The flow rule is associated in the cap region (f_c) and nonassociated in the shear failure region (f_s) and transition region (f_t), as shown in Figure 6.2. The Drucker-Prager shear failure segment is a perfectly plastic yield surface, on which the plastic flow results in volumetric dilation that causes the cap yield surface to soften.

6.3.1 Failure surface

The shear failure surface of the Modified Drucker-Prager/Cap model (Hibbitt *et*

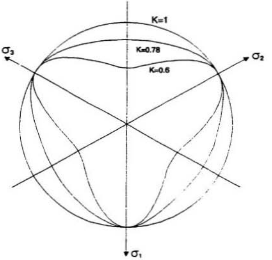

Figure 6.3: Yield Surfaces of the ABAQUS Drucker-Prager model in the π-Plane

al., 1994) is a straight line in the p-t space defined by

$$f_s = t - p \tan\beta - d = 0 \tag{6.40}$$

in which

$$t = \frac{1}{2} q \left[1 + \frac{1}{K} + \left(1 - \frac{1}{K}\right) \left(\frac{r}{q}\right)^3 \right] \tag{6.41}$$

$$r = \left[\frac{1}{2} (2\sigma_1 - \sigma_2 - \sigma_3)(2\sigma_2 - \sigma_3 - \sigma_1)(2\sigma_3 - \sigma_1 - \sigma_2) \right]^{1/3} \tag{6.42}$$

where β, d and K are soil parameters, p is the mean principal stress and q is the deviator stress.

In Equations (6.40) and (6.41), β is the friction angle of soil in the t-p plane. K controls the dependence of the yield surface on the intermediate principal stress. $K = 1$ implies that the yield surface is the von Mises circle in the π-plane, as shown in Figure 6.3. The convexity of yield surface requires $K \geq 0.778$.

It is known that the Mohr-Coulomb strength parameters c and ϕ are independent of the intermediate principal stress (σ_2). It can be assumed that the value of ϕ determined from triaxial compression test is equal to that from triaxial extension test (Sutherland and Mesdare, 1969). However, the Drucker-Prager parameters β, K and d are influenced by σ_2. To use c and ϕ to determine the value of β and K, it is preferable to make the Mohr-Coulomb model and the Drucker-Prager model provide the same failure definition in triaxial compression and extension. Hibbitt *et al.* (1994) deduced that to match the response of triaxial compression and extension, the Drucker-Prager parameters are given by

$$\tan \beta_{tr} = \frac{6 \sin \phi}{3 - \sin \phi} \tag{6.43}$$

$$K_{tr} = \frac{3 - \sin \phi}{3 + \sin \phi} \tag{6.44}$$

and

$$d_{tr} = c \frac{6 \cos \phi}{3 - \sin \phi} \tag{6.45}$$

where β_{tr}, K_{tr} and d_{tr} represent β, K and d respectively under triaxial conditions.

The three equations above provide the Drucker-Prager model parameters which match the Mohr-Coulomb model in triaxial compression and extension. Because $K_{tr} \geq 0.78$ is required for the convexity of yield surface, Equation (6.44) implies $\phi \leq 22°$. Therefore, if ϕ is significantly greater that 22°, this approach may yield a poor Drucker-Prager match of the Mohr-Coulomb parameters.

As described in chapter 3, the values of ϕ of the dense sand are typically between 32° and 47°, depending on stress level. In this study, in order to adapt the Drucker-Prager model for those high triaxial ϕ values, the failure surface f of the sand determined by the calculated β_{tr} and K_{tr}, as shown in Figure 6.4, is replaced by an equivalent yield failure surface f_m defined by β'_{tr} and K'_{tr}. The rule for defining f_m is that the distance between points a and b in triaxial compression is equal to the distance between points

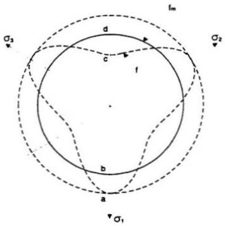

Figure 6.4: Modification of Drucker-Prager yield surface

c and d. Using this rule, β'_{tr} is given by

$$\tan \beta'_{tr} = \frac{K_{tr}^2 + 2}{K'^2_{tr} + 2} \tan \beta_{tr} - \frac{K'^2_{tr} - K_{tr}^2}{K'^2_{tr} + 2} \frac{d_{tr}}{p} \tag{6.46}$$

with

$$d'_{tr} = d_{tr} \tag{6.47}$$

where p is the mean principal stress in soil. When d_{tr} is zero or very small, the above equation for β'_{tr} can be expressed as

$$\tan \beta'_{tr} = \frac{K_{tr}^2 + 2}{K'^2_{tr} + 2} \tan \beta_{tr} \tag{6.48}$$

where $0.78 \leq K'_{tr} \leq 1.0$. For K'_{tr}=1,

$$\tan \beta'_{tr} = \frac{K_{tr}^2 + 2}{3} \tan \beta_{tr} \tag{6.49}$$

in which β'_{tr}, K'_{tr} and d'_{tr} are modified Drucker-Prager parameters for triaxial matching.

For plane strain problems such as strip foundations, the Drucker-Prager model parameters should be matched to provide the same flow and failure response as Mohr-Coulomb model. It is known that the value of friction angle (ϕ) is about 10% higher under plane strain conditions than under triaxial conditions. That is

$$\phi_{pl} = (1 + \xi)\phi_{tr} \tag{6.50}$$

where ξ is about 10% (Bishop, 1961, 1966; Meyerhof, 1963; and Hansen, 1970).

Under plane strain conditions, the Drucker-Prager model parameters β, K and d are represented by β_{pl}, K_{pl} and d_{pl} respectively. Assuming K_{pl}=1 which means t=q, Hibbitt *et al.* (1994) demonstrated that β_{pl} and d_{pl} are related to Mohr-Coulomb parameters c and ϕ_{pl} by

$$\sin\phi_{pl} = \frac{\tan\beta_{pl}\sqrt{3(9-\tan^2\psi)}}{9-\tan\beta_{pl}\tan\psi} \tag{6.51}$$

$$c\cos\phi_{pl} = \frac{\sqrt{3(9-\tan^2\psi)}}{9-\tan\beta_{pl}\tan\psi}d_{pl} \tag{6.52}$$

where ψ is the dilation angle in the p-t plane as shown in Figure 6.2. For associated flow ($\psi = \beta_{pl}$), this yields

$$\tan\beta_{pl} = \frac{3\sin\phi_{pl}}{\sqrt{3+\sin^2\phi_{pl}}} \tag{6.53}$$

$$\frac{d_{pl}}{c} = \frac{3\cos\phi_{pl}}{\sqrt{3+\sin^2\phi_{pl}}} \tag{6.54}$$

and for nondilatant flow ($\psi = 0$), it can be derived that

$$\tan\beta_{pl} = \sqrt{3}\sin\phi_{pl} \tag{6.55}$$

$$\frac{d_{pl}}{c} = \sqrt{3}\cos\phi_{pl} \tag{6.56}$$

For the Drucker-Prager/Cap model, ψ under shear failure conditions is typically between 0 to β. By averaging the values of $\tan\beta_{pl}$ and d_{pl} for associated flow and nondila-

Table 6.1: Drucker-Prager parameters converted from c and ϕ (for $K'_{tr}=K_{pl}=1$)

Friction angle ϕ (degree)	Triaxial matching ($\phi_{tr} = \phi$)		Plane strain matching ($\phi_{pl} = 1.1\phi$)	
	β'_{tr} (degree)	d'_{tr}/c	β_{pl} (degree)	d_{pl}/c
20	34.12	2.12	32.68	1.59
25	40.09	2.11	38.18	1.51
30	45.12	2.08	42.66	1.42
35	49.32	2.03	46.30	1.32
40	52.83	1.95	49.24	1.20
45	55.76	1.85	51.60	1.08
50	58.20	1.73	53.49	0.95

tant flow using the four equations above, the approximate estimations of the Drucker-Prager parameters for plane strain matching can be obtained from

$$\tan \beta_{pl} = \frac{\sqrt{3}\sin\phi_{pl}}{2}\left(1 + \frac{\sqrt{3}}{\sqrt{3+\sin^2\phi_{pl}}}\right) \tag{6.57}$$

$$\frac{d_{pl}}{c} = \frac{\sqrt{3}\cos\phi_{pl}}{2}\left(1 + \frac{\sqrt{3}}{\sqrt{3+\sin^2\phi_{pl}}}\right) \tag{6.58}$$

The Drucker-Prager model parameters derived from c and ϕ under triaxial condition (ξ=0) and plane strain condition (ξ=0.1) are listed in Table 6.1.

In ring foundation analysis, soil under a circular footing (ring radii ratio n=0) is in a condition close to triaxial testing (Okamura *et al.*, 1997); the Drucker-Prager β, K and d can be approximated by β'_{tr}, K'_{tr} and d'_{tr}. The results of centrifuge tests presented in Chapter 4 indicate that the behaviour of a ring footing is similar to a circular footing when the ring radii ratio is within 0.35. When n is increased to 0.9, the soil under the footing can be considered under plane strain conditions and β_{pl}, d_{pl} and K_{pl}=1 are used in analysis. Therefore, the values of β and d when K=1 for a ring footing with a radii ratio n can be obtained as

$$\beta = \beta'_{tr} - \alpha_n(\beta'_{tr} - \beta_{pl}) \tag{6.59}$$

$$d = d'_{tr} - \alpha_n(d'_{tr} - d_{pl}) \tag{6.60}$$

where

$$\alpha_n = \begin{cases} 0 & \text{if } n \leq 0.35 \\ 1.82(n - 0.35) & \text{if } 0.35 \leq n \leq 0.9 \end{cases} \tag{6.61}$$

In analysis, when the value of d is small, the load increment required may be too small; with the increase of d, the yield stress may be too low and the cap may be in tension space and a fatal error may occur. Reducing the value of R (see Sections 6.3.2 and 6.3.3) will improve the conditions. When d is too small, convergence may not be guaranteed. In analysis, a relatively small c value is used for each footings. The value of soil cohesion c used is assumed to be proportional to footing dimension. For a circular footing 1 m in diameter, c is assumed to be equal to 5 kPa, in order that the bearing capacity is not significantly increased and the convergence of the analysis is ensured.

6.3.2 Yield surface

The yield surface of a soil element is a boundary in the stress space within which the soil behaves elastically; an increment of stress from the yield surface may lead to a plastic deformation depending on the flow rule. Accordingly, the plastic deformation may result in a change of the yield surface and a new yield surface may be formed, depending on the hardening law. The current yield surface of a soil is related to the (effective) stress history of the soil.

The yield surface of the modified Drucker-Prager/Cap model in the p-t space consists of a straight line and a curved cap. The straight line is a Drucker-Prager shear failure segment defined by Equation (6.40). This failure segment is a perfectly plastic yield surface without hardening or softening. Plastic flow on the failure segment results in plastic volumentric increase which only causes the cap to soften. The cap yield surface, which hardens or softens as a function of plastic volumetric strain, is of elliptical shape written as

$$f_c = \sqrt{(p-p_a)^2 + \left[\frac{Rt}{(1+\alpha-\alpha\cos\beta)}\right]^2} - R(d + p_a\tan\beta) = 0 \qquad (6.62)$$

and the transition yield surface is expressed as

$$f_t = \sqrt{(p-p_a)^2 + \left[t - \left(1 - \frac{\alpha}{\cos\beta}\right)(d + p_a\tan\beta)\right]^2} - \alpha(d + p_a\tan\beta) = 0 \qquad (6.63)$$

in which R is a soil parameter which controls the shape of the cap, α is a small number for defining the transition yield surface. The parameter p_a is in the form of

$$p_a = \frac{p_b - Rd}{1 + R\tan\beta} \qquad (6.64)$$

where the isotropic compression yield stress, p_b, defines the hardening law, which will be discussed later in the following section.

Hibbitt *et al.* (1994) suggests that an α value between 0.01 and 0.05 should be used. Preliminary computational results indicate that the loading capacity of a footing is not significantly affected by the value of α. Therefore, an α value of 0.03 is selected in the analysis, as suggested by ABAQUS manuals. The loading capacity decreases slightly with R, which varies typically from 0 to 1. For the dense sand in this study, an R value of 0.5 is adopted.

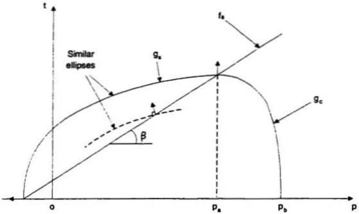

Figure 6.5: Plastic potential of modified Drucker-Prager/Cap model

6.3.3 Flow rule and hardening law

To define the flow rule of a soil, a plastic potential (surface) is used to indicate the direction of the plastic strain vector on the yield surface. The plastic strain vector is perpendicular to the plastic potential. When the strain vector is also perpendicular to the yield surface, the flow rule is termed associated. Otherwise, it is nonassociated. For associated flow rule, the yield surface can be used as a plastic potential.

The surfaces of plastic potential of the modified Drucker-Prager/Cap model are shown in Figure 6.5. On the cap yield surface, the plastic potential is associated, and is given by

$$g_c = \sqrt{(p - p_a)^2 + \left[\frac{Rt}{(1 + \alpha - \alpha \cos \beta)}\right]^2} \tag{6.65}$$

On the shear failure surface and the transition yield surface, the plastic potential is nonassociated, defined by

$$g_s = \sqrt{[(p-p_a)\tan\beta]^2 + \left[\frac{t}{(1+\alpha-\alpha\cos\beta)}\right]^2} \tag{6.66}$$

Therefore, g_c and g_s form a continuous and smooth potential surface. It should be mentioned that the nonassociated plastic flow implies that the soil stiffness matrix is not symmetric.

In the analysis, when the stress state of an element is outside the initially defined cap yield surface, ABAQUS will adjust the cap position so that the stress state lies on the yield surface.

The hardening law is defined by a piecewise relationship between the isotropic compression yield stress (p_b) and the volumetric plastic strain (ε_v^p), as shown in Figure 3.7. This relationship is obtained in isotropic triaxial compression test. In analysis, the initial volumetric plastic strain (ε_v^o) employed is corresponding to the initial stress state when the analysis begins. It defines the cap yield surface at the start of analysis.

6.4 Finite Element Technique

This section introduces some basic techniques used in the analysis of the ring footings. The main ideas presented here come from the ABAQUS manuals (Hibbitt *et al.*, 1994).

6.4.1 Element selection and isoparametric formulation

In ABAQUS (Hibbitt *et al.*, 1994), the axisymmetric elements are formulated in an r-z coordinate system. Isoparametric formulation is used in order to exactly represent rigid body modes and homogeneous deformation modes, which is necessary for convergence to the exact solution when the mesh is refined. All the elements are integrated numerically and the virtual work integral is replaced by a summation at the integration points. The integration can be "full" or "reduced". For full integration, the number of integration points is sufficient to exactly integrate the virtual work. For the reduced integration, the number of integration points is sufficient to exactly integrate the strain field contributions which are one order less than the order of interpolation; the higher-order contributions to the strain field will be ignored.

In reduced integration elements, the strains and stresses are calculated at locations which provide optimal accuracy. In addition, the reduced number of integration points decreases CPU time. A disadvantage of this procedure is that it may admit deformation modes causing no straining at the integration points. These zero-energy modes cause a phenomenon named "hourglassing" and result in inaccurate solution. This problem is particularly severe in first-order quadrilateral and hexahedra elements.

The isoparametric elements include quadrilaterals in two dimensions for plane and axisymmetric problems and "brick" (hexahedra) in three dimensions. Non-isoparametric elements such as wedge elements are only be used for awkward parts of the mesh. Standard first-order elements are of constant strains. Although first-order isoparametric elements can provide more than constant strain response, the higher-order content is usually not accurate and has little value. The second-order elements are of linear strains. For elliptic problems such as elasticity analysis, in which smoothness of solutions is assured, the second-order elements usually provide higher solution accuracy per degree of freedom.

For plasticity problems such as the foundation analysis in the present study, when the solution approaches the limit loads, the plasticity modes usually tend towards hyperbolic behaviour and localizations arise. These discontinuities in the gradient field should be well modelled. For a given number of nodes, the first-order elements are likely to be the best, as they provide the most locations at which some component of the solution gradient can be discontinuous (the element edges). Therefore first-order

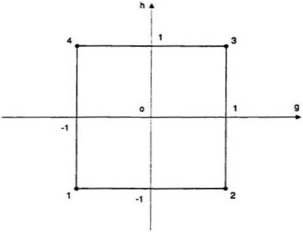

Figure 6.6: Isoparametric element

elements are preferred in such a case (Hibbitt *et al.*, 1994, Nagtegall *et al.*, 1974; and Nagtegaal and De Jong, 1981).

In this study, 4-node first-order quadrilateral elements of soil are chosen for the axisymmetric analysis. In the analysis, isoparametric interpolation and full integration are used. The isoparametric element is shown in Figure 6.6. The isoparametric element coordinates are g and h, ranging from -1 to +1 in an element. The interpolation function of the first-order quadrilaterals is

$$\begin{aligned} u = {} & \frac{1}{4}(1-g)(1-h)u_1 + \frac{1}{4}(1+g)(1-h)u_2 \\ & + \frac{1}{4}(1+g)(1+h)u_3 + \frac{1}{4}(1-g)(1+h)u_4 \end{aligned} \tag{6.67}$$

6.4.2 Interaction between soil and footings

In order to model the interaction between the deformable soil and the relatively stiff aluminum footing, interface elements are used. The footing is idealized as a rigid

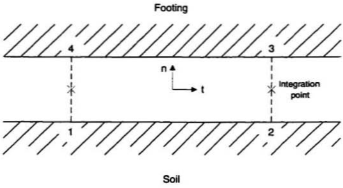

Figure 6.7: Node ordering of interface element INTER2A

body; the surface of the footing contacting the soil is treated as a rigid surface and is represented by rigid surface elements. For the surface of the soil contacting the footing, the interface elements use the nodes corresponding to the discretized soil domain. For each 4-node interface element (INTER2A), there are 2 nodes on each side of the contacting surfaces of the soil and the footing. The two integration points are located at the two ends. The node ordering of the interface elements is shown in Figure 6.7.

A rigid body representing a footing has a master reference node common to all of the rigid surface element nodes. The nodes for defining the rigid surface elements are slave nodes, on which kinematic constraints such as boundary conditions cannot be applied, but to which other elements can be connected. For the reference node, transitional and rotational degrees of freedom are allowed. Kinematic constraints controlling the over all motion of the rigid body must be defined at the reference node. Point loads can be applied to both the reference node and the rigid surface element nodes. Distributed

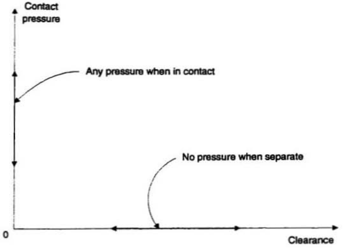

Figure 6.8: Contact pressure-clearance relationship for interface elements

loads can be applied to the rigid surface elements. The reference node can be used for nodal output.

For the interface elements between the rigid surface and the soil, a finite-sliding formulation is adopted. This formulation allows for separation and relative finite displacement. These elements satisfy the conditions of equilibrium and continuity of displacement in the normal contact direction and are able to transmit tangential shear stress and normal pressure stress. When the normal stress is reduced to zero, the surfaces begin to separate, as illustrated in Figure 6.8. Separated surfaces come into contact when the clearance becomes zero.

The tangential shear stress is coupled with the normal stress by the effect of friction between the two surfaces. The standard Coulomb friction model is used to define the shear response. Using this friction model, the contact surfaces do not slide as long as the equivalent shear stress is less than the critical shear stress (τ_{cr}), or

$$\tau_{eq} = \sqrt{\tau_1^2 + \tau_2^2} < \tau_{cr} \tag{6.68}$$

where τ_1 and τ_2 is the shear stresses in direction 1 and 2 respectively. The critical shear stress is related to the normal stress by

$$\tau_{cr} = \mu_f \sigma_n \tag{6.69}$$

where σ_n is the normal stress and μ_f is the coefficient of friction of the interface.

For isotropic friction, the direction of the frictional slip is identical to the direction of the shear stress, expressed by

$$\frac{\tau_i}{\tau_{eq}} = \frac{\dot{\gamma}_i}{\dot{\gamma}_{eq}} \tag{6.70}$$

where $\dot{\gamma}_i$ is the slip rate in direction i ($i = 1$ or 2), and $\dot{\gamma}_{eq}$ is the equivalent slip rate given by

$$\dot{\gamma}_{eq} = \sqrt{\dot{\gamma}_1^2 + \dot{\gamma}_2^2} \tag{6.71}$$

A stiffness method is used to implement the friction theory. The condition of no relative motion is approximately modelled by stiff elastic behaviour. No relative motion exists until frictional slip occurs. A larger value of the stiffness will more reasonably model the actual problem. As shown in Figure 6.9, the elastic stiffness is defined so that the relative motion (elastic slip) from the point of zero shear stress is bounded by the allowable maximum elastic slip (γ_{cr}) after which frictional slip occurs. The elastic slip is selected according to the value of a characteristic element length ($\bar{l}_i$) calculated by ABAQUS from the whole model. The maximum elastic slip is chosen as a small fraction (F_f) of $\bar{l}_i$. A better approximation can be achieved with a smaller value of F_f, at the expense of a slower convergence rate of the solution. As suggested by Hibbitt *et al.* (1994), a default F_f value of 0.005 is selected in the analysis.

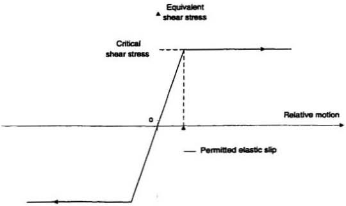

Figure 6.9: Friction model of interface elements

6.4.3 Nonlinear solution technique

The finite element models for the foundation analysis are nonlinear and involve many thousands of variables. The equilibrium equations may be symbolically expressed as

$$F^N(u^M) = 0 \tag{6.72}$$

where F^N is the force component conjugate to the N^{th} variable and u^M represents value of the M^{th} variable.

ABAQUS provides Newton's method and Quasi-Newton's method for solving the nonlinear problem of Equation (6.72) by developing a series of increments (Hibbitt *et al.*, 1994). Because the nonassociated flow rule is used in the elasto-plastic Drucker-Prager/Cap model for the soil, the stiffness matrix of the problem is not symmetric. Therefore, the Quasi-Newton's method, which requires that the Jacobian matrix should be symmetric and not change greatly from one iteration to the next, can not be used. The (standard) Newton's method is adopted as a numerical technique for solving the nonlinear equilibrium equations throughout the history of interest.

In the Newton's method, when an approximate solution of u_i^M has been obtained after an iteration i, if c_{i+1}^M is the difference between this approximate solution and the exact solution, Equation (6.72) can be written as

$$F^N(u_i^M + c_{i+1}^M) = 0 \tag{6.73}$$

Expanding this equation in a Taylor series about the approximate solution u_i^M yields

$$F^N(u_i^M) + \frac{\partial F^N}{\partial u^P}(u_i^M)c_{i+1}^P + \frac{\partial^2 F^N}{\partial u^P \partial u^Q}(u_i^M)c_{i+1}^P c_{i+1}^Q + \ldots = 0 \tag{6.74}$$

If u_i^M is a close approximation to the solution, each c_{i+1}^M will be small. Therefore, the above equation can be substituted by

$$K_i^{NP} c_{i+1}^P = -F_i^N \tag{6.75}$$

where

$$F_i^N = F^N(u_i^M) \tag{6.76}$$

and

$$K_i^{NP} = \frac{\partial F^N}{\partial u^P}(u_i^M) \tag{6.77}$$

is the Jacobian matrix. In this way, the next approximation to the solution is

$$u_{i+1}^M = u_i^M + c_{i+1}^M \tag{6.78}$$

and the iteration can be repeated to reach a required accuracy.

The advantage of this method is its quadratic convergence rate when convergence is ensured. However, Newton's method is expensive, because the Jacobian must be formed and solved at each iteration. Another major disadvantage of this method is that the calculation of the Jacobian matrix may be a problem, because in some cases it is difficult to obtain the form of the matrix algebraically. To ensure convergence, all entries in F_i^N and c_{i+1}^N must be sufficiently small. In ABAQUS, the magnitude of the increments can be controlled automatically. The time step is controlled based on the maximum force residuals following each iteration. By comparing the consecutive values of the force residuals, ABAQUS can determine whether convergence is likely. If convergence is unlikely in a reasonable number of iterations, the load increment will be adjusted.

6.5 Implementation of Analysis

6.5.1 Introduction to ABAQUS

The finite element analysis of footings is carried out using a general purpose finite element program, ABAQUS, which runs as a batch application (Hibbitt *et al.*, 1994). The input file indicates options required and gives data corresponding to these options. ABAQUS data consist of model data and history data. Model data define a finite element model including the elements, nodes, element properties and material behaviour; history data indicate the sequence of events and loads applied to the model. The program can be used to conduct various types of analyses, including static and dynamic stress-displacement analysis, heat transfer and thermal stress analysis, coupled pore fluid flow and stress analysis and mass diffusion analysis. In ABAQUS, a basic concept is that a problem history can be divided into steps. A step is any phase of the history: a thermal transient or a dynamic transient. In static stress analysis, a step just means an analysis of a load change from one magnitude to another. In each step, a procedure for defining the type of analysis (i.e., static or dynamic stress analysis) can be chosen, and loading definitions and boundary conditions can be given. The procedure can be changed from step to step to provide the user great flexibility in performing analyses.

An analysis process may include different steps. Each new step will start the analysis from the final state of the last step.

The element library in ABAQUS provides various choices of element types: solid (continuum) elements, interface elements, rigid elements, infinite elements, membrane elements, beam elements, elbow elements, hydrostatic fluid elements, shell elements and other special purpose elements. In an analysis, any meaningful combination of elements can be used to make up the model. In the foundation analysis of this study, solid elements are used in the soil domain, rigid elements are adopted to represent the foundation, and interface elements are employed to model the friction between soil and foundation.

ABAQUS provides a broad range of material behaviour: elasticity, plasticity, thermal properties, hydrostatic fluid and pore fluid flow properties, mass diffusion and other material properties. The material library provides both linear and nonlinear, isotropic and anisotropic material models. The properties related to a material are specified in a data block. A name is given to the material specified in order to reference it when corresponding element properties are defined. Some material data can be defined as functions of independent variables such as temperature and stress.

ABAQUS is well designed for result output including both nodal and element data. It offers a printed data file written during the analysis, containing information of model definitions, history definitions, and nodal and element output results specified by the user. ABAQUS also offers a results file and a restart file for postprocessing. The results file, in either ASCII or binary format, is a computer readable output file. The restart file may be read by ABAQUS to continue the analysis or may be processed by ABAQUS/POST to display the results. The program of ABAQUS/POST provides graphical postprocessing capacities including model plotting, deformed shape plotting, contour line plotting, vector plotting and X-Y plotting. It can be conveniently used to display plots interactively or generate hardcopy plots.

6.5.2 Finite element meshes

For circular and ring footings under axial loading, 4-node axisymmetric quadrilateral elements (CAX4) are adopted in the soil domain. Each footing is represented by a rigid body consisting of 6 two-node rigid surface elements (RAX2) and a reference node. Between the rigid surface and the soil, 6 interface elements (INTER2A) are defined to model the interaction between the footing and soil. Each 4-node interface element shares two nodes with a rigid surface element and other two nodes with a soil element. The finite element meshes for footings with ring radii ratios of 0, 0.2, 0.35, 0.5, 0.7, 0.8 and 0.9 are shown in Figure B.1 to B.7 in Appendix B, with 336, 368, 432, 400, 392, 324 and 336 soil elements respectively.

In the soil domain of the meshes, the nodes on the left vertical boundary which is the center line of axisymmetry, can only move in the vertical direction; rotation and horizontal movement are restrained. For nodes on the horizontal line at the bottom of the meshes, both vertical and horizontal movements are not allowed. For nodes on the right side boundary, only horizontal movement is restrained.

6.5.3 Loading of footings

The initial stresses in soil are the hydrostatic stresses due to gravity. The vertical stress (σ_1) of a soil element is calculated according to the depth of the element and the unit weight of the soil. The horizontal stress (σ_2 or σ_3) can be estimated using the coefficient of earth pressure at rest (K_o), measured using an oedometer ring as introduced in chapter 3. The initial stresses are applied to the soil elements by a loading step taking into account the soil body (gravity) force. In the process of loading, the measured K_o value of 0.42 is not directly used. A Poisson's ratio (ν) of 0.30 calculated from K_o using Equation (3.4) is used in the analysis. In this way, the initial stress state in the soil can be modelled.

In the finite element analysis, a footing is represented by a rigid body consisting of rigid surface elements and a reference node. The rigid surface elements are connected with soil elements using interface elements. The nodes of the rigid surface elements are slave nodes; kinematic constraints or boundary conditions cannot be applied on them. Boundary conditions of a footing must be defined on the reference node which can also be used for nodal output of loads and displacements. The reference node is a point where the load on the footing is applied.

Loading is applied on a footing by giving a prescribed vertical displacement on the reference node of the rigid body in a number of increments. The magnitude of a loading (displacement) increment is automatically selected by ABAQUS depending on the conditions of convergence. To ensure accuracy of analysis, the load is applied in 30 or more increments for each footing.

6.6 Analysis of Circular Footings

6.6.1 Procedure of analysis

Circular footings on the dense sand under axial loads have been analysed using the FE technique. Because the friction angle of soil decreases with stress level, an equivalent friction angle has been adopted for each footing. The technique of iteration has been employed in the finite element analysis. For each footing, an initial bearing capacity is assumed in order to calculated the mean stress (s) in soil using Equation (5.54). Using the estimated s, the friction angles at peak and critical state can be obtained by Equation (3.20) to (3.21); the Young's modulus can be obtained using Equation (3.9). After calculating the parameters of Drucker-Prager model by Equation (6.47) and (6.49), finite element analysis of the footing can be carried out to obtain a new bearing capacity. Then the calculated bearing capacity is used to repeat the analysis until a required accuracy for the bearing capacity is reached. Analysis shows that the convergency rate of iteration for the bearing capacity is very quick. For an assumed initial bearing capacity which is about one half of or twice the accurate bearing capacity of a footing, a bearing capacity with an accuracy of 0.1 percent can be obtained by repeating the iteration process for 3 or 4 times.

Preliminary analysis indicates that using the peak friction angle in the finite element analysis leads to an over-estimated bearing capacity when compared with centrifuge results. This suggests that a friction angle between the peak and critical state friction angles should be used. The friction angle from triaxial data for FE analysis is expressed as

$$\phi_{tr} = \phi_{cs} + m_\phi(\phi_{max} - \phi_{cs}) \tag{6.79}$$

where m_ϕ is a coefficient having a value from 0 to 1, ϕ_{max} and ϕ_{cs} are peak and critical friction angles expressed by Equation (3.20) and (3.21) respectively and are dependent on stress level. Preliminary analysis of circular footings indicate that to best fit the centrifuge data, an m_ϕ value of 0.5 should be used in the finite element analysis. This m_ϕ value of 0.5 has been chosen so that the bearing capacity obtained from the FE analysis is in accordance with that from the centrifuge tests when the footing diameter is 1.0 m. A footing of 1.0 m in diameter is considered an intermediate footing in size in the centrifuge tests and FE analysis.

The initial plastic volumetric strain (ε_v^o) in the soil under a footing is estimated according to a mean principal stress, by using the relationship between the plastic volumetric strain and mean principal stress as shown in Figure 3.7. This mean principal stress in the soil is the average value to a depth of three times the footing diameter.

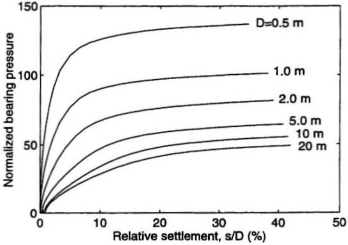

Figure 6.10: Normalized bearing pressure (R_p) versus relative settlement (s/D) of circular footings from FE analysis

6.6.2 Effect of footing size

Centrifuge test results presented in Chapter 4 show that the bearing capacity of circular footings increases linearly with footing diameter in a double-log scale diagram. The failure mode of footings tends to move from general shear failure to local shear failure when the size of footings is increased. The effects of foundation size on the behaviour of bearing capacity have been widely discussed (De Beer, 1965a; and Vesic, 1973; Clark, 1998).

To investigate the influence of footing size using FE technique, several circular footings under axial loads have been analyzed. The finite element model used for the analysis is shown in Figure B.1. The relationships between the normalized bearing pressure R_p expressed in Equation (4.18) and the relative settlement of footings with diameters of 0.5, 1.0, 2.0, 5.0, 10 and 20 m are presented in Figure 6.10. In the figure, s represents the settlement of a footing; D is the footing diameter. The normalized bearing pressure is in the form of

$$R_p = \frac{p}{\gamma D} \tag{6.80}$$

where p is the averaged pressure acting on the footing, and γ is soil unit weight.

From Figure 6.10, it can be seen that the normalized bearing pressure decreases with footing size. When the footing diameter is increased from 0.5 m to 20 m, the normalized bearing pressure at failure is reduced from approximately 125 to 42; the relative settlement is increased from approximately 8% to 22%. It can also be seen that the slope of the curves before failure loads decreases significantly with footing size. The failure mode of the circular footings tends to move from general shear failure to local shear failure when the footing diameter is increased.

The behaviour of load and settlement of circular footings from the FE analysis is very close to that of circular footings in centrifuge tests as seen in Figure 4.12. A major difference is that in centrifuge tests, there are peak loads for small footings, while in the FE analysis there is no peak load for all footings.

The bearing capacity obtained from FE analysis is plotted against footing diameter in Figure 6.11. The values of bearing capacity are 660, 960, 1450, 2300, 4400, 7600 and 13000 kPa when the footing diameters are 0.2, 0.5, 1.0, 2.0, 5.0, 10 and 20 m respectively. The bearing capacity calculated increases approximately linearly with footing diameter in the double-log scale diagram. For comparison, the bearing capacity of circular footings from centrifuge tests, represented by Equation (4.22) is also shown in Figure 6.11. It can be seen that the bearing capacity of circular footings from FE analysis is very close to that obtained from centrifuge tests. The difference is very small when the footing diameter is greater than 0.5 m. For smaller footings, the bearing capacity from FE analysis is higher.

The bearing capacity of circular footings of up to 20 m in diameter has been calculated in the FE analysis. In the centrifuge tests described in Chapter 4, the footing

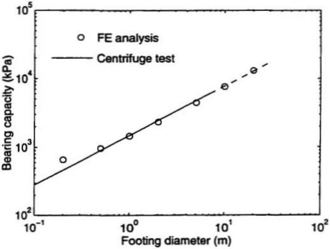

Figure 6.11: Bearing capacity versus diameter of circular footings

diameter is limited to 7 m. The relationship between the bearing capacity and footing diameter from centrifuge tests can be extrapolated as shown by the dotted line in Figure 6.11. The bearing capacity of footing with diameters of 10 m and 20 m is on the dotted line extrapolated from centrifuge test data. This indicates that when calibrated with test data, the FE technique developed can be used to estimate the bearing capacity of large foundations.

With the increase of footing size from 0.2 m to 20 m, the bearing capacity obtained from the FE analysis is increased from 660 kPa to 13,000 kPa, which leads to an significant increase of stress level in the soil and a decrease of friction angle shown in Figure 6.12. The equivalent friction angle mobilized is reduced from 42.4° to 36.4° when the footing diameter increases from 0.2 m to 20 m. For a log-cycle increase of footing size, the mobilized friction angle of soil in reduced by 3°.

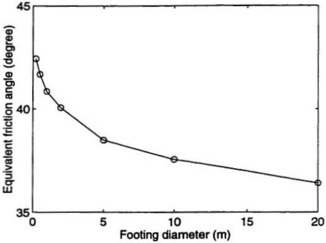

Figure 6.12: Equivalent friction angle versus footing diameter in FE analysis

6.7 Axially Loaded Ring Footings

The behaviour of ring footings under axial loads has been analyzed using the FE technique. The meshes for the FE analysis of footings with ring radii ratios of 0, 0.2, 0.35, 0.5, 0.7, 0.8 and 0.9 are shown in Figure B.1 to Figure B.7. To investigate the effect of footing size, four groups of footings with areas of 0.785, 1.57, 19.6 and 78.5 m^2 are analyzed. The corresponding circular footing diameters are 1.0, 2.0, 5.0 and 10 m respectively.

6.7.1 Load and settlement

Figure 6.13 presents the relationship between the average pressure applied and the settlement of two groups of footings, in which s represents the settlement of footings, and D is the outside diameter. In Figure 6.13(a), the area of the footings is 0.785 m^2, in which the outside footing diameters (D) are 1.0, 1.068, 1.155, 1.400 and 2.294 m

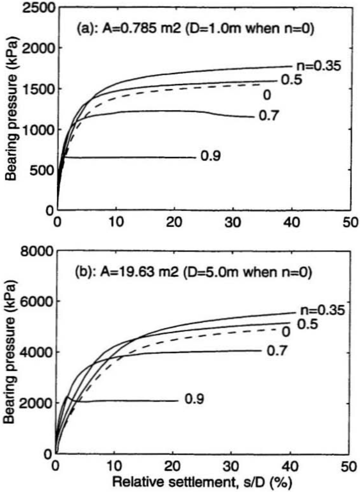

Figure 6.13: Load versus settlement of ring footings from FE analysis

when the ring radii ratios are 0, 0.35, 0.5, 0.7 and 0.9 respectively. The load-settlement relationship is influenced greatly by the ring radii ratio (n). The slope of the curves before failure loads increases with ring radii ratio. The failure load is maximum when n=0.35; when n=0 and 0.5, the failure loads are approximately equal; for a ring footing with n=0.9, the failure bearing pressure is 660 kPa, which is about one half of that of the circular footing (n=0). When n=0, 0.35 and 0.5, there are no peak loads; the loads increase slightly with settlements after failure loads. For n=0.7 and 0.9, there are peak loads; the load is decreased after the failure of footings.

For the larger footings with an area of 19.63 m^2 in Figure 6.13(b), in which the footing outside diameters are 5.0, 5.34, 5.77, 7.00, 11.5 m when the ring radii ratios are 0, 0.35, 0.5, 0.7 and 0.9 respectively, the relationship between load and settlement is similar to that of the smaller footings in Figure 6.13(a). It is seen that there are differences between the two groups of footings. In Figure 6.13(b), there is no peak load for the footing with n=0.7. The decrease of load after failure is more obvious for the footing with n=0.9. More importantly, the relative settlement (s/D) at failure becomes greater. The slope of the curves is smaller than that of the footings in Figure 6.13(a). With the increase of footing size, the bearing capacity increases but the failure mode becomes more and more local.

Compared with the centrifuge test data shown in Figure 4.16 to 4.19, the FE technique is not very good for modelling the strain softening behaviour of footings after failure loads. In centrifuge tests, all ring footings with various dimensions have failed in general shear mode; the failure loads are the peak ones. In the FE modelling, only footings with large ring radii ratio (n is greater than 0.7) fails in general shear model; when n is smaller, the failure mode is local shear. However, in both centrifuge tests and FE analysis, the load-settlement patterns are very similar before failure loads. Therefore, from the view point of bearing capacity, the results of the FE analysis of

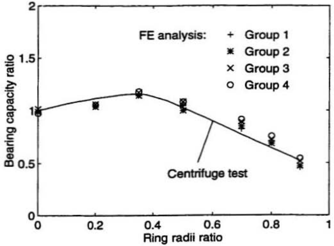

Figure 6.14: Bearing capacity ratio (B_r) versus ring radii ratio (n) from FE analysis (Group 1: A=0.785 m^2; Group 2: A=1.57 m^2; Group 3: A=19.6 m^2; Group 4: A=78.5 m^2)

ring footings are satisfactory.

6.7.2 Bearing capacity

As described in Section 6.6, the values of bearing capacity of circular footings of 1.0, 2.0, 5.0, and 10.0 m in diameter are 1450, 2300, 4400 and 7600 kPa respectively. Four groups of ring footings with the same areas as these four circular footings have been analyzed using FE technique to investigate the effect of footing size and ring radii ratio on bearing capacity. The calculated values of bearing capacity ratio (B_r) as given by Equation (4.27), which is defined as the ratio of the bearing capacity of a ring footing over the bearing capacity of a circular footing with the same area, are shown in Figure 6.14.

It is seen that at a given n value, the difference of the calculated B_r values of the four groups of footings is very small. This suggests that the footing size has little effect on the value of bearing capacity ratio. The B_r values from the FE analysis are very close to those from centrifuge tests. The FE technique adopted is good for calculating the bearing capacity of ring footings under axial loads.

6.8 Summarizing Remarks

The FE technique has been used for bearing capacity analysis of ring footings on dense sand under axial loads. In the analysis, a footing is represented by a rigid body with rigid surface elements. In the soil domain, 4-node axisymmetric elements are used. Between the footing and soil, interface elements have been adopted. Drucker-Prager/Cap constitutive model is chosen to simulate the elasto-plastic behaviour of soil. The analysis has been carried out using a general purpose finite element program, ABAQUS. The footings were loaded by applying a prescribed vertical displacement in a number of increments.

The effect of footing size on bearing capacity has been investigated by analyzing circular footings of 0.2 to 20 m in diameter. The normalized bearing pressure decreases with footing size. The failure mode of the circular footings tends to move from general shear to local shear when the footing size is increased. The bearing capacity increases from 660 to 13000 kPa when the footing diameter is from 0.2 to 20 m. As a result, the mobilized soil friction angle estimated is reduced from 42.4° to 36.4°, due to the increase of stress level in soil. The relationship between the calculated bearing capacity and footing diameter is approximately linear in a double-log scale diagram. The bearing capacity from FE analysis is very close to that obtained in centrifuge tests. Footings with ring radii ratios of 0.2, 0.35, 0.5, 0.7, 0.8 and 0.9 have been analyzed to examine the effect of footing shape and size. The load-settlement pattern and the bearing capacity behavior of the ring footings analyzed are similar to those observed on centrifuge tests.

In the literature, very few good results of the bearing capacity of foundations on sand from finite element analysis have been reported. It is believed that the difficulty is due to the complexity of soil behaviour. In this study, an attempt has been made to use the FE technique to investigate the bearing capacity behaviour of ring foundations on a dense sand. Satisfactory results have been obtained. The parameters of the Drucker-Prager/Cap constitutive model are chosen according to the triaxial behaviour and other properties of soil. Some soil parameters are determined by comparing the bearing capacities obtained from the FE analysis to those from the centrifuge tests. The finite element technique is helpful for further understanding of ring foundation behaviour. It can be very useful when experimental modelling is difficult, such as in the case of very large foundation analysis. The procedure of the FE analysis developed could be helpful for future research on the behaviour of foundations on cohesionless soils.

Chapter 7

Summary and Conclusions

7.1 Summary

This thesis presents research on the bearing capacity of ring foundations on a dense sand by means of centrifuge modelling, the method of characteristics and FE analysis. The work has summarized the past research on ring foundations and has presented a comprehensive review of the fundamentals of bearing capacity in order to provide an insight to the behaviour of foundations. The silica sand used had an effective grain size (d_{10}) of 0.22 mm and a uniformity coefficient of 1.69. Triaxial tests have been carried out to determine the the variations of friction angle and plastic volumetric strain of the sand at a density index of 90%. In situ stresses and elastic moduli were measured by oedometer compression tests. The friction between the sand and the aluminum footings used in centrifuge tests was measured using a direct shear device.

Over 40 centrifuge tests of ring footings on the sand have been carried out at accelerations from 10 to 160 gravities to investigate the effect of footing size, ring radii ratio and load eccentricity on bearing capacity. The aluminum model footings of 15 cm^2 in area each have ring radii ratios of 0, 0.2, 0.35, 0.5, 0.7, 0.8 and 0.9. Footings were loaded vertically at a constant rate of 0.1 mm per second, with load eccentricity ratios ranging from 0 to 0.375. A steel ball was positioned on each footing to transfer load from a load cell so that the footing could rotate during loading. Three linear displacement transducers were used to measure the vertical displacement and rotation of footings. Sand samples of up to 430 kg were prepared by a raining technique using a diffuser consisting of three 200 mm sieves and a shutter with 19 holes, resulting in a density index of 90%. During the raining of sand, the falling height was kept at 50 cm while the deposition intensity was 0.103 g/cm^2 per second. Centrifuge model tests have been verified using the principle of modelling of models. Based on the test results, a procedure for evaluating the bearing capacity of ring foundations under axial and eccentric loads has been presented.

The bearing capacity of circular footings under axisymmetric conditions has been estimated by the method of characteristics (or slip-line method) using the Mohr-Coulomb yield criterion of soil. The analysis has been carried out to investigate the effect of footing size on bearing capacity. An elastic wedge under a rough footing has been assumed. The wedge angle can be derived from the average mobilized friction angle according to the stress level along the wedge surface. A program written in C has been developed to implement the analysis. Analyses have been conducted using both a constant equivalent friction angle and variable friction angle which depends on the stress level in the soil.

Circular and ring footings under axial loads have been analyzed by the finite element (FE) technique. A footing is represented by a rigid body consisting of rigid surface elements. In the soil domain, 4-node axisymmetric element are used. Interface elements are used to model the interaction between the footing and soil. The elasto-plastic constitutive relationship of soil is represented by the Drucker-Prager/Cap model. The FE analysis has been conducted on circular footings of 0.2 to 20 m in diameter and on ring footings of different dimensions and ring radii ratios. The effect of footing size and shape on bearing capacity has been investigated.

7.2 Conclusions

According to the results obtained regarding to the soil behaviour, the centrifuge modelling and numerical analysis of circular and ring footings, the following conclusions can be drawn:

1. In triaxial compression tests, both the peak and critical state friction angles of the silica sand with density index of 90% decrease with stress level. When the cell pressure is increased from 25 to 2500 kPa, the peak friction angle is reduced from 46.9° to 37.3°, while the critical state friction angle is reduced from 40.1° to 31.9°. For a log-cycle increase of stress, the friction angles are reduced by 4° to 5°. The difference between the peak friction angle and the critical state one ranges from 5° to 7°, decreasing with stress level.

2. The coefficient of earth pressure at rest (K_o) of the sand measured using an oedometer ring is 0.42. The value of Poisson's ratio determined from the value of K_o is 0.30. The measured elastic modulus, which increases with stress, is close to that proposed by Hardin and Richart (1963).

3. The coefficient of friction between the sand and the aluminum footings, measured using a direct shear device, is 0.53. This value is equivalent to a friction angle of 28° between the sand and the footings.

4. Using the raining technique developed, dense uniform sand samples can be obtained with good repeatability. The method is very effective for preparing large sand samples.

5. For the circular footings in the centrifuge, the bearing capacity increases linearly with footing diameter in a double-log scale diagram. For a footing with a prototype diameter of 7 m, the measured bearing capacity is as high as 6200 kPa. The bearing capacity factor N_γ decreases with increasing footing size due to the reduction of soil

friction angle with stress level and the effect of progressive failure of soil.

6. In centrifuge tests, the bearing capacity of constant area ring footings under axial loads increases slightly when the ring radii ratio (n) is from 0 to 0.35. When n is greater than 0.35, the bearing capacity decreases significantly. For a ring footing with n=0.9, the bearing capacity is about one half of that of the circular footing. Test results indicate that the bearing capacity of a ring footing can be obtained from the bearing capacity of a circular footing with the same area using a bearing capacity ratio. B_r. The value of B_r is related only to the ring radii ratio, and is independent of footing size.

7. For eccentrically loaded ring footings in centrifuge, the bearing capacity decreases with load eccentricity. The bearing capacity of a ring footing under eccentric load can be expressed in terms of a reduction factor (R_e) and the bearing capacity of the footing under axial load. The value of R_e is related only to load eccentricity, and is independent of ring radii ratio and footing size.

8. The centrifuge test results indicate that the bearing capacity of an eccentrically loaded ring footing on the sand (q_u) can be estimated from the bearing capacity ratio, B_r, the reduction factor, R_e, and the bearing capacity of an axially loaded circular footing with the same area (q_{uc}). That is

$$q_u = R_e B_r q_{uc}$$

This procedure for evaluating the bearing capacity of ring footings under vertical loads is very practical, because the bearing capacity of a circular footing can be obtained using the generally accepted experimental data and theories available in the literature.

9. The bearing capacity of circular footings can be calculated by the method of characteristics using variable soil friction angle or equivalent constant friction angle. The bearing capacities calculated also increase approximately linearly with footing dimension in a double-log scale diagram, and are close to the results obtained in centrifuge

tests. The method for bearing capacity using an equivalent friction angle provides a basis for the FE analysis of footings using constant friction angles.

10. In the FE analysis, the bearing capacity of circular footings is increased from 660 to 13000 kPa when the footing diameter is from 0.2 to 20 m. As a result, the mobilized soil friction angle is reduced from 42.4° to 36.4°, due to the increase of stress level in soil. The load-settlement pattern and bearing capacity of ring footings obtained from the FE analysis are very close to those from centrifuge tests.

11. This study presents an attempt at applying the finite element technique for the bearing capacity of ring foundations on sand. The results from the analysis of circular and ring footings are satisfactory. It should be mentioned that some soil parameters for the FE analysis have been determined by comparing the results of FE analysis with centrifuge test data. The finite element model calibrated with experimental data is very useful for analysis of very large foundations or for other cases when experimental results are not available or difficult to obtain.

7.3 Future Research

In this study, centrifuge tests have been carried out to investigate the bearing capacity behaviour of ring footings on sand under axial and eccentric vertical loads. The method of characteristics has been employed to study the effect of footing size on the bearing capacity of circular footings. The FE analysis has been carried out to calculate the bearing capacity of circular and ring footings under axial loads. Good results have been obtained. According to the results and experience obtained in this research, it is recommended that future research on the bearing capacity of ring foundations should be concentrated on the following.

1. Centrifuge modelling of ring foundations under inclined or torsional loads should be conducted, because ring foundations are often used for tall structures which are

subject to horizontal as well as vertical loads.

2. Centrifuge tests may be carried out to investigate the effect of other factors on the bearing capacity of ring foundations, such as the density of sand, the embedment depth of foundations and the cohesion of soil. The presently available theories and experience of strip and circular foundations should be very helpful to guide the design of the experiment. It is expected that the results of a limited number of tests will be enough to provide a insight to the influence of those factors.

3. Three dimensional finite element analysis can be carried out for ring foundations under eccentric and inclined loads. Three dimensional FE analysis will be more difficult to conduct due to the large number of variables and slower convergence rate in analysis of foundations under eccentric and inclined loads. The analysis should be focused on large foundations as they are more practical. For small footings on sand such as one of 0.1 m in dimension, the FE analysis may be difficult due to the high friction angle of soil as the stress level is low.

REFERENCES

Aiban, S.A., and Znidarcic, D. (1991). "Shallow Footings on Sand under Vertical Central, Eccentrical and Inclined Loads." *Centrifuge 91*, Balkema, Rotterdam, pp. 201-208.

Al-Hussaini, D.M., and Perry, E.B. (1978). "Field Experiment of Reinforced Earth Wall." *ASCE Journal of Geotechnical Engineering Division*, Vol. 104, No. GT3, pp. 307-322.

Al-Sanad, H.A., Ismael, N.F., and Brenner, R.P. (1993). "Settlement of Circular and Ring Plates in Very Dense Calcareous Sands." *ASCE Journal of Geotechnical Engineering*, Vol. 119, No. 4, pp. 622-638.

Andrawes, K.Z., and El-Sohby, M.A. (1973). "Factors Affecting Coefficient of Earth Pressure K_o". *ASCE Journal of Soil Mechanics and Foundation Engineering*, Vol. 99, No. SM7, pp. 527-539.

Bakir, N.E., and Garnier, J. (1994). "Loading of Shallow Foundations: Importance of Testing Procedures." *Centrifuge 94*, Balkema, Rotterdam, pp. 553-558.

Bhushan, K., and Boniadi, F. (1988). "Settlement of a Ring Foundation using Cone Data." *Cone penetration Testing 1988*, ISOPT-1, Balkema, Rotterdam.

Biarez, J., Burel, M., and Wack, B. (1961). "Contribution a l'etude de la force portant des fondations." *Proceedings of the 5th International Conference on Soil Mechanics and Foundation Engineering*, Vol. 1, pp. 603-609.

Bishop, A.W. (1961). Discussions on "Soil Properties and their Measurement." *Proceedings of the 5th International Conference on Soil Mechanics and Foundation Engineering*, Paris, Vol. 3, pp. 97-100.

Bishop, A.W. (1966). "The Strength of Soils as Engineering Materials." *Geotechnique*, Vol. 16, No. 2, pp. 91-128.

Bjerrum, L. (1973). "Problem of Soil Mechanics and Construction on Soft Clays." *Proceedings of the 8th International Conference on Soil Mechanics and Foundation Engineering*, Moscow, State of the Art Report, Vol. 3, pp. 111-159.

Bolton, M.D. (1986). "The Strength and Dilatancy of Sands." *Geotechnique*, Vol. 36, No. 1, pp. 65-78.

Bolton, M.D., and Lau, C.K. (1993). "Vertical Bearing Capacity Factors for Circular and Strip Footings on Mohr-Coulomb Soil." *Canadian Geotechnical Journal*, Vol. 30, pp. 1024-1033.

Bonding, N. (1977). "Kinematical Admissibility of the Pure N_γ Rupture Figure." *Proceedings of the 9th International Conference on Soil Mechanics and Foundation Engineering*, Vol. 1.

Bowles, J.E. (1975). "Combined and Special Footings." in *Foundation Engineering Handbook,* edited by H. F. Winterkorn and H. Y. Fang, Van Nostrand Reinhold Company, New York, pp. 504-527.

Bowles, J.E. (1977). *Foundation Analysis and Design,* 2nd ed., McGraw-Hill, New York, 750 p.

Bozozuk, M. (1974). "Bearing Capacity of Clays for Tower Silos." *Canadian Agricultural Engineering,* Vol. 16, No. 1, pp. 13-17.

Bozozuk, M. (1979a). "Problems with Concrete Tower Silos." *Canadian Agricultural Engineering,* Vol. 21, No. 2, pp. 69-77.

Bozozuk, M. (1979b). "The Instrumented Tower Silo at Hammond, Ontario." *Canadian Agricultural Engineering,* Vol. 21, No. 2, pp. 79-84.

Brenner, R.P., Kunzi, B., Jeragh, A., and Gunatilaka, A. (1990). "Site Investigation for Tower Structure on Ring-Shaped Raft on Sand." *Proceedings of the 6th International Congress of the International Association of Engineering Geology,* Balkema, Rotterdam, pp. 1813-1820.

Britto, A.M., Gunn, M.J. (1987). *Critical State Soil Mechanics Via Finite Elements,* John Wiley & Sons, New York, 488 p.

Brooker, E.W., and Ireland, H.O. (1965). "Earth Pressures at Rest Related to Stress History." *Canadian Geotechnical Journal,* Vol. 2, No. 1, pp. 1-15.

Caquot, A., Kerisel, J. (1953). "Sur le terme de surface dans le calcul des fondations en milieu pulverulent." *Proceedings of the 3rd International Conference on Soil Mechanics and Foundation Engineering,* Zurich, Switzerland, Vol. 1, pp. 336-337.

Canadian Geotechnical Society. 1992. *Canadian Foundation Engineering Manual,* 3rd Edition, BiTech Publishers Ltd., Vancouver.

Chen, W.F. (1975). *Limit Analysis and Soil Plasticity,* Elsevier, New York, 638 p.

Christian, J.T. (1977). *Numerical Methods in Geotechnical Engineering,* Shallow Foundation, Ch. 6, McGraw Hill Book Company.

Chu, J. (1995). "An Experimental Examination of the Critical State and Other Similar Concepts for Granular Soils." *Canadian Geotechnical Journal,* Vol. 32, pp. 1065-1075.

Clark, J.I. (1972). "Evaluation and Performance of the Calgary Tower Foundation." *Proceedings of the 25th Canadian Geotechnical Conference*, Ottawa.

Clark, J.I. (1998). "The Settlement and Bearing Capacity of Very Large Foundations on Strong Soils: The 1996 R.M. Hardy Lecture." *Canadian Geotechnical Journal*. Vol. 35, No. 1, pp. 131-145.

Corte, J.F., Faigeix, D., Gainier, J., Bagge, G., Fuglsang, L., James, R.G., Shi, Q., and Tan, F. (1988). "Centrifugal Modelling of Behaviour of Shallow Foundation - A Cooperative Test Program." *Centrifuge 88*, Balkema, Rotterdam, pp. 325-336.

Corte, J.F., Garnier, J., Cottineau, L.M., and Rault, G. (1991). "Determination of Model Soil Properties in the Centrifuge." *Centrifuge 91*, ed. by H.Y. Ko, Balkema, Rotterdam, pp. 607-614.

Cox, A.D. (1962). "Axially-Symmetric Plastic Deformation in Soils-II. Indentation of Ponderable Soils." *Int. J. Mech. Sci.*, 4: 371-380.

Cox, A.D., Eason, G. and Hopkins, H.G. (1961). "Axially Symmetric Plastic Deformation in Soils." *Trans. R. Soc. London, Ser. A*, 254: 1.

Craig, W.H. (1989). "Edouard Phillips (1821-89) and the Idea of Centrifuge Modelling." *Geotechnique*, Vol. 39, No. 4, pp. 679-700.

Cunard, C.G. (1993). "Design of an In-Flight Cone Penetrometer for the Acutronic 680-2 Geotechnical Centrifuge." C-CORE Internal *Report*, Memorial University of Newfoundland, St. John's, Canada.

Das, B.M. (1990) *Principles of Foundation Engineering*. Second Edition, PWS-Kent Publishing Company, Boston, 731 p.

Dasgupta, S., and Sengupta, D. (1989). "Analysis of Ring Foundation and Circular Footing on Elastic Foundation using Curved Isoparametric Beam Element." *Journal of the Institution of Engineers (India)*, Civil Engineering Division, Vol. 69, Part CI 4, January, pp. 252-256.

Davidson, H.L., and Chen, W.F. (1976). "Nonlinear Analyses in Soil and Solid Mechanics." In *Numerical Methods in Geomechanics* (ed. C.S. Desai), pp. 205-218. American Society of Civil Engineers (ASCE), New York.

De Beer, E.E. (1965a). "Bearing Capacity and Settlement of Shallow Foundations on Sand." *Proceedings of Bearing Capacity and Settlement of Foundation Symposium*, Duke University, pp. 15-34.

De Beer, E.E. (1965b). "The Scale Effect on the Phenomenon of Progressive Rupture in Cohesionless Soils." *Proceedings of the 6th International Conference on Soil Mechanics and Foundation Engineering*, Montreal, Vol. 2, pp. 13-17.

De Beer, E.E. (1970). "Experimental Determination of the Shape Factors and Bearing Capacity Factors of Sand." *Geotechnique*, Vol. 20, No. 4, pp. 387-411.

De Beer, E.E. (1987). "Analysis of Shallow Foundations." in *Geotechnical Modeling and Applications*, edited by Sayed M. Sayed, Gulf Publishing Company, Houston, pp. 212-321.

De Josselin de Jong, G. (1976). "Rowe's Stress-Dilatancy Relation Based on Friction." *Geotechnique*, Vol. 26, No. 3, pp. 527-534.

Desai, C.S. (1968). "Solution of Stress-Deformation Problems in Soil and Rock Mechanics Using the Finite Element Methods." *Ph.D. Thesis*, University of Texas, Austin.

Desai, C.S. (1971). "Nonlinear Analyses Using Spline Functions." *ASCE Journal of Soil Mechanics and Foundation Division*, Vol. 97, No. SM10.

Desai, C.S., and Christian, J.T. (ed.). (1977). "Numerical Methods in Geotechnical Enginering," McGraw-Hill Book Company, New York, 783p.

Desai, C.S., and Reese, L.C. (1970). "Analysis of Circular Footings on Layered Soils." *ASCE Journal of Soil Mechanics and Foundation Division*, Vol. 96, No. SM4.

Drucker, D.C., Prager, W. (1952). "Soil Mechanics and Plasticity Analysis or Limit Design." *Quarterly of Applied Mathematics*, Vol. 10, No. 2, pp. 157-165.

Durgunoglu, H.T., and Mitchell, J.K. (1975). "Static Penetration Resistance of Soils." *Proceedings of ASCE Conference on In Situ Measurement of Soil Properties*, Raleigh, pp. 151-188.

Egorov, K.E. (1965). "Calculation of Bed for Foundation With Ring Footing." *Proceedings of the 6th International Conference on Soil Mechanics and Foundation Engineering*, Montreal, Vol. 2, pp. 41-45.

Eid, W.K. (1987). "Scaling Effect in Cone Penetration Testing in Sand." *Ph.D. Thesis*, Virginia Polytechnic Institute and State University, 244 p.

Feda, J. (1976). "Skin Friction of Piles." *Proceedings of the 6th European Conference on Soil Mechanics and Foundation Engineering*, Vol. 1.2, International Society for Soil Mechanics and Foundation Engineering, pp. 423-428.

Feng, G. and Hu, Y. (1988). "Centrifuge Model Test of a Highway Embankment on Soft Clay." in *Centrifuge 88*, ed. by Corte, Balkema, Rotterdam, pp. 153-162.

Ferguson, K.A., and Ko, H.Y. (1985). "Application of Centrifuge Modelling to Cone Penetrometer Technology." *Proceedings of the Symposium on the Application Centrifuge Modelling to Geotechnical Design*, Balkema, Rotterdam.

Fuglsang, L.D., and Ovesen, N.K. (1988). "The Application of the Theory of Modelling to Centrifuge Studies." in *Centrifuge in Soil Mechanics*, ed. by W.H. Craig *et al.*, Balkema, Rotterdam, pp. 119-138.

Garnier, J., and Canepa, Y. (1991). "Effect of Different Footing Conditions on the Ultimate Bearing Pressure." *Centrifuge 91*, Balkema, Rotterdam, pp. 209-216.

Gorbunov-Possadov, M.I. (1965). "Calculations for the Stability of Sand Bed by a Solution Combining Theories of Elasticity and Plasticity." *Proceedings of the 6th International Conference on Soil Mechanics and Foundation Engineering*, Vol. 2. pp. 51-55.

Graham, J. (1968). "Plane Plastic Failure in Cohesionless Soils." *Geotechnique*, Vol. 18, No. 3, pp. 301-316.

Graham, J., and Hovan, J.M. (1986). "Stress Characteristics for Bearing Capacity in Sand Using a Critical Model." *Canadian Geotechnical Journal*, Vol. 23, No. 2, pp. 195-202.

Graham, J., and Stuart, J.G. (1971). "Scale and Boundary Effects in Foundation Analysis." *ASCE Journal of Soil Mechanics and Foundation Engineering Division*, Vol. 97, No. SM11, pp. 1533-1548.

Griffith, D.U. (1982). "Computation of Bearing Capacity Factors Using Finite Elements." *Geotechnique*, Vol. 32, No. 3, pp. 195-202.

Hanna, A.M., and Meyerhof, G.G. (1981). "Experimental Evaluation of Bearing Capacity." *Canadian Geotechnical Journal*, Vol. 18, No. 4, pp. 599-603.

Hansen, J.B. (1970). "A Revised and Extended Formula for Bearing Capacity." Danish Geotechnical Institute, Copenhagen, Bulletin 28, pp. 5-11.

Hansen, B., and Christensen, N. H. (1969). Discussion of "Theoretical Bearing Capacity of Very Shallow Footings." by Lawrence A. Larkin, *ASCE Journal of the Soil Mechanics and Foundations Division*, Vol. 95, No. SM6, pp. 1568-1572. (MUN Lib, Microfilm)

Hardin, B.O. (1985). "Crushing of Soil Particles." *ASCE Journal of Geotechnical Engineering*, Vol. 111, No. 10, pp. 1177-1192.

Hardin, B.O., and Richart, F.E. (1963). "Elastic Wave Velocities in Granular Soils." *ASCE Journal of Soil Mechanics and Foundation Engineering*, Vol. 89, No. SM1, pp. 33-65.

Hibbitt, H.D., Karlsson, B.I., and Sorenson, E.P. 1994. "User's Manuals and Theory Manual." *ABAQUS/Standard Version 5.4 Documentation*, Hibbitt, Karlsson & Sorenson Ltd., Providence, Rhode Island.

Hill, R. (1950). "The Mathematical Theory of Plasticity." Oxford University Press. London.

Hoeg, K., Christian, J.T., and Whitman, R.V. (1968). "Settlement of Strip Load on Elastic Plastic Soil." *ASCE Journal of Soil Mechanics and Foundation Division*, Vol. 94, No. SM2, pp. 431-445.

Hrennikoff, A. (1941). "Solution of Problems in Elasticity by the Frame Work Method." *Journal of Applied Mechanics*, Vol. 8, No. 4, pp. 59-82.

Hushmand, B., Scott, R.F., and Grouse, C.B. (1988). "Centrifuge Liquefaction Tests in a Laminar Box." *Geotechnique*, Vol. 38, No. 2, pp. 253-262.

Ismael, N.F. (1996). "Loading Tests on Circular and Ring Plates in Very Dense Cemented Sands." *ASCE Journal of Geotechnical Engineering*, Vol. 122, No. 4, pp. 281-287.

James, R.G., and Shi, Q. (1988). "Centrifuge Modelling of the Behaviour of Surface Footings under Combined Loading." *Centrifuge 88*, Balkema, Rotterdam, pp. 307-311.

Jamiolkowski, M. (1985). "New Developments in Field and Laboratory Testing of Soils." *Theme Lecture, the 11th International Conference on Soil Mechanics and Foundation Engineering*, San Francisco.

Juilie, Y., and Sherwood, D.E. (1983). "Improvement of Sabkha Soil of the Arabian Gulf Coast." *Proceedings of the 8th European Conference on Soil Mechanics and Foundations*, Helsinki, pp. 781-788.

Kathroli, S., Madhav, S.K., and Iyengar, N.G. (1982). "Analysis of Rigid Ring Foundations." *Proceedings of the International Symposium on Numerical Models in Geotechnics,* Edited by R. Dungar *et al.*, Zurich, pp. 687-692.

Kimura, T., Kusakabe, O., and Saitoh, K. (1985). "Geotechnical Model Tests of Bearing Capacity Problems in a Centrifuge." *Geotechnique,* Vol. 35, No. 1, pp. 33-45.

Ko, H.Y., and Davidson, L.W. (1973). "Bearing Capacity of Footings in Plane Strain." *ASCE Journal of Soil Mechanics and Foundations Division*, Vol. 99, No. SM1, pp. 1-23.

Kolbuszeski, J.J. (1948a). "An Experimental Study of the Maximum and Minimum Porosities of Sands." *Proceedings of the 2nd International Conference on Soil Mechanics and Foundation Engineering*, London, Vol. 1, pp. 158-165.

Kolbuszeski, J.J. (1948b). "General Investigation of the Fundamental Factors Controlling Loose Packing of Sand." *Proceedings of the 2nd International Conference on Soil Mechanics and Foundation Engineering*, London, Vol. 1, pp. 47-49.

Kosar, K.M., Walter, D.J., and Burwash, W.J. 1994. "Design of Foundations to Resist High Lateral Loads for Northumberland Strait Crossing." *Proceedings of the 4th Conference on Developments in Short and Medium Span Bridge Engineering '94*, Halifax, Canada, pp. 1363-1375.

Kusakabe, O., Yamaguchi, H., and Morikage, A. (1991). "Experiment and Analysis of Scale Effect of N_γ for Circular and Rectangular Footings." *Centrifuge 91*, Balkema, Rotterdam, pp. 179-186.

Kutter, B.L., Abghari, A., and Shinde, S.B. (1988). "Modelling of Circular Foundations on Relatively Thin Clay Layers." *Centrifuge 88*, Balkema, Rotterdam, pp. 337-344.

Lacasse, S.K., and Olsen, T.S. (1988). "Evaluation of Foundation Stability of Platform MCP-01." *Report*, Norwegian Geotechnical Institute.

Ladd, C.C., Foott, R., Ishihara, K., Schlosser, F., and Poulos, H.G. (1977). "Stress-Deformation and Strength Characteristics." *Proceedings of the 9th International Conference on Soil Mechanics and Foundation Engineering*, Tokyo, Vol. 2, pp. 421-494.

Lade, P.V., and Duncan, J.M. (1975). "Elastoplastic Stress-Strain Theory for Cohesionless Soil." *ASCE Journal of Geotechnical Engineering Division*, Vol. 101, pp. 1037-1053.

Lade, P.V., Yamamuro, J.A., and Bopp, P.A. (1996). "Significance of Particle Crushing in Granular Materials." *ASCE Journal of Geotechnical Engineering*, Vol. 122, No. 4, pp. 309-316.

Larkin, L.A. (1968). "Theoretical Bearing Capacity of Very Shallow Footings." *ASCE Journal of Soil Mechanics and Foundations Division*, Vol. 94, No. SM6, pp. 1347-1357.

Lau, C.K. (1988). "Scale Effects in Tests on Footings." *Ph.D. Thesis*, Cambridge University, U.K.

Lee, F.H. (1985). "Centrifuge Modelling of Earthquake Effects on Sand Embankments and Islands." *Ph.D. Thesis*, Cambridge University, U.K.

Lee, F.H., and Schofield, A.N. (1988). "Centrifuge Modelling of Sand Embankments and Islands in Earthquake." *Geotechnique*, Vol. 38, No. 1, pp. 45-58.

Lin, L. (1995). "Strength Characteristics of a Modelling Silty Clay." *M.Eng. Thesis*, Memorial University of Newfoundland, St. John's, 120 p.

Lo, K.Y., and Becker, D.E. (1979). "Pore-Pressure Response beneath a Ring Foundation on Clay." *Canadian Geotechnical Journal*, Vol. 16, pp. 551-566.

Logan, D.L. (1992). "A First Course in the Finite Element Method." 2nd Edition, PWS-KENT Publishing Company, Boston, 662p.

Lundgren, H., and Mortensen, K. (1953). "Determination by the Theory of Plasticity of the Bearing Capacity of Continuous Footings on Sand." *Proceedings of the 3rd International Conference on Soil Mechanics and Foundation Engineering*, Zurich, Switzerland, Vol. 1, pp. 409-412.

Lunne, T., and Kleven, A. (1981). "Role of CPT in North Sea Foundation Engineering." *Cone Penetration Testing and Experience*, Ed. by G.M. Norris and R.D. Holtz, pp. 201-227.

Madhav, M.R. (1980). "Settlement and Allowable Pressures for Ring or Annular Footings." *Indian Geotechnical Journal*, Vol. 10, pp. 267-271.

Madhav, M.R., and Karmarkar, R.S. (1982). "Elasto-Plastic Settlement of Rigid Footings." *ASCE Journal of Geotechnical Engineering Division*, Vol. 108, No. GT3, pp. 483-488.

Marsland, A., and Quarterman, R.S. (1982). "Factors Affecting the Measurements and Interpretation of Quasi-Static Penetration Tests in Clays." *Proceedings of the 2nd European Symposium on Penetration Testing*, Amsterdam, pp. 697-702.

Mayne, P.W., and Kulhawy, F.H. (1982). "K_o-OCR Relationship in Soil." *ASCE Journal of Geotechnical Engineering Division*, Vol. 108, No. GT6, pp. 851-872.

McHenry, D. (1943). "A Lattice Analogy for the Solution of Plane Stress Problems." *Journal of Institution of Civil Engineers*, Vol. 21, pp. 59-82.

Meigh, A.C. (1987). *Cone Penetration Testing: Methods and Interpretation.* Butterworths, United Kingdom.

Menard, L. (1965). "Regle pour le calcul de la force portante et du tassement des fondations en fonction des resultats pressiometriques." *Proceedings of the 6th International Conference on Soil Mechanics and Foundation Engineering*, Montreal, Vol. 2, pp. 295-299.

Meyerhof, G.G. (1950). "The Bearing Capacity of Sand." *Ph.D. Thesis,* University of London.

Meyerhof, G.G. (1951). "The Ultimate Bearing Capacity of Foundations." *Geotechnique,* Vol. 2, pp. 301-332.

Meyerhof, G.G. (1953). "The Bearing Capacity of Foundations Under Eccentric and Inclined Loads." *Proceedings of the 3rd International Conference on Soil Mechanics and Foundation Engineering,* Zurich, Vol. 1, pp. 440-445.

Meyerhof, G.G. (1955). "Influence of Roughness of Base and Groundwater Conditions on the Ultimate Bearing Capacity of Foundations." *Geotechnique.* Vol. 5, pp. 227-242.

Meyerhof, G.G. (1963). "Some Recent Research on The Bearing Capacity of Foundations." *Canadian Geotechnical Journal,* Vol. 1, No. 1, pp. 16-26.

Meyerhof, G.G. (1956). "Penetration Tests and Bearing Capacity of Cohesionless Soils." *ASCE Journal of Soil Mechanics and Foundation Engineering,* Vol. 82, No. SM1, pp. 1-19.

Mikasa, M., and Takasa, N. (1973). "Significance of Centrifugal Model Test in Soil mechanics." *Proceedings of the 8th International Conference on Soil Mechanics and Foundation Engineering,* Moscow, Vol. 1.2, pp. 273-278.

Milovic, D.M. (1973). "Stresses and Displacements Produced by a Ring Foundation." *Proceedings of the 8th International Conference on Soil Mechanics and Foundation Engineering,* Vol. 1, Moscow, pp. 167-171.

Milovic, D.M. (1982). "Stresses and Displacements Produced by Various Shapes of Foundation." *Proceedings of the International Symposium on Numerical Models in Geotechnics,* Ed. by R. Dungar *et al.*, Zurich, pp. 721-731.

Mitchell, J.K., Vivatrat, V., and Lambe, T.W. (1977). "Foundation Performance of Tower of Pisa." *ASCE Journal of Geotechnical Engineering Division.* Vol. 103, No. GT3, pp. 227-249.

Morin, J.P., and Bozozuk, M. (1983). "Performance of Concrete Tower Silos on Clays in Quebec." *Canadian Agricultural Engineering,* Vol. 25, No. 1, pp. 81-88.

Morin, J.P., Gervais, R. (1985). "Settlement Record of Tower Silos Built on Champlain Clays." *Proceedings of the 38th Canadian Geotechnical Conference,* Edmonton, pp. 285-294.

Muhs, H. (1965). "On the Phenomenon of Progressive Rupture in Connection with the Failure Load: Discussion." *Proceedings of the 6th International Conference on Soil Mechanics and Foundation Engineering,* Montreal, Vol. 3, pp. 419-421.

Nagtegaal, J.C., Parks, D.M., and Rice, J.R. 1974. "On Numerical Accurate Finite Element Solution in the Full Plastic Range." *Computer Methods in the Applied Mechanics and Engineering,* North Holland Publishing, Vol. 33, pp. 469-484.

Nagtegaal, J.C., and De Jong, J.E. 1981. "Some Computational Aspects of Elastic-Plastic Large Strain Analysis." *International Journal for Numerical Methods in Engineering,* Vol. 17, pp. 15-41.

Ofer, Z. (1981). "Laboratory Instrument for Measuring Lateral Soil Pressure and Swelling Pressure." *Geotechnical Testing Journal*, Vol. 4, No. 4, pp. 177-182.

Okamura, M., Takemura, J., and Kimura, T. (1997). "Experimental and Analytical Studies on Bearing Capacities of Rectangular Footings on Sand." Presented on *The 3rd International Geotechnical Engineering Conference*, Cairo University, Egypt.

Ovesen, N.K. (1975). "Centrifugal Testing Applied to Bearing Capacity Problems of Footings on Sand." *Geotechnique*, Vol. 25, No. 2, pp. 394-401.

Phillips, R. (1995). "Centrifuge Modelling: Practical Considerations." in *Geotechnical Centrifuge Technology*, ed. by R.N. Taylor, Blackie Academic & Professional, London, pp. 34-60.

Pooroshasb, H.B., Holubec, I., and Sherborne, A.N. (1967). "Yielding and Flow of Sand in Triaxial Compression: Parts II and III." *Canadian Geotechnical Journal*, Vol. 4, No. 4, pp. 376-397.

Potyondy, J.G. (1961). "Skin Friction Between Various Soil and Construction Materials." *Geotechnique*, Vol. 11, No. 4, pp. 339-353.

Prandtl, L. (1921). "Uber die Eindringungsfestigkeit plastischer Baustoffe und die Festigkeit von Schneiden." *Zeitschrift fur Angewandte Mathematik und Mechanik*, Basel, Switzerland, Vol. 1, pp. 15-20.

Pu, J.L., and Ko, H.Y. (1988). "Experimental Determination of Bearing Capacity in Sand by Centrifuge Footing Test." *Centrifuge 88*, Balkema, Rotterdam, pp. 293-299.

Rad, N.S., and Tumay, M.T. (1987). "Factors Affecting Sand Specimen Preparation by Raining." *Geotechnical Testing Journal*, Vol. 10, No. 1, pp. 31-37.

Reissner, H. (1924). "Zum Erddruckproblem." *Proceedings of the 1st International Conference on Applied Mechanics*, Delft, Netherlands, pp. 295-311.

Roscoe, K.H., and Burland, J.B. (1968). "On the Generalized Stress-Strain Behaviour of 'Wet' Clay." *Engineering Plasticity*, ed. by J. Heyman and F.K. Leckie, Cambridge University Press, Cambridge, pp. 535-609.

Rowe, P.W. (1962). "The Stress-Dilatancy Relation for Static Equilibrium of an Assembly of Particles in Contact." *Proceedings of Royal Society*, Vol. 269A, pp. 500-527.

Rowe, P.W. (1969). "The Relation between the Shear Strength of Sands in Triaxial Compression, Plane Strain and Direct Shear." *Geotechnique*, Vol. 9, No. 1, pp. 75-86.

Roscoe, K.H., Schofield, A.N., and Wroth, C.P. (1958). "On the Yielding of Soils." *Geotechnique*, Vol. 8, pp. 22-53.

Rowe, P.W. (1975). "Displacement and Failure Modes of Model Offshore Gravity Platforms Founded on Clay." in *Conference on Offshore Europe*, Spearhead Publications, Aberdeen.

Schcherbina, V.I. (1988)." Earth Pressure Studies on Retaining Walls by Centrifuge Modelling." *Centrifuge 88*, ed. by Corte, Balkema, Rotterdam, pp. 421-428.

Schmertmann, J.H. (1975). "Measurement of In Situ Shear Strength." *Proceedings of ASCE Conference on In Situ Measurement of Soil Properties*, Raleigh, pp. 57-138.

Schofield, A.N. (1980). "Cambridge Geotechnical Centrifuge Operation." *Geotechnique*, Vol. 30, No. 3, pp. 227-268.

Schofield, A.N., and Wroth, C.P. (1968). *Critical State Soil Mechanics*, McGraw Hill, Inc., London.

Selig, E. T., and McKee, K. E. (1961). "Static and Dynamic Behaviour of Small Footings." *ASCE Journal of Soil Mechanics of and Foundations Division*, Vol. 87, No. SM6, pp. 69-81.

Shield, T.R. (1955). "On Coulomb's Law of Failure of Soils." *J. Mech. Phys. Solids*, Vol. 4, No. 1, pp. 10-16.

Sokolovskii, V.V. (1960). *Statics of Soil Media*, Butterworths Scientific Publications, London, 237 p. (Translated by D.H. Jones and A.N. Schofield from 1954 Second Russian edition)

Sokolovskii, V.V. (1965). Statics of Granular Media, Pergamon Press, New York.

Sutherland, H.B., and Mesdary, M.S. (1969). "The Influence of the Intermediate Principal Stress on the Strength of Sand." *Proceedings of the 7th International Conference on Soil Mechanics and Foundation Engineering*, Mexico, Vol. 1, pp. 391-399.

Tan, F.S. (1990). "Centrifuge and Theoretical Modelling of Conical Footings on Sand." *Ph.D. Thesis*, Cambridge University.

Tassoulas, J.L., and Kausel, E. (1984). "On the Dynamic Stiffness of Circular Ring Footing on an Elastic Stratum." *International Journal for Numerical and Analytical Methods in Geomechanics*, Vol. 8, No. 5, pp. 411-426.

Tatsuoka, F., and Ishihara, K. (1974). "Yielding of Sand in Triaxial Compression." *Soils and Foundations*, Vol. 14, No. 2, pp. 63-76.

Taylor, D.W. (1948). *Fundamentals of Soil Mechanics*, Wiley, New York.

Terzaghi, K. (1943). *Theoretical Soil Mechanics*, John Wiley and Sons, New York, 510 p.

Ueno, K., Nakatomi, T., Mito, K., and Kusakabe, O. (1994). "Influence of Initial Conditions on Bearing Characteristics of Sand." *Centrifuge 94*, Balkema, Rotterdam, pp. 541-546.

Veletsos, A.S., and Tang, Y. (1987). "Vertical Vibration of Ring Foundations." *Earthquake Engineering and Structural Dynamics*, Vol 15, No. 1, pp. 1-21.

Vesic, A.S. (1963). "Bearing Capacity of Deep Foundations in Sand." *Highway Research Record*, No. 39, pp. 112-153.

Vesic, A.S. (1965). "Ultimate Loads and Settlements of Deep foundation." *Bearing Capacity and Settlement of Foundation*, Proceedings of a Symposium Held at Duke University in 1965, pp. 63-68.

Vesic, A.S. (1969). Discussion "Effects of Scale and Compressibility on Bearing Capacity of Surface Foundations." *Proceedings of 7th International Conference on Soil Mechanics and Foundation Engineering*, Mexico City, Vol. 3, pp. 270.

Vesic, A.S. (1973). "Analysis of Ultimate Loads of Shallow Foundations." *ASCE Journal of Soil Mechanics and Foundation Engineering Division*, Vol. 99, No. SM1, pp. 45-73.

Vesic, A.S. (1975). "Bearing Capacity of Shallow Foundations." *Foundation Engineering Handbook*. Van Nostrand Reinhold Company, New York, Chapter 3, pp. 121-147.

Vesic, A.S., Banks, D.C., and Woodard, J.M. (1965). "An Experimental Study of Dynamic Bearing Capacity of Footing on Sand." *Proceeding of 6th International Conference on Soil Mechanics and Foundation Engineering*, Montreal, Vol. 2, pp. 209-213.

Vesic, A.S., and Johnson, W.H. (1963). "Model Study of Beams Resting on a Silt Subgrade" *ASCE Journal of Soil Mechanics and Foundations Division*, Vol. 89, No. SM1, pp. 1-31.

Wood, D.M. (1990). "Soil Behaviour and Critical State Soil Mechanics." Cambridge University Press, Cambridge, 462 p.

Yoshimi, Y., and Kishida, T. (1981). "A Ring Torsion Apparatus for Evaluating Friction between Soil and Metal Surfaces." *Geotechnical Testing Journal*, Vol. 4, No. 4, pp. 145-152.

Zhou, S.G. (1981). "Evaluation of the Liquefaction of Sand by Static Cone Penetration Test." *Proceedings of the 7th World Conference on Earthquake Engineering*, Istanbul, Vol. 1, pp. 156-162.

Zhu, F., Clark, J.I., and Paulin, M.J. (1995). "Factors Affecting At-Rest Lateral Stress in Artificially Cemented Sands." *Canadian Geotechnical Journal*, Vol. 32, pp. 195-203.

Zhu, F., Clark, J.I., and Phillips, R. (1998). "Bearing Capacity of Ring Foundations under Vertical Load", *Centrifuge 98.*

Zienkiewicz, O.C., and Cormeau, I.C. (1972). "Viscoplastic Solution by the Finite Element Process." *Arch. Mech.*, Vol. 24, pp. 873-888.

Zienkiewicz, O.C., and Cormeau, I.C. (1974). "Viscoplasticity, Plasticity and Creep in Elastic Solids: A United Numerical Solution Approach", *International Journal for Numerical Methods in Engineering*, Vol. 8, pp. 8321-845.

Zienkiewicz, O.C., Humpheson, C., and Lewis, R.W. (1975). "Associated and Non-Associated Viscoplasticity and Plasticity in Soil Mechanics." *Geotechnique*, Vol. 25, No. 4, pp. 671-689.

Zienkiewicz, O.C., Norris, V.A., Winnicki, L.A., Naylor, D.J., and Lewis, R.W. (1978). "A United Approach to the Soil Mechanics Problems of Offshore Foundations." In *Numerical Methods in Offshore Engineering*, John Wiley & Sons, New York, pp. 361-411.

Appendix A

Load and Displacement of Eccentrically Loaded Ring Footings

Centrifuge tests of eccentrically loaded circular and ring footings with an area of $15cm^2$ were conducted at an acceleration of 100 gravities, as described in Chapter 4. The footings are in five groups, with ring radii ratio n = 0, 0.35, 0.5, 0.7 and 0.9 respectively. The loading eccentricity varies from 0 to 0.375. The load, settlement and rotation angle of 20 tests conducted at various ring radii ratio and loading eccentricity are given in Figure A.1 to A.20 as follows.

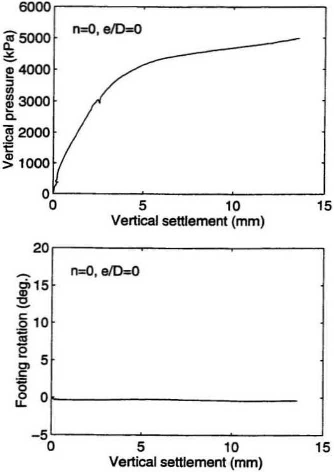

Figure A.1: Load and rotation angle versus vertical settlement (n=0, e/D=0)

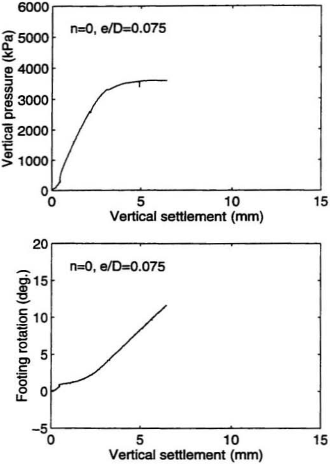

Figure A.2: Load and rotation angle versus vertical settlement (n=0, e/D=0.075)

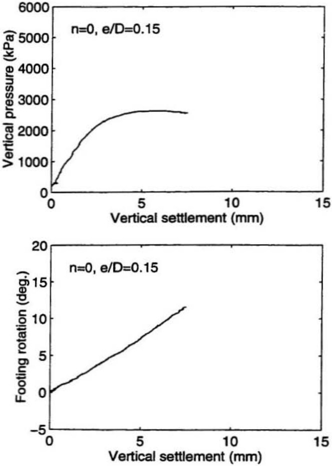

Figure A.3: Load and rotation angle versus vertical settlement (n=0, e/D=0.15)

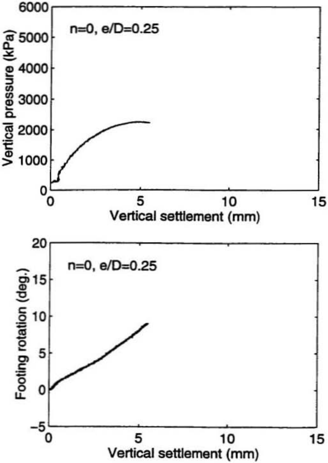

Figure A.4: Load and rotation angle versus vertical settlement (n=0, e/D=0.25)

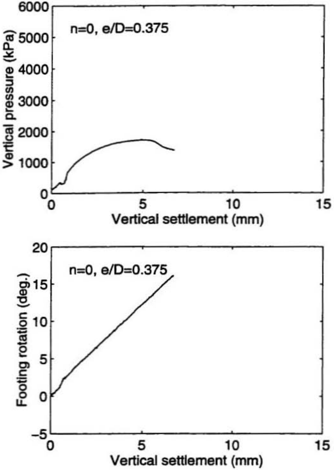

Figure A.5: Load and rotation angle versus vertical settlement (n=0, e/D=0.375)

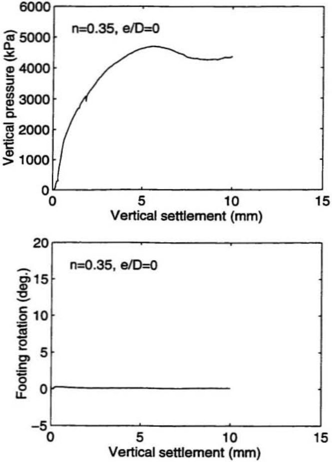

Figure A.6: Load and rotation angle versus vertical settlement (n=0.35, e/D=0)

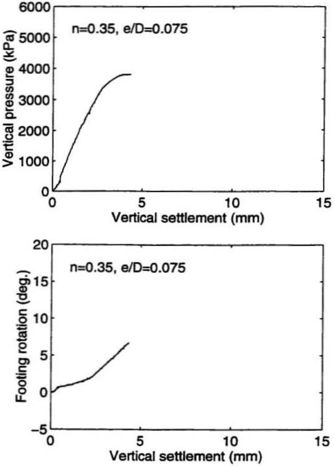

Figure A.7: Load and rotation angle versus vertical settlement (n=0.35, e/D=0.075)

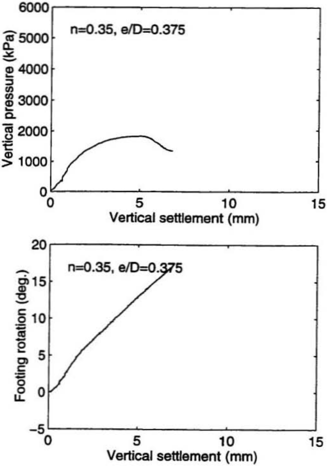

Figure A.8: Load and rotation angle versus vertical settlement (n=0.35, e/D=0.375)

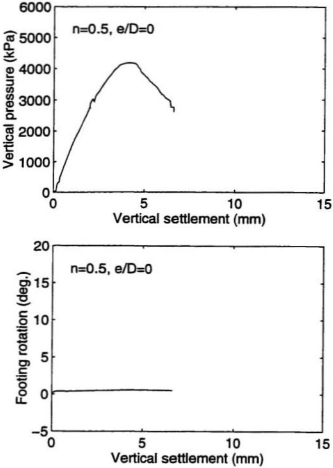

Figure A.9: Load and rotation angle versus vertical settlement (n=0.5, e/D=0)

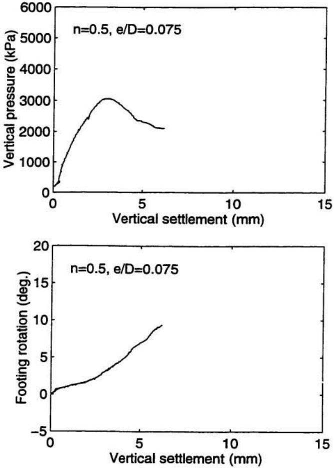

Figure A.10: Load and rotation angle versus vertical settlement (n=0.5, e/D=0.075)

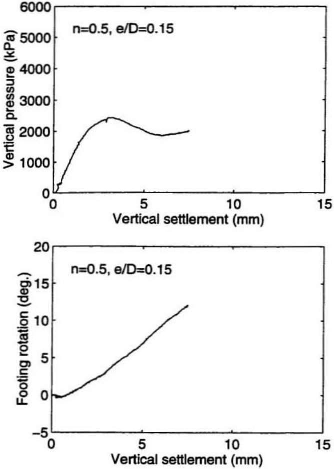

Figure A.11: Load and rotation angle versus vertical settlement (n=0.5, e/D=0.15)

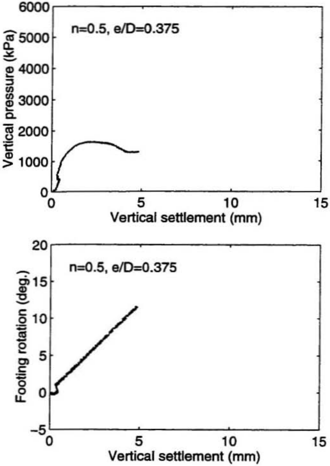

Figure A.12: Load and rotation angle versus vertical settlement (n=0.5, e/D=0.375)

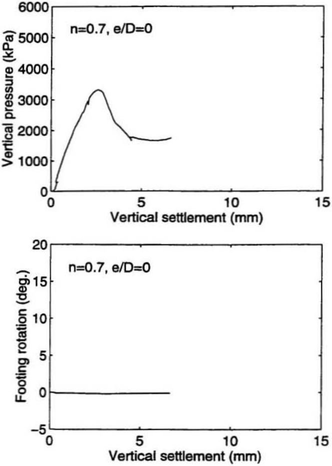

Figure A.13: Load and rotation angle versus vertical settlement (n=0.7, e/D=0)

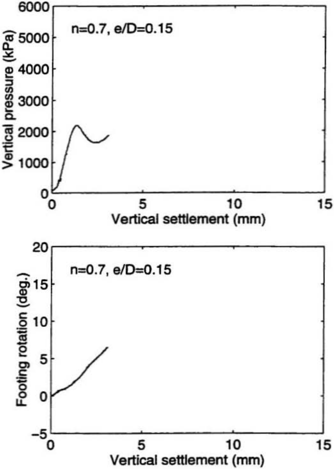

Figure A.14: Load and rotation angle versus vertical settlement (n=0.7, e/D=0.15)

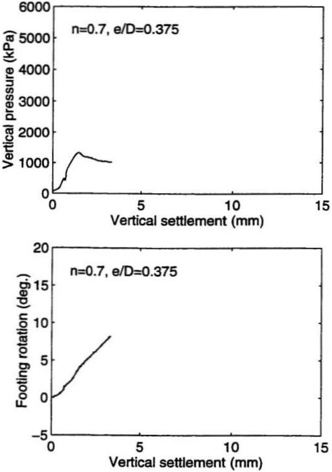

Figure A.15: Load and rotation angle versus vertical settlement (n=0.7, e/D=0.375)

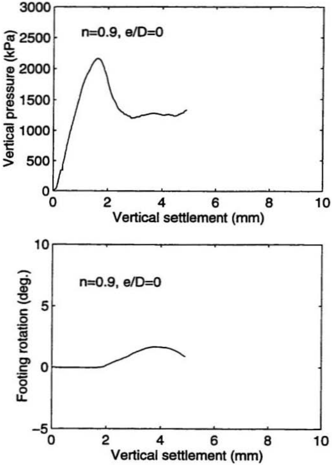

Figure A.16: Load and rotation angle versus vertical settlement (n=0.9, e/D=0)

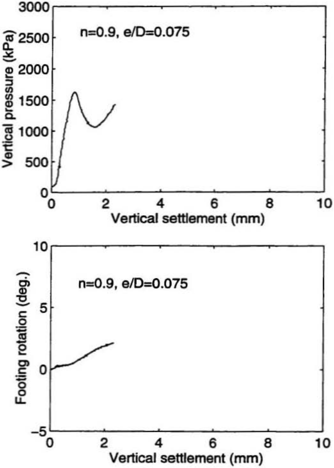

Figure A.17: Load and rotation angle versus vertical settlement (n=0.9, e/D=0.075)

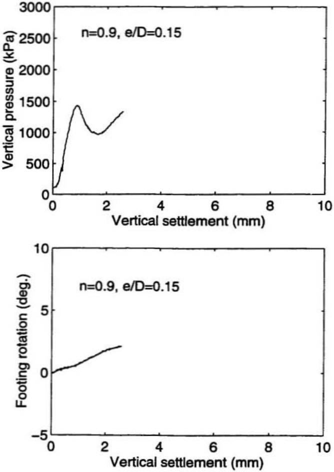

Figure A.18: Load and rotation angle versus vertical settlement (n=0.9, e/D=0.15)

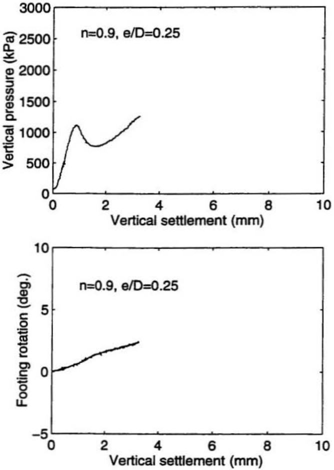

Figure A.19: Load and rotation angle versus vertical settlement (n=0.9, e/D=0.25)

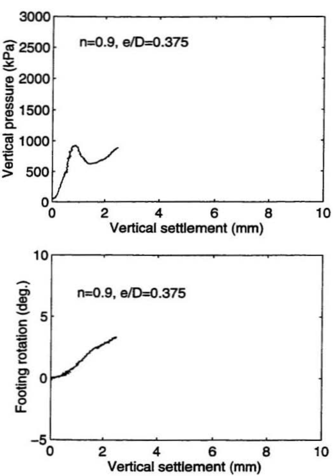

Figure A.20: Load and rotation angle versus vertical settlement (n=0.9, e/D=0.375)

Appendix B

Finite Element Meshes for Axially Loaded Ring Footings

The finite element meshes for seven circular and ring footings under axisymmetric conditions with ring radii ratio n=0, 0.2, 0.35, 0.5, 0.7, 0.8 and 0.9 are shown in Figure B1 to B7 respectively. The meshes have been used in the finite element analysis of the bearing capacity of ring footings on sand, as presented in Chapter 6. In each figure, the dashed line on the left side represents the axisymmetric center. At the bottom of each mesh, both vertical and horizontal displacements are constrained; at the right side of the mesh, only horizontal displacement is not allowed.

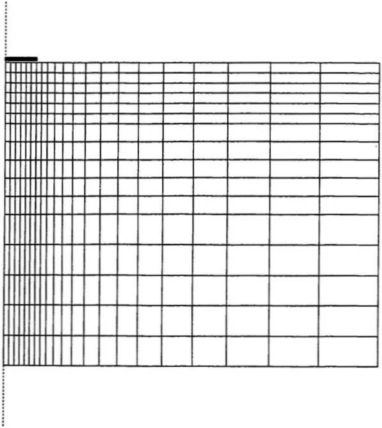

Figure B.1: Finite element mesh for circular footing (n=0)

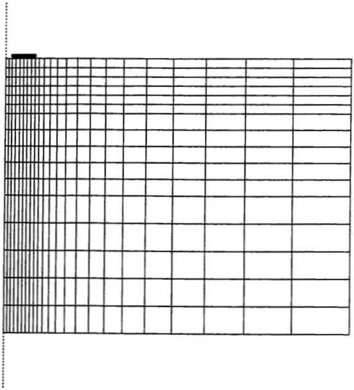

Figure B.2: Finite element mesh for ring footing with n=0.2

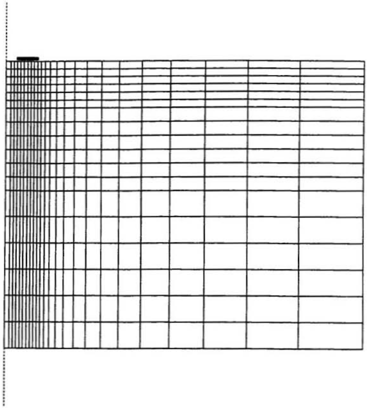

Figure B.3: Finite element mesh for ring footing with n=0.35

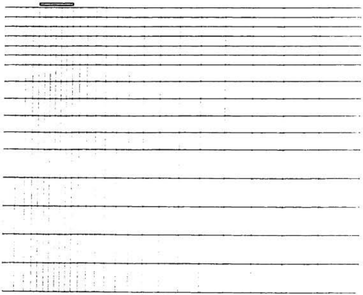

Figure B.4: Finite element mesh for ring footing with n=0.5

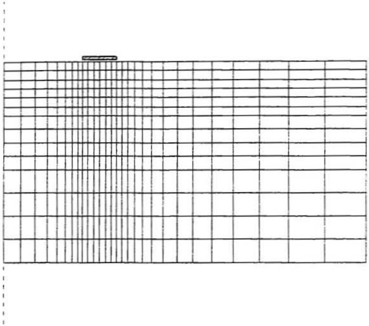

Figure B.5: Finite element mesh for ring footing with n=0.7

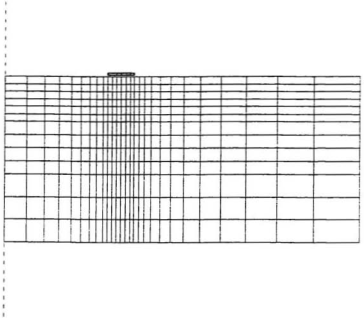

Figure B.6: Finite element mesh for ring footing with n=0.8

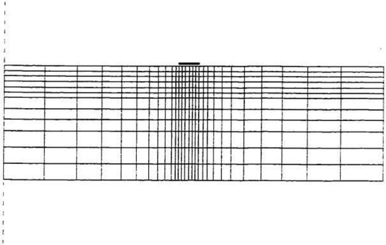

Figure B.7: Finite element mesh for ring footing with n=0.9

IMAGE EVALUATION
TEST TARGET (QA-3)

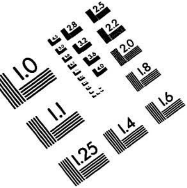

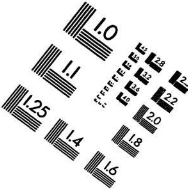

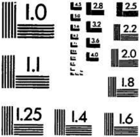

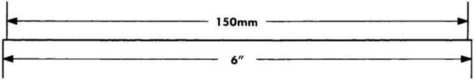

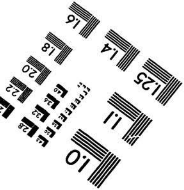

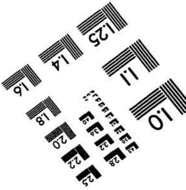

APPLIED IMAGE . Inc
1653 East Main Street
Rochester, NY 14609 USA
Phone: 716/482-0300
Fax: 716/288-5989

© 1993, Applied Image, Inc., All Rights Reserved

CENTRE FOR NFLD. STUDIES
JUL 18 1978
MEMORIAL UNIVERSITY
OF NEWFOUNDLAND